Universidad de Guanajuato

División de Ciencias e Ingenierías

Campus León

Validation of muon energy scale fit with medium energy flux using the low-ν method on MINERvA experiment

Thesis presented by

FRANCISCO JAVIER ROSAS TORRES

This dissertation is submitted for the degree of

Master of Physics

Advisor

Dr. Julián Félix Valdez

Co-advisor

Dr. Laura Fields

March 18, 2021

Abstract

The research to understand the universe has been present since a long time ago. In recent time, the MINERνA collaboration has done a good measurement of the neutrino cross section in five nuclear targets, implementing the neutrino beam-line NuMI. For the medium energy configuration of the beam, the data events measured and simulation presented a discrepancy. The collaboration implemented the low-ν method to investigate the source of the disagreement and fixed that. In this work, a validation of the fit developed to remove the discrepancy between the data and simulation for the charged-current quasi-elastic sample of events in MINERνA is presented. This study validates that the mis-modeling is coming from the muon energy scale parameter in the MINOS detector.

Dedicado a mi familia y amigos.

Acknowledgements

My complete gratitude to my parents, Alicia and Javier, and my brother, Fernando, who were always supporting me. None of this would have been achieved without your help. They even shown me that in the darkness, the light persists. They are my motivation to improve myself day by day.

I thank my advisor, Julián Félix, who introduced me to the high energy physics and he provided me with all the necessary material to develop my knowledge in the area of particle detectors, all this through the international laboratory of elementary particles of the University of Guanajuato. In addition to teaching me the importance of always addressing the greatest goal and thinking that everything can be achieved using the right tool.

Thanks to my supervisor at Fermilab, Laura Fields, who guided me to develop the present thesis, giving me great advice and teaching me to make a correct interpretation of the measured data. Besides teaching me the importance of knowing how to ask for help and trusting your colleagues to collaborate together and thus improve our work.

I thank Jorge G. Morfin, for helping me to understand the physical phenomena of the MINERνA experiment, and for all the support given to be able to carry out a one-year stay at Fermilab, without their continuous interest in supporting all young Latin American scientists, this could not be possible.

Thanks to my extended family who have provided comments, suggestions and good advice; that have led me to be a good citizen wanting to continue growing in my society. My acknowledgement to the institutions that gave me an economical support, CONACyT, Fermilab, and the University of Guanajuato.

Finally, thank you to my friends (Karla, Eduardo R., Miguel, Daniel, Raúl, Cristina, Jazmín, Eduardo G., and Leonardo) who are with me every day, either to make a comment that can help me with my work, or simply to generate a smile to be able to continue with energy every day. You have shown me that I am never alone, and the day I think that I can no longer, you will be there and guide me to move on.

Contents

1 Introduction **8**

2 Neutrino research **10**

2.1 Standard Model . . . 10

2.2 Neutrino oscillations . . . 11

3 NuMI Beam-line **15**

3.1 Target . . . 16

3.2 Focusing horns . . . 17

3.3 Decay pipe . . . 20

3.4 Absorber and monitors of hadrons and muons . . . 21

4 MINERνA **24**

4.1 Types of Charged-Current interactions at MINERνA . . . 24

4.1.1 Charged-Current Quasielastic Scattering (CCQE) . . . 25

4.1.2 Resonance . . . 25

4.1.3 Deep Inelastic Scattering (DIS) . . . 26

4.2 MINERνA detector . . . 27

4.2.1 Steel Shield and Veto Wall . . . 31

4.2.2 Nuclear Target Region . . . 31

4.2.3 Active Tracker Region . . . 32

4.2.4 Electromagnetic calorimeter (ECAL) . . . 33

4.2.5 Hadronic calorimeter (HCAL) . . . 33

4.3 MINOS detector . . . 33

5 Wiggle **36**

6 Low-ν method **38**

6.1 Charged Current Neutrino-Nucleus interaction . . . 38

6.2 Charged current scattering cross section . . . 40

6.3 Low-ν in the flux fit investigation . . . 40

7 Systematic uncertainties **42**
7.1 Central Value and the universes . . . 42
7.2 Source of the uncertainties . . . 43
7.3 Systematic error band in the ratio of the data and simulation . . . 45

8 Fits implemented **48**
8.1 Measurement of E_μ and ν . . . 48
8.2 Vertical and lateral affectation generated by shifts to the parameters . . . 50
8.3 Performing a weight function . . . 54
8.4 Weight function of the focusing parameters . . . 57
8.5 Shift to the muon energy scale . . . 60
8.6 Weight function of the focusing parameters and muon reconstruction parameters . . . 63
8.7 Comparing between the shape distribution of all hypotheses . . . 68

9 Variations to the sample **70**
9.1 Samples of muons reconstructed by curvature . . . 70
9.2 Samples of muons reconstructed by range . . . 73
9.3 Samples of MINOS muon momentum $<$ 1 GeV . . . 76
9.4 Sample of MINOS muon momentum $>$ 1 GeV . . . 83
9.5 Contribution of the hadronic recoil energy to the E_ν . . . 85
9.5.1 Sample of $\mathbf{0 < y < 0.1}$ . . . 89
9.5.2 Sample of $\mathbf{0.1 < y < 0.3}$ . . . 91
9.5.3 Sample of $\mathbf{0.3 < y < 0.5}$ . . . 94

10 Conclusions **100**

A Supplementary plots **102**

Bibliography **109**

Chapter 1. Introduction

In this thesis is presented the comparison of applying independently three different fits to remove the discrepancy between data and simulation on the MINERνA experiment; for this analysis the low-ν method is implemented. The goal is to validate previous studies that show that the muon energy scale is the origin of the problem of the discrepancy between data and simulation in the neutrino flux when it is measured in the MINERνA detector.

In chapter 2 a brief description of the neutrino physics and some projects that are running to learn more about these particles are mentioned.

In chapter 3 the NUMI beam line is shown, with a description of each component that make up the beam, used by the experiments developed in Fermilab.

Chapter 4 includes a short explanation of the geometry, materials, and goals of the MINERνA experiment. This detector was located on-axis in the neutrino beam of Fermilab, and studies the interactions of neutrinos with five different targets.

In chapter 5 the discrepancy between data and simulation of the MINERνA experiment found in the neutrino flux of the NuMI beam line using the medium energy configuration, known as wiggle, is showed.

In chapter 6 the explanation and definition of low-ν method is described. Also a brief description of why it is used to analyze the neutrino flux in the MINERνA detector and what cuts are made to the data and simulation to apply this method is depicted.

In chapter 7 the systematic uncertainties used in the analysis and the importance of a right implementation to get a better fit between data and simulation in the investigation of flux discrepancy are discussed.

In chapter 8 the three fits that are implemented to fix the discrepancy observed between data and simulation are presented, and how they are applied to the sample. These

were development by the MINERνA collaboration.

In chapter 9 the histograms of different samples of data and simulation are shown, to analyze how the shape of histograms changes for each sample when the weight functions are implemented. The weight functions used are mentioned in the previous chapter.

In chapter 10 the conclusions of this validation for these studies with the three fits applied to the different samples of the events measured using the low-ν method are discussed.

Chapter 2. Neutrino research

Throughout human history, the curiosity to know and understand everything that surrounds us has existed. Humans began to try to understand how things they saw happen. However to understand these phenomena, first we need to comprehend what things are made of. Eventually this line of study led scientists to investigate the elementary particles that make up our universe. Many particles were discovered, but it was not enough just to discover them. Developing a model that unifies all the particles to create a better understanding of the universe was the next objective. The standard model was developed to have a better understanding of the fundamental interactions of matter and to unify all the acquired knowledge of the known elementary particles.

2.1 Standard Model

The Standard Model is conformed by six quarks that are represented by the letters *u, d, s, c, b* and *t*. This letters means *up, down, strange, charm, bottom and top*; in order of how they are enlisted. The model additionally includes three charged leptons: e (electron), μ (muon), and τ (tau). Each one has a neutral lepton partner named neutrinos: ν_μ, ν_e, and ν_τ. All these particles, six leptons and six quarks, have an equivalent antiparticle. These antiparticles are represented in different forms, the antiparticles of the quarks and neutrinos are denoted by the same symbol but with an upper bar, for example $\overline{\nu}_\mu$. For the charged leptons, they are denoted by a superscript symbol that represent the charge of the particle, for example $\mu^\pm$.

In nature quarks are not observed in free state, they are found in clusters of two-quarks or three-quarks. They are assigned names according to the number of quarks binded, mesons for two-quarks, and baryons for three-quarks, in general they are called hadrons. With the arrangement of the lightest quarks, u and d, we get protons (uud), and neutrons (udd), that collectively are called "nucleons". When the nucleons and the electrons are together, atoms are obtained. From these the matter of our universe is formed.

In addition to the description of the particles that form the matter of the universe,

the Standard Model describes the interactions between the particles, which are: electromagnetic, strong and weak. These interactions happen by the exchange of gauge bosons. The electromagnetic interaction occurs in the attraction or repulsion of a charged particle immersed in an electric field, or changing the trajectory of a charged particle when it is crossing a magnetic field, in this kind of interactions photons are liberated. The strong interaction is responsible for the formation of nucleons and the nucleus, having the exchange of gluons. The weak interaction is responsible for the beta decay in the heavy elements, it is mediated by the exchange of a charged W boson. The neutrino is the principal particle to analyze for this investigation, and the only that participates of the weak interactions, since these are a neutral particles, without electric charge.

Focusing our attention on weak interactions, which can occur through two types of exchanges, with the W boson or by the Z boson. Depending on which boson is involved in the interaction it is named differently. When the W boson is in the interaction the type of channel is known as "charged-current" because the W boson carries a unit of electric charge. In the figure 2.1 one type of charged current is shown, this is illustrated using a Feynman diagram for a neutrino scattering interaction. This can happen for a beam-line of muon neutrinos, ν_μ, colliding with a fixed target. Then the neutrino is converted to its charged lepton partner, a μ^- for this example, besides a d quark is converted to a u quark which will produce a hadron when interacting with other particles.

If the weak interaction occurs with a Z boson, then the channel is termed "neutral-current", because the Z carries no charge. In the figure 2.2 a Feynman diagram of the scattering between ν_μ and target is shown. In the diagram it is observed that the incoming neutrino particle is the same as in the final state. This kind of interaction is less probable than the charged-current.

2.2 Neutrino oscillations

In nature thousands of sources of neutrinos exist, for example: in the interaction of cosmic rays with the atmosphere of the Earth, in stars, and supernovae. The Sun is the principal source of neutrinos in the Solar System, for this reason the scientists have taken great interest to analyze the process that neutrinos go through, since they leave the Sun until

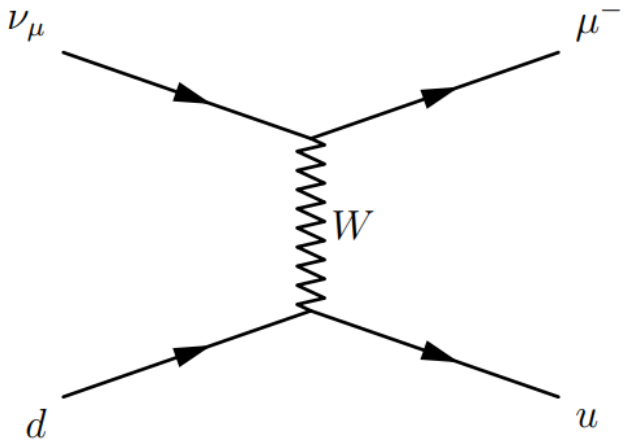

Figure 2.1. Feynman diagram for a Charged-Current interaction. The muon neutrino (ν_μ) incoming is converted to a muon (μ^-) by the interaction with a d quark, this by the exchange of a W boson (carries a unit of charge), in addition the d quark is converted to a u quark.

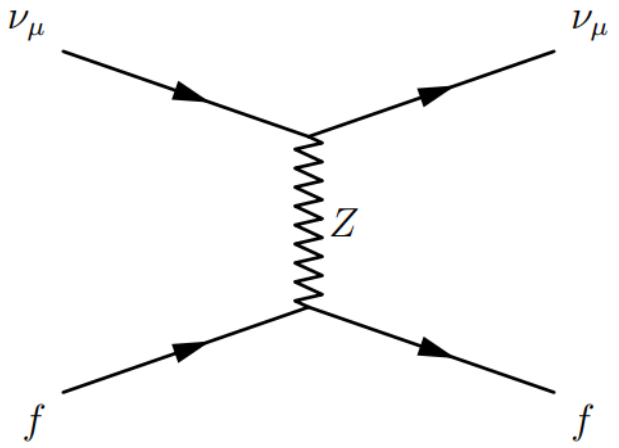

Figure 2.2. Feynman diagram for a Neutral-Current interaction. The muon neutrino (ν_μ) incoming exchanges a Z boson with either a quark or lepton, f. For this kind of interaction the particles of the initial state are the same that in the final state.

they reach the Earth. The fusion process occurs in the Sun and creates a flux of electron neutrino, ν_e, with an energy scale of MeV, these leave the Sun and travel in space until arriving at the Earth and even cross it.

With the work of John Bahcall [29], in 1960 it was possible to calculate the neutrino flux incoming from the Sun. In addition to the calculation of Bahcall, Raymond Davis [19] performed the experiment to measure the ν_e incoming from the Sun. From this measurement it was possible to identify that the number of electron neutrinos does not match with the number calculated. The disagreement observed between the calculation and the measurement was that the number of electron neutrinos measured was 1/3 (one third) the number of electron neutrinos predicted.

The answer to the discrepancy observed was found in the works of Bruno Pontecorvo [5], where he explained that if the neutrino mass is different to zero, then a change of flavor between the three types of neutrinos should be possible. This would happen while they are traveling in space. To describe the *flavor state* of the neutrinos, the *mass state*, (ν_1, ν_2, ν_3) of them can be used. If the flavor states are expressed as a linear combination of the mass states, then a mixing matrix can be used, as given in the next equation:

$$|\nu_\alpha\rangle = \sum_k U_{\alpha k} \, |\nu_k\rangle \ , \tag{2.1}$$

where $\alpha \in \{e, \mu, \tau\}$, and $k \in \{1, 2, 3\}$. Furthermore, the mixing matrix implemented is known as the PMNS matrix, this is for the surnames of: Bruno Pontecorvo, Ziro Maki, Masami Nakagawa, and Shoichi Sakata [32]; the matrix can be parameterized by the three mixing angles $(\theta_{12}, \theta_{13}, \theta_{23})$, and the CP-violating phase (δ_{CP}), the parametrization is shown next:

$$U = \begin{pmatrix} 1 & 0 & 0 \\ 0 & \cos\theta_{23} & \sin\theta_{23} \\ 0 & -\sin\theta_{23} & \cos\theta_{23} \end{pmatrix} \times \begin{pmatrix} \cos\theta_{13} & 0 & e^{-i\delta_{CP}}\sin\theta_{13} \\ 0 & 1 & 0 \\ -e^{-i\delta_{CP}}\sin\theta_{13} & 0 & \cos\theta_{13} \end{pmatrix} \times \begin{pmatrix} \cos\theta_{12} & \sin\theta_{12} & 0 \\ -\sin\theta_{12} & \cos\theta_{12} & 0 \\ 0 & 0 & 1 \end{pmatrix} . \tag{2.2}$$

It is important to highlight that the neutrino oscillation probabilities do not have a direct dependence of the neutrino masses. The indirect dependence is coming from the difference of masses squared, $(\Delta m^2)_{kk'}$, that is a factor in the oscillation probability be-

tween two states. Considering all these parameters it is possible to note that the oscillation probabilities between the three flavor states is a complex mix of the different parameters with too many combinations. For example, the probability between two flavor state is shown in the next equation:

$$P_{\alpha\to\beta} = \sin^2(2\theta)\sin^2\left(\frac{\Delta m^2 L}{4E}\right). \tag{2.3}$$

This equation describes the probability that a neutrino with the initial flavor state α oscillates to the neutrino with the flavor state β, where, θ is the mixing angle, Δm^2 is the difference of the neutrino masses squared. For the last two variables the subscripts have been removed because the equation is only for the two particles mentioned above. In addition to these variables, that are difficult to measure, we need to know the length that the neutrinos travel, L, and the energy of the particle, E.

All the factors to be measured to obtain the oscillation probability generate a difficult condition to carry out an experiment using the neutrinos formed in nature. When it is possible to elaborate the best combination of the parameters that maximizes the probability of neutrino oscillation, better results in neutrino measurement can be get and reduced the construction costs of the particle detector.

In order to optimize the measurement processes to develop experiments related to neutrino research, the NuMI beam-line was built at Fermilab. In this beam-line many neutrino experiments have been run, for example: MINOS (Main Injector Neutrino Oscillation Search), NOνA (NuMI Off-axis ν_e Appearance) and MINERνA (Main Injector Experiment ν - A). The description of the components used in the NuMI beam-line and the process to get a neutrino beam are described in chapter 3.

Chapter 3. NuMI Beam-line

Fermilab [15] is the premier particle physics laboratory in the United States, it has worked since 1967. In this laboratory, the scientists work to understand what the universe is made of, analyzing the fundamental particles of matter, in addition to dark matter and dark energy. To do these investigations, the Fermi Research Alliance LLC of the U.S. Department of Energy Office of Science builds the most advanced particle accelerators of the world. The accelerator complex located in Fermilab is shown in the figure 3.1. In the complex, beam-lines of neutrinos, muons and hadrons are generated, the beams cross the particles detector at Fermilab to study the particle interaction in them, one of the beam-line is known as NuMI beam.

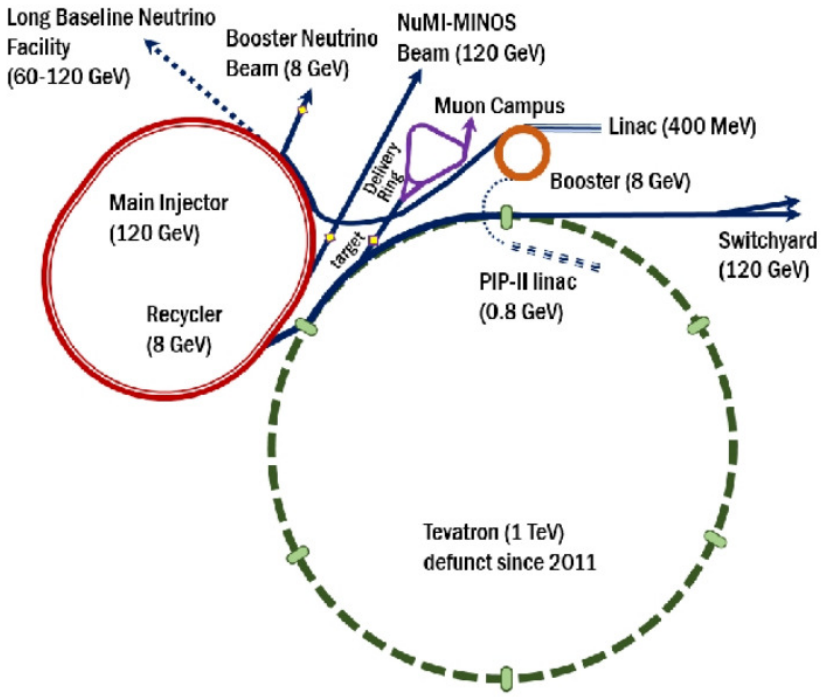

Figure 3.1. The accelerator complex built at Fermilab. The point of origin of the protons is the Linac. The PIP-II linac is currently being built to have a beam with higher energy. Figure from the reference [30].

Neutrinos at the Main Injector (NuMI) is in charge of producing the neutrinos beam-line at Fermilab. It produces the most high energetic neutrino beamline for the following

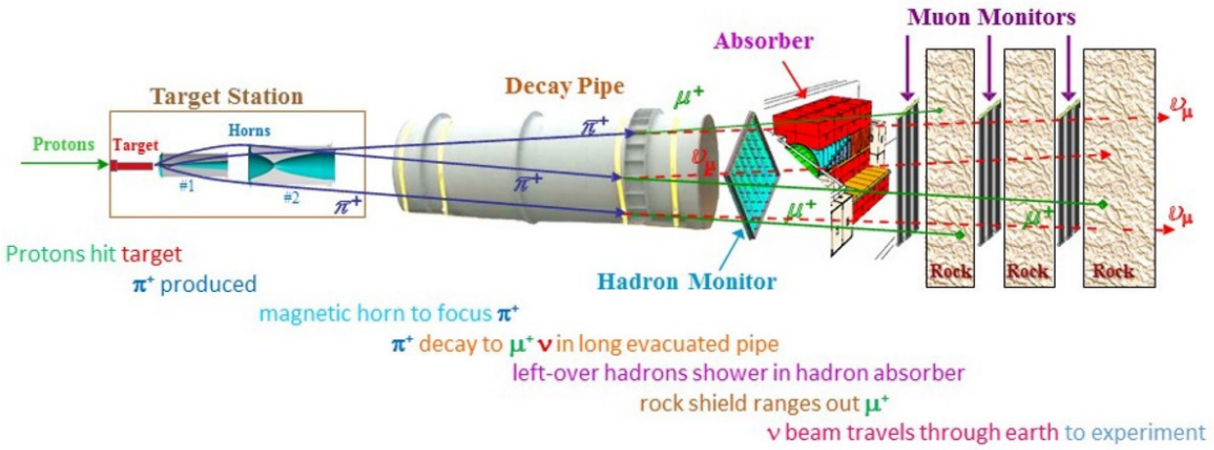

Figure 3.2. Diagram of the NuMI beamline. Figure from the reference [2].

experiments: MINERvA, MINOS, and NOvA; for this reason, it is the most important neutrino beam-line in the world. In the figure 3.2 a diagram of the components in the NuMI beam-line is shown. The NuMI beam begins at 1 km upstream of the MINOS Near Detector with a protons beam of 120 GeV coming from the Main Injector, which do not arrive continuously, they are separated by spill. Each spill has around 25 to 50 millions protons, and the spill has a duration of 1.33 seconds. The main parts to perform the neutrino beam-line are the Target Hall (composed of the target and the focusing horns), the Decay Pipe, absorber, and the downstream monitoring.

3.1 Target

The first element through which the protons from the main injector pass is the target, which is made up of graphite with density of 1.78 $g/cm3$. The objective that the protons hit the target and produce $pions^{\pm}$, π, and kaons from the interaction with the graphite, given that the predominant decay of these particles are the following:

$$\pi^{\pm} \rightarrow \mu^{\pm} + \nu_{\mu}\,, \qquad\qquad K^{+} \rightarrow \mu^{+} + \nu_{\mu}\,. \tag{3.1}$$

The array consists of 48 fins of graphite, each one having the same dimensions: 25 mm of width, 7.4 mm of length, and 63 mm of height. Between each fin exists a gap of

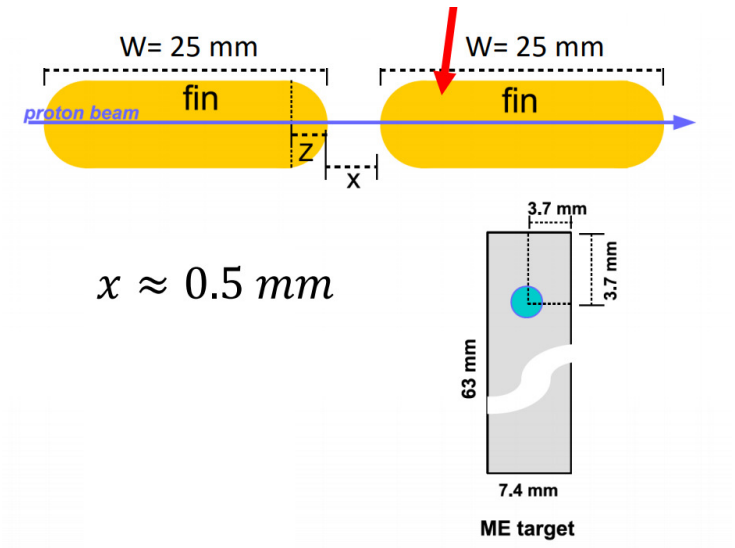

Figure 3.3. Diagram of the fins of graphite to form the target of NuMI beamline. Figure from the reference [2].

0.5 mm, for this reason the total length of the target is 1200 mm, with a cross sectional view of 7.4×63 mm2. In the figure 3.3 a diagram with the configuration of the fins is shown.

The target is inside of a canister, in which a cooling water is flowing to keep the graphite fins in low temperature, see figure 3.4. Furthermore the position of the target on the z-axis can be changed according to the configuration of the beam, if you want to have a beam of low neutrino energies, then the target position is 35 cm inside the first focusing horn.

For a medium energy configuration, the target position is 143 cm upstream from the low energy position. In addition to this change to vary the energy of the beam, the number of fins and the cross section of them need to change. The characteristic of the fins mentioned above corresponds to the dimensions for the medium energy beam-line.

3.2 Focusing horns

To focus the particles generated from the interaction between protons and the target, two aluminum horns were created. In this horn a toroidal magnetic field is produced. To do this, the horns consist of two parts, inner and outer layer of conductive material. When a charged particle travels through the horns, this particle feels a transverse momentum

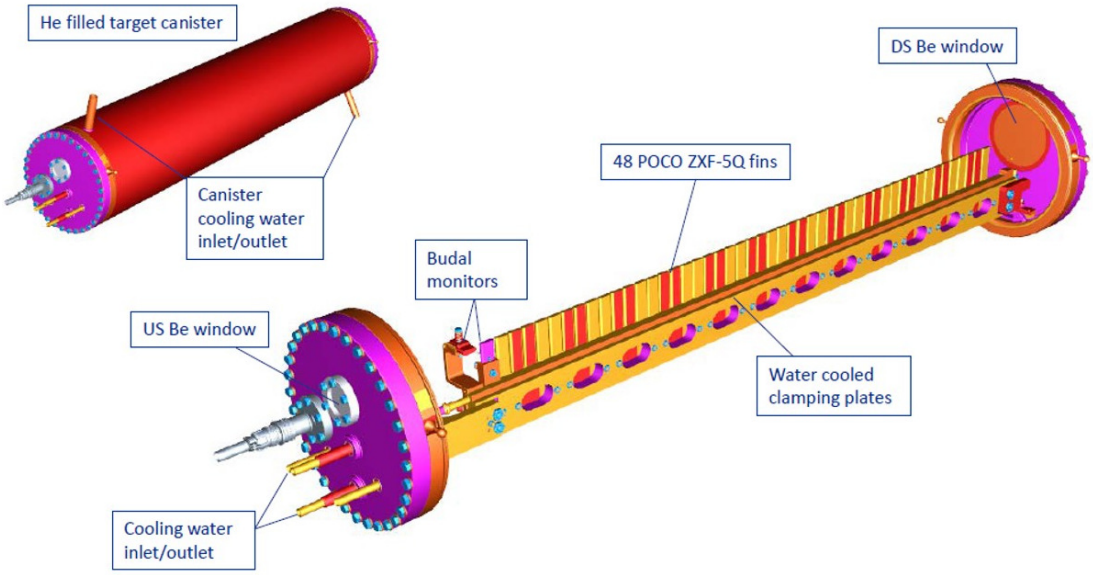

Figure 3.4. Diagram of the canister with the graphite fins array in the target sector of NuMI beam-line. Figure from the reference [12].

p_t kick, causing that particle to change its direction, which can focus one type of particle and defocus another, according to the charge of the particle. For this reason, according to the direction of the current in the horns, the switch between neutrino or anti-neutrino in the beam-line can be done.

In the figure 3.5 a diagram of the trajectory of the particles when they travel through the horns is shown. This system with a two focusing horns is used with the idea to reduce the divergence of the beam. Because if one particle is improperly focused by the first horn, then the second horn could focus the particle and get a greater number of particles focused by the horns, and this ends up increasing the number of neutrinos in the particle beam.

The current in the horns is pulsed with a maximum amplitude of 205 kA, the duration of the pulse is 2.3 ms. In figure 3.6 a schematic of a focusing horn is shown. The direction of the current shown in the schematic generates a magnetic field, $\vec{B}$. For this configuration, the positive particles are focused in the direction of the beam, and the particles of negative charge are defocused. Then the resulting beam corresponds to the neutrino beam-line.

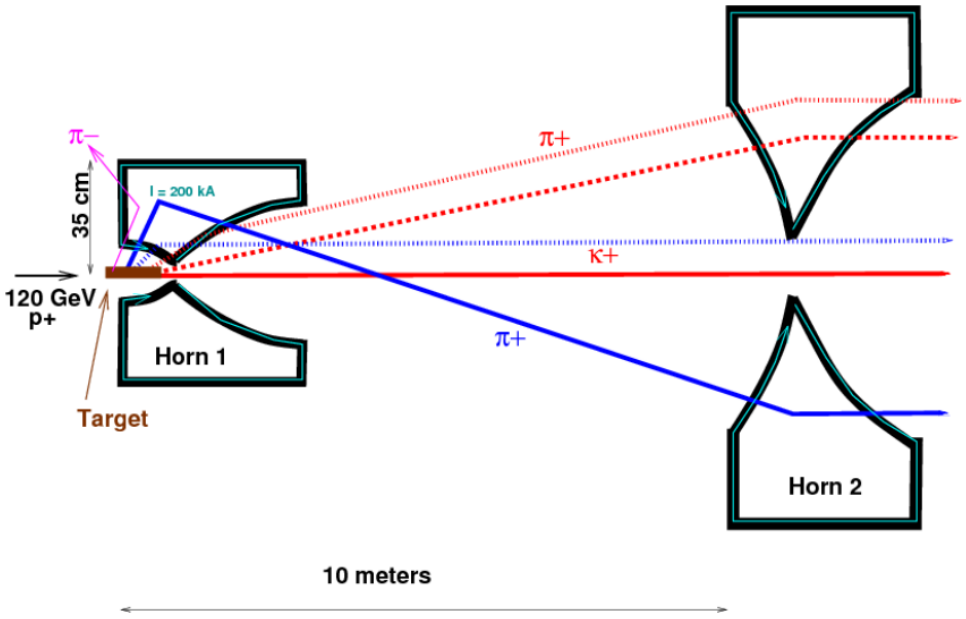

Figure 3.5. Diagram of the NuMI focusing system, which is composed of two magnetic horns, where each one creates a toroidal magnetic field to focus the mesons particles. Figure from the reference [26].

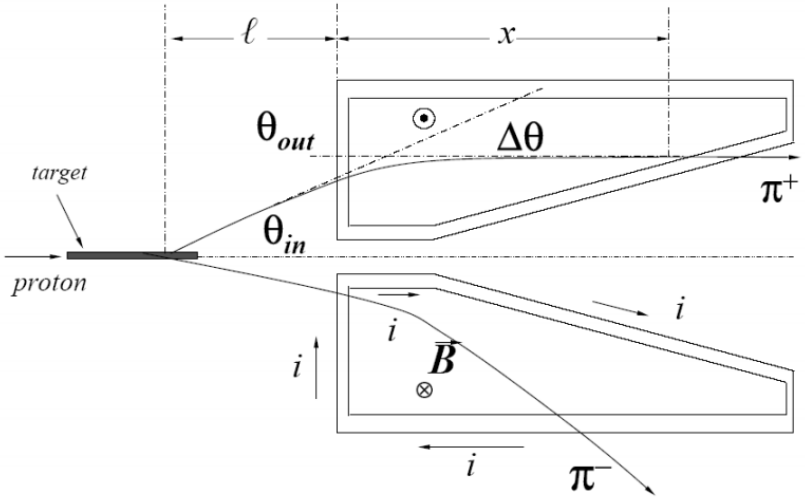

Figure 3.6. Diagram with the side-view of a horn of the NuMI focusing system. Indicating the current, i, that passes through the outside layer of the horn to create a magnetic field $\vec{B}$. For this configuration, the positive particles are focused. Figure from the reference [26].

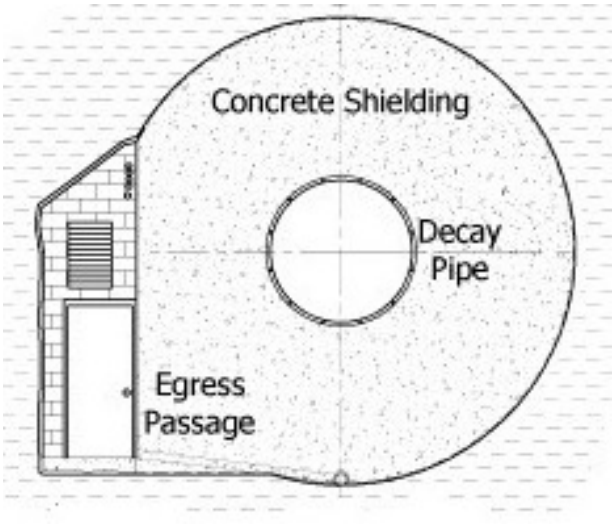

Figure 3.7. Diagram with the frontal-view of the decay pipe covered by the concrete shielding to reduce the noise of particles produce by outside sources. Figure from the reference [14].

3.3 Decay pipe

After particle to be focused, the pions and kaons produced by the interaction of the protons with the graphite target travel through the decay pipe. This is done to give the particles time and space to decay into neutrinos. The decay pipe literally is a pipe made up of steel with 0.95 cm of thickness, 675 m long, and 1.8 m of diameter; it is filled with helium, because it is inert and will reduce the probability that the focused particles scatter before they decay, reducing the meson interactions.

It is very important to reduce the interaction inside the pipe because this could contaminate the neutrino beam. It is expected that after the decay pipe, the beam is formed of neutrinos, muons, electrons, and mesons. In figure 3.7 it is shows a scheme with a frontal view of the decay pipe and the concrete shield that covers around the pipe to reduce the interaction of particles coming from other sources.

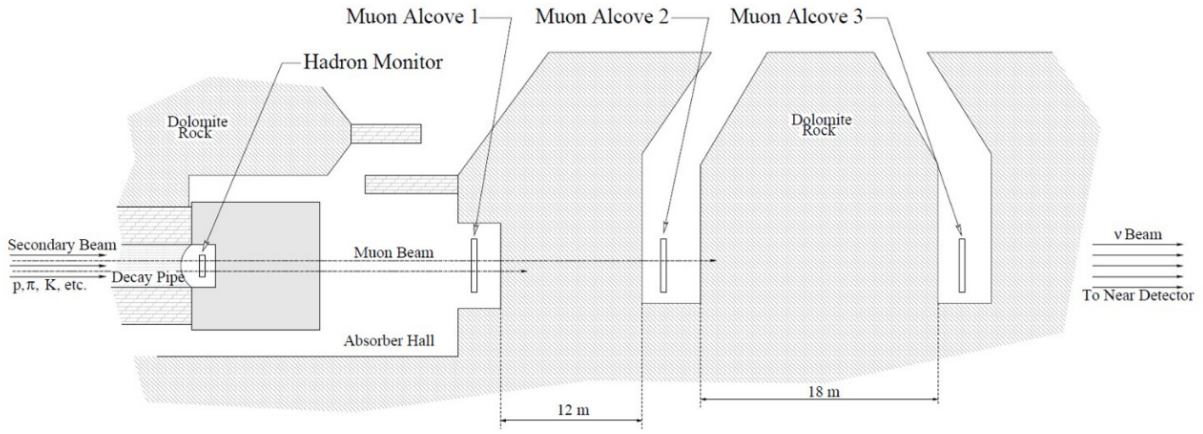

Figure 3.8. Scheme of the complete monitor system of the NuMI beam-line that includes the Hadronic Monitor, and three Muons Monitors. Also the Absorber Hall is indicated in this scheme. Figure from the reference [11].

3.4 Absorber and monitors of hadrons and muons

When the particles leave the decay pipe, they travel to the *Hadron Monitor*, see figure 3.8, its function is measure the hadron flux, with this information we can estimate the number of protons on the beam. Furthermore, the number of neutrinos can be estimated using this information.

Downstream to the hadron monitor, the next component in the NuMI is the *Absorber* which is used to reduce the number of muon particles with high energy, this absorbs $\sim 40\%$ of beam power. This is very helpful to reduce the background noise in the detectors that are on-axis of the beam-line. In figure 3.9 the elements of the absorber are presented. It is elaborated with a central core made of aluminum blocks, followed by steel blocks. Both elements of the absorber core are surrounded by 88 Duratek steel blocks that are used as radiation shielding. Because the second function of the absorber is to reduce the contamination generated by the radiation, to keep the water of the underground free of radiation produced by the NuMI beam.

In addition to the hadron monitor, downstream of the absorber are located three *Muon monitors* which are used to measure the spatial distributions of the muon beam, and measure the different energy ranges of muons. To do the measurements, the muon monitors are composed of three identical 9 x 9 arrays of ionization chambers, figure 3.10 shows the

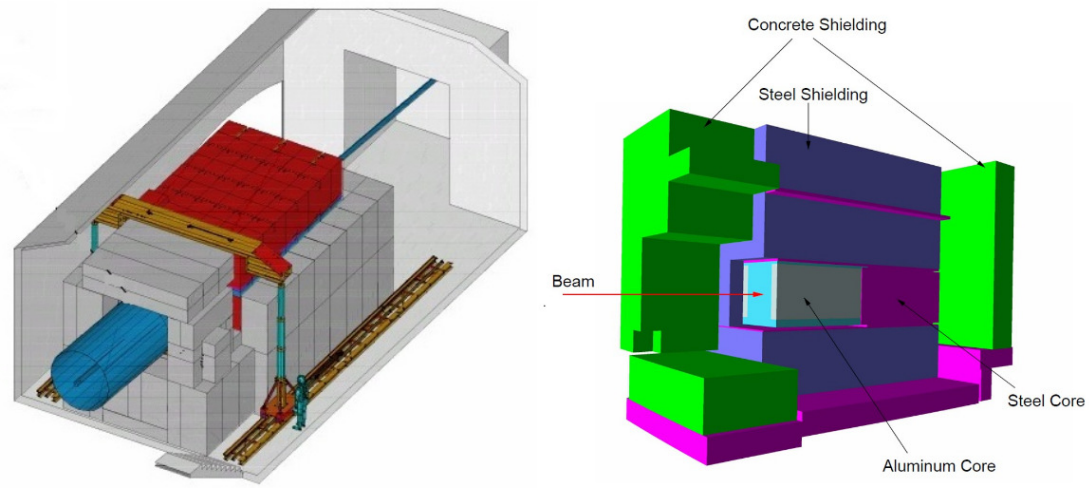

Figure 3.9. Diagram of the Absorber representing each layer of shield with different colors to be more illustrative. Figure from the reference [10].

array of the muon monitor, this arrangement is the same for the three muon monitors used. The monitors are designed to resist high levels of radiation, as they are immersed in the flow of the beam.

Between the Underground MINOS Hall and the last Muon monitor the particles travel through 240 m of solid rock, that is used as a natural muon shield. The Underground MINOS Hall is the cave where the MINERνA, MINOS and NOνA detectors are located. As explained above, MINERνA and MINOS are on-axis of NuMI beam-line, more about these detectors is discussed in chapter 4.

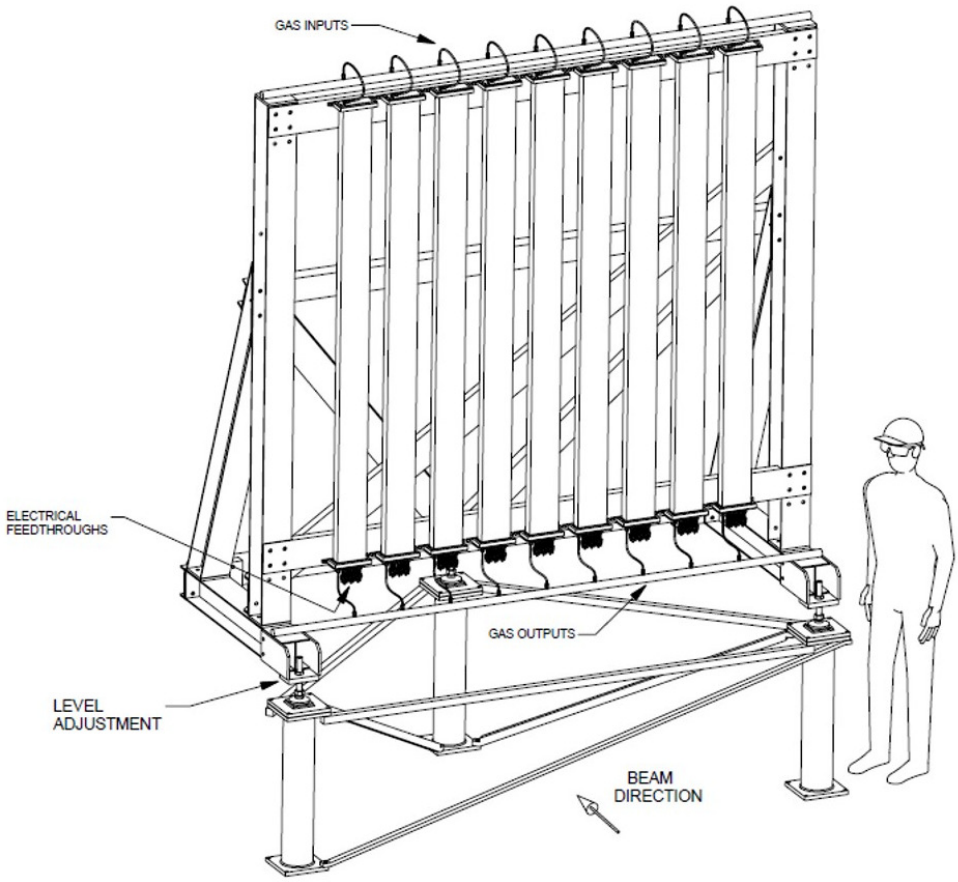

Figure 3.10. Diagram of the Muon monitor used in the NuMI beam-line to measure the spacial distribution of the muons and their energy. The figure shows only one of the three muon monitors, all are identical. Figure from the reference [11].

Chapter 4. MINERνA

With the aim of following the line of research about the neutrino oscillation, the Main Injector Experiment ν - A (MINERνA) was developed with the goal to achieve the most precise measurement of the neutrino cross sections in five nuclei(carbon, lead, iron, water and helium). In addition to achieve dozens of measurements, the design of this detector allows us to identify the neutrino interactions on a variety of channels to get a better reconstruction of events. These characteristics of the experiment are helpful for future experiments of neutrino oscillation, because new techniques can be tested to probe models that will be used for future experiments.

4.1 Types of Charged-Current interactions at MINERνA

In the neutrino detectors, to measure the neutrino it is necessary that an interaction with the matter of the detector take place, because the neutrinos are observed indirectly through the interactions occurring between neutrinos and the matter. For this reason the materials used in these detectors usually have high densities. As mentioned before, neutrinos are weakly-interacting particles, generally they penetrate the nucleus and scatter off of a single nucleon.

The MINERνA experiment is focused in analyzing the charged-current interactions, given that for this interaction the production of a muon is induced if a muon neutrino (ν_μ) interacted with a nucleus, or an electron is observed in the final state if the interaction occurred by an electron neutrino and the nucleus or nucleon. These final states make an easier way to identify the flavor between these two neutrinos. Furthermore, the process to identify the type of particle in the detector is conveniently simple, measuring the charge deposited by the particles produced in the interaction neutrino-nucleus. To identify the muons in the detector, they tend to travel in a long straight line. In the case of identifying an electron, they tend to initiate an electromagnetic shower with a shape similar to a cone.

The three types of charged-current (CC) interaction observed in the MINERνA experiment will be discussed below. Remembering that the charged-current interactions occur

with weak interaction charges mediated by the $W^{\pm}$ boson.

4.1.1 Charged-Current Quasielastic Scattering (CCQE)

This kind of interaction is defined by the reaction $\nu_l + N \rightarrow l + N'$. Where ν_l refers to one of the neutrino flavors $l \in \{e, \mu, \tau\}$, and N refer to the nucleon before the interaction, and N' is after the interaction. In this interaction the scattering is quasielastic, because the nucleon that interacts is bound in the nucleus. This is an important interaction for the experiment, because it dominates the region of low energies in the spectrum of neutrino energy. This region is very important to analyze the events, because dozens of experiments work in this region of energy, and future experiments will operate in this region too. In figure 4.1 the Feynman diagram for the charged-current quasielastic interaction (red box) and the neutrino energy distribution for this interaction are shown.

4.1.2 Resonance

This interaction is a single pion production that can be identified by the reaction $\nu_l + N \rightarrow l + N' + \pi$. The principal characteristic of this reaction is the production of a pion (π). In the model of this interaction, it is considered that the neutrino interacting with the nucleon begins a baryon resonance, which quickly decays into a pion and a nucleon. There is an important situation to highlight when analyzing this type of interaction, in the MINERνA detector is only possible to measure the single pion production in the final state. But in the model we attribute the resonance production to observable final state, this for the case of single pion production.

The problem with the situation of not being able to observe the resonance process in the detector, is that multiple interactions occur in the detector with the possibility to find the same particles in the final state but generated by different interactions. This causes a variety of theoretical models to be compared with the neutrino interaction channels in the simulation until the best agreement is found between the simulation and data to describe the interaction occurred in the detector; as expected, this analysis of the models in the experiment can require some care. In figure 4.1 with the blue box the Feynman diagram for the resonance, single pion production, is shown.

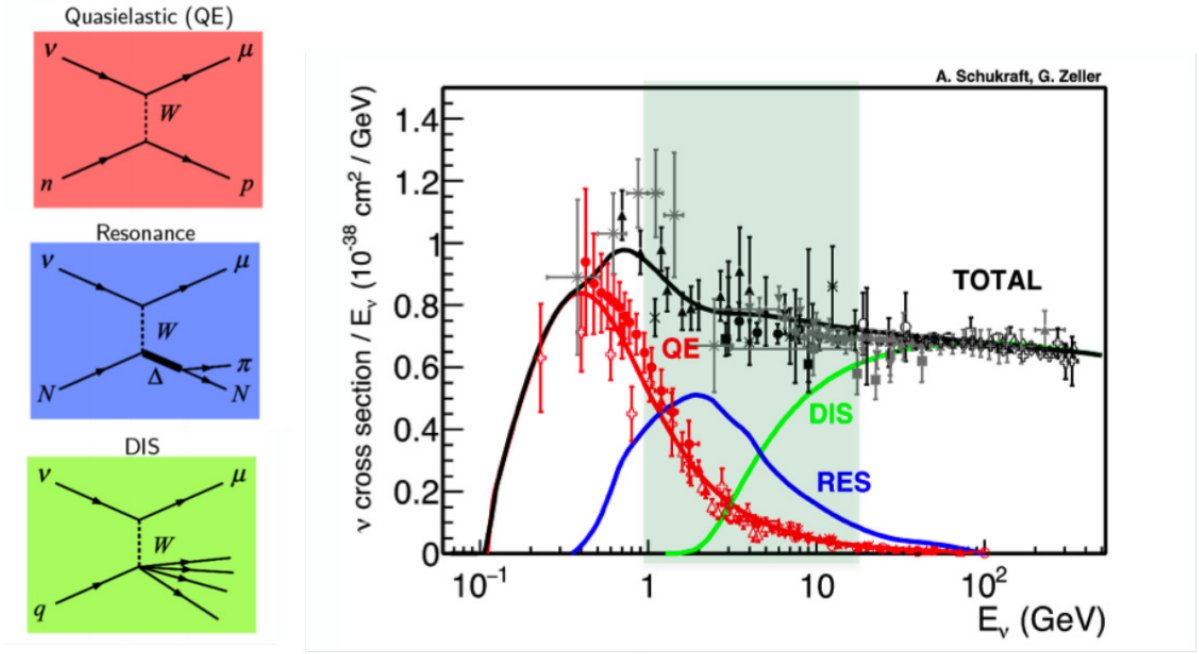

Figure 4.1. In the left side, diagrams of the charged-current quasielastic, resonance, and deep inelastic scattering interactions are shown. In the right side, the distribution of the cross section of the corresponding interaction are presented. The solid lines are predictions of the events obtained with the NUANCE neutrino event generator [8], and circa 2013 [16]. The green vertical band is the region of energy in which MINERνA works. Figure from the reference [27].

4.1.3 Deep Inelastic Scattering (DIS)

The last interaction to mention for the charged-current interactions in the MINERνA experiment is the deep inelastic scattering (DIS). The model for this interaction begins with the neutrino scattering off of a quark inside the nucleon, causing the nucleon to break apart. The strong nuclear force prevents the quark from existing outside of the nucleon. In this interaction the final state includes an hadronic shower, known as "hadronization". The reaction can be identified by the following $\nu_l + N \rightarrow l + N' + X$, for this reaction, X represents an arbitrary number of hadrons produced. In the figure 4.1, the green box shows the Feynman diagram for the deep inelastic scattering (DIS) interaction.

Due to the difficult process to identify every hadron produced in the DIS interaction,

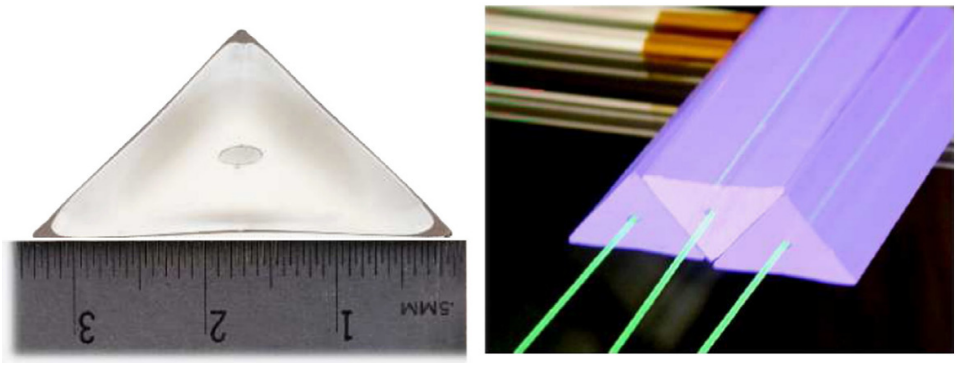

Figure 4.2. MINERνA scintillator strips used in the planes to track the particles. The triangular form is to minimize the uncertainty of the spatial position. The strips are stack to conform a scintillator plane, the right side. Figure from the reference [21].

this interaction is classified as *inclusive* reconstruction, this means that all the hadrons are reconstructed and added as one group of particles for this final state. Because it is very difficult to identify each one of the hadrons produced. In comparison with the two interactions mentioned before, they are considered *exclusive* reconstructions, because all the particles can be identified in the final state.

4.2 MINERνA detector

The MINERνA detector is made of hexagonal modules, one behind the other, with a frame to support all the modules along the axis of the neutrino beam-line. The thickness of each module is of 17 mm, and the distance point-to-point in the hexagonal is of 2.5 m. Each hexagonal module is conformed of 127 triangular scintillator strips, see figure 4.2 to observe the form of the scintillator strips used. The strips are triangular in form to have a precise tracking of the particles.

Three different arrangements of the strips are used, that alternate the orientation of the strip with a rotation of 60° with respect to the vertical position. Implementing these different orientations of the strips, the uncertainty of the spatial position in the measurement is reduced, see figure 4.3 that shows the arrangement of the strips, these are known as U, V and X orientations. Also, an example of a particle crossing the modules with the strips is represented with a red line.

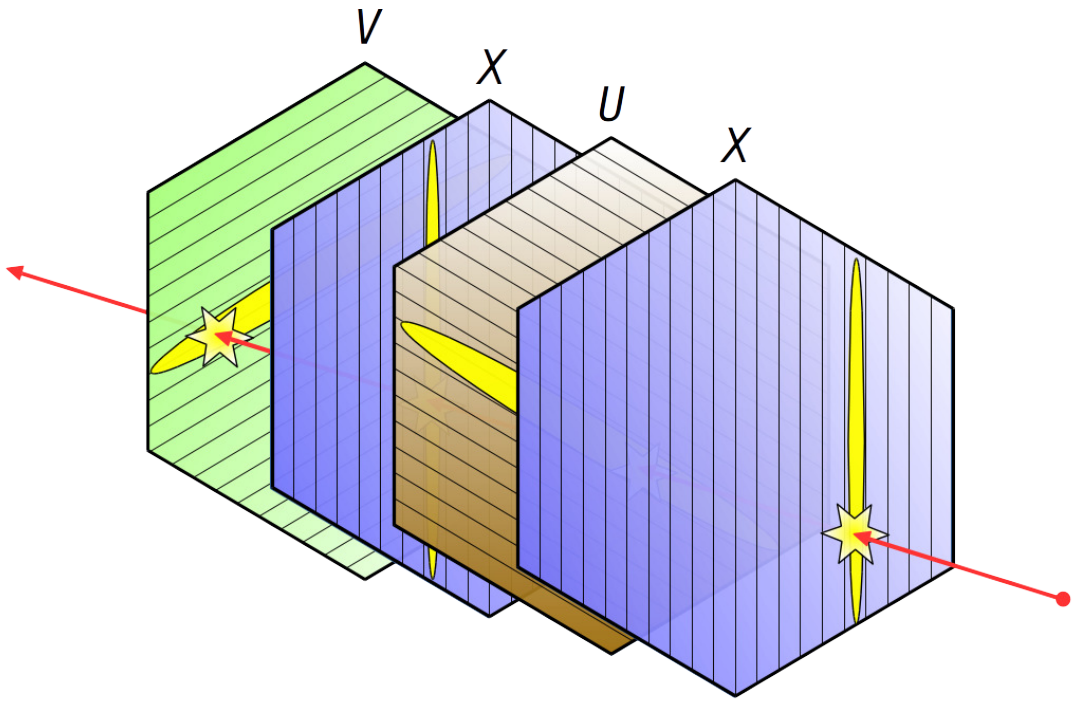

Figure 4.3. Scintillator planes of the MINERνA experiment, three different arrangement are used: X, U, and V. The X configuration is intercalated between the other two positions. The yellow region represents the strip with the energy deposited by the trajectory of a particle. Figure from the MINERνA Collaboration [28].

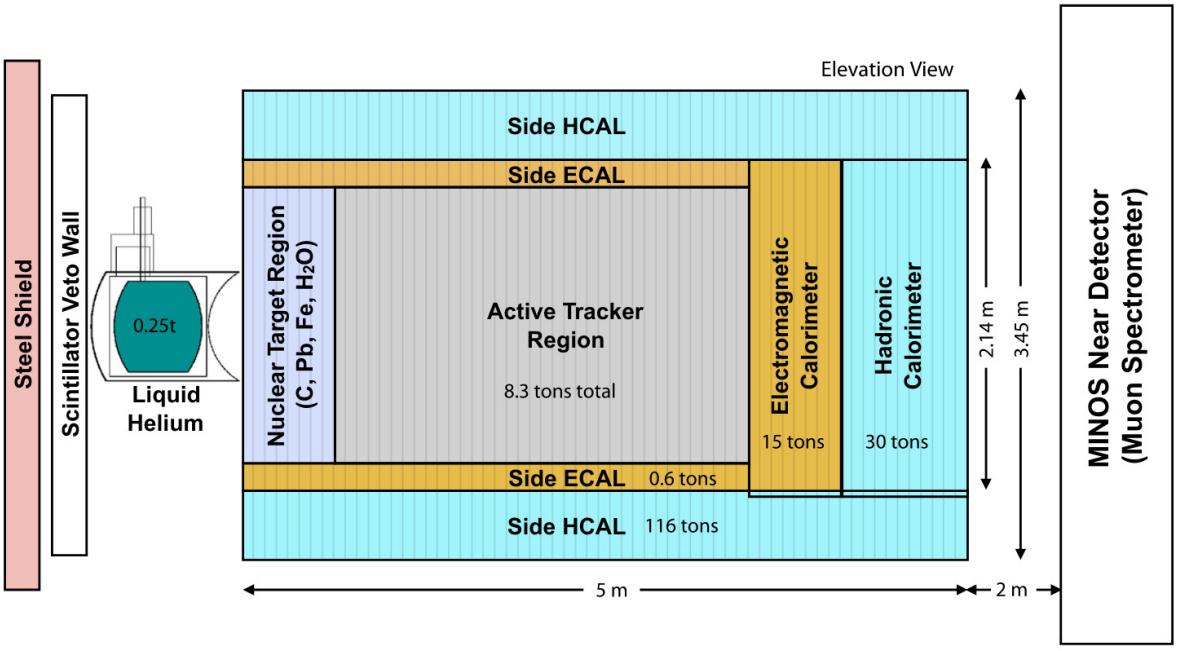

Figure 4.4. Schematic view of the MINERνA detector. Side view of the complete detector to identify all the sections: nuclear target, active tracker, surrounding calorimeter regions, and veto wall. Figure from the reference [21].

To measure the passage of a particle in the detector, the particle must have an electric charge. When this particle passes through the plastic scintillator it ionizes the atoms, and free electrons are generated. In the next step protons are produced by the recombination of the electrons with atoms. The protons produced travel through the optical fibers that are placed in the center of each scintillator strip; the optical fibers are connected to a PMT (Photomultiplier tube) that transforms the light received into electric pulses. According to the electric pulses generated the energy deposited by the particle is measured.

The parts of the detector are shown in the figure 4.4, this is an elevation view with the name of each of the parts that conform the detector, the regions of the detector are divided in the following sections: The Steel Shield, Veto Wall, Nuclear target Region, Tracker Region, Electromagnetic Calorimeter, and the Hadronic Calorimeter. Furthermore, if the detector is observed with a front view perspective, see figure 4.5, we can identify that it is separated by two regions: Inner detector (ID) and Outer Detector (OD).

The **Inner detector** region includes the Nuclear target region, the active tracker region, and the downstream calorimeters (electromagnetic and hadronic). Otherwise, the

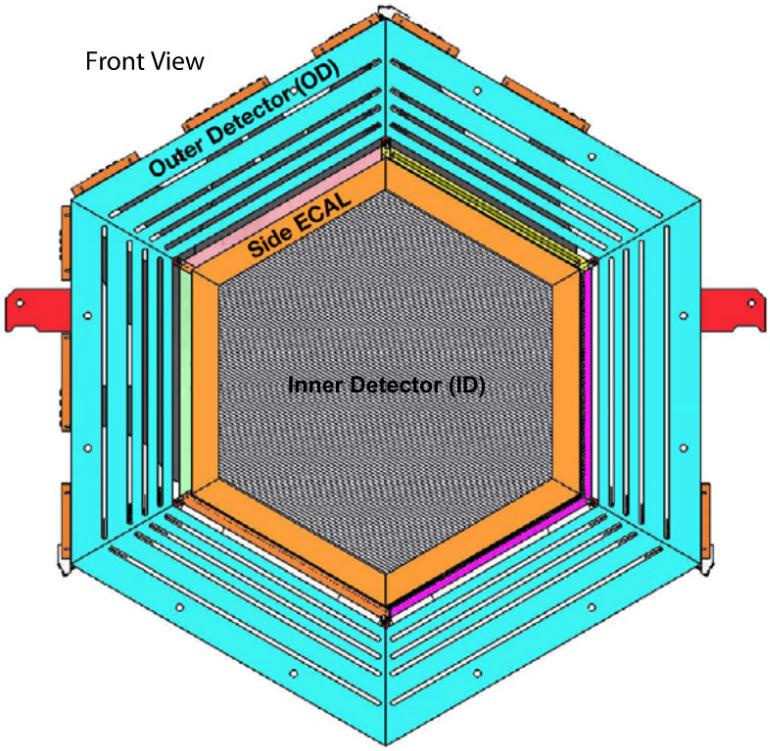

Figure 4.5. Schematic view of the MINERνA detector. Front view of the detector to identify the inner and outer sections of the detector. Figure from the reference [21].

Outer detector region is formed by the side electromagnetic calorimeter and the side hadronic calorimeter. These are used to stop and collect the energy of the particles that leave the tracker region.

4.2.1 Steel Shield and Veto Wall

The first element of the detector, taking into account the input direction of the neutrino beam, is a **steel shield**, this is used to reduce the number of muon particles that could not be stopped by the rock upstream of the detector.

After the steel shield, the next part of the detector is the **Scintillator Veto Wall**, the main function of this is to identify the muon particles that could not be stopped by the rock and the steel shield, these muons are known as "rock muons". Identifying these muons is very important, because they will be measured in MINERνA and MINOS, but they will not be produced by the interaction of a neutrino in the detector, then the rock muons measured will be added to the background noise of the detector. The Veto Wall has two steel plates and 2 planes of scintillators intercalated.

4.2.2 Nuclear Target Region

The next section after the Veto Wall according to the direction of the beam-line is an one cubic meter container of liquid helium, this is the first nuclear target in the detector. Behind the liquid helium is located the **Nuclear Target Region** in which the four layers of the nuclear targets are placed, the targets are made of carbon, lead, iron, and water. In figure 4.6 the distribution of the four nuclear targets is shown. Each layer of the target is intercalated by four modules of scintillator, where each module is formed by two planes of scintillator. The modules can be of two types, UX module and UV module, depending on the combination of the arrangement of the planes used.

The intercalated configuration of the nuclear targets and the scintillator modules is to do a better identification of the interactions occurring between neutrinos and each target. The distribution of the different materials in the layers has the goal to obtain a similar density of the materials for all the regions in a frontal view of the detector when neutrinos

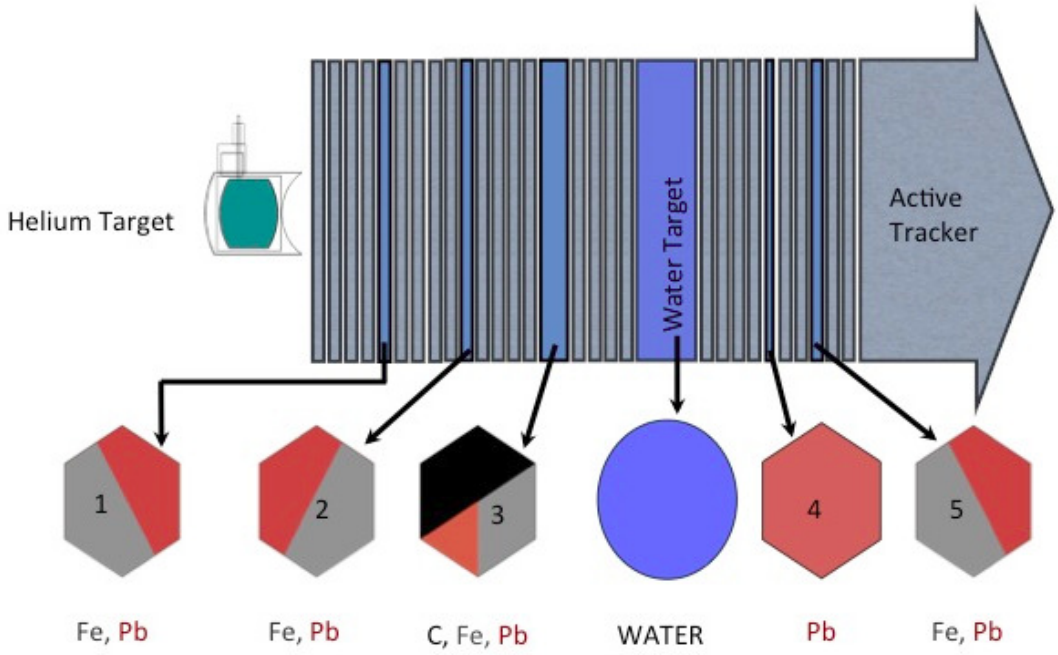

Figure 4.6. Schematic side view of the nuclear target region on the MINERνA detector. The distribution of the materials in each layer of target is shown. Figure from the reference [23].

are crossing the nuclear target region.

4.2.3 Active Tracker Region

The tracker region contains 62 modules, as mentioned above each module is constructed of two scintillator planes. In addition to this planes, the tracker region is surrounded by a lead collar, with a 15 mm wide and 2 mm thick. This collar is used by the side electromagnetic calorimeter. Furthermore, in the tracker region interaction studies are carried out, the number of neutrino interactions are reduced in comparison with the events in the nuclear target region. The scintillator strips are comprised of 87.6 % carbon, 7.4 % hydrogen, 3.2 % oxygen and 1.8 % miscellaneous; these are mass percentages [21].

4.2.4 Electromagnetic calorimeter (ECAL)

The electromagnetic calorimeter is located downstream of the tracker region and it is used to measure the energy of protons and electrons. This consists of lead sheets of 2 mm of thickness, each sheet is covering the entire surface of each scintillator plane used. In total the ECAL implements 10 modules of scintillator, recall that each module is formed by two planes of plastic scintillator.

For the side electromagnetic calorimeter that surrounds the nuclear target and the active tracker regions, the construction is the same as that of the ECAL located behind the tracker region.

4.2.5 Hadronic calorimeter (HCAL)

The hadronic calorimeter is located downstream of the electromagnetic calorimeter, unlike the ECAL is composed of 20 modules, but for this each module consists of a single scintillator plane. Between each scintillator plane a steel absorber sheet with 2.54 cm of thickness is located, obtaining a total thickness of 50 cm. For the side hadronic calorimeter the number of scintillator planes is reduced to only five, each one with 2.5 cm of thickness, and the thickness of the steel sheets changes to 8.64 cm each one. Getting a total thickness of 55.9 cm.

In figure 4.7 the visualization of a neutrino interaction in the MINERνA detector is shown. This kind of event display is obtained to process the signals of each channel and test the different models to do the best reconstruction of the event. According to the color of each triangle the magnitude of the energy deposited in each scintillator strip is represented.

4.3 MINOS detector

The Main Injector Neutrino Oscillation Search (MINOS) [13] was constructed to measure neutrino oscillations of ν_μ. For this, two detectors were constructed, a near detector located at Fermilab and a far detector located to 735 km away at northern Minnesota. The near detector is located 2.1 m downstream from the MINERνA detector, and it is used as

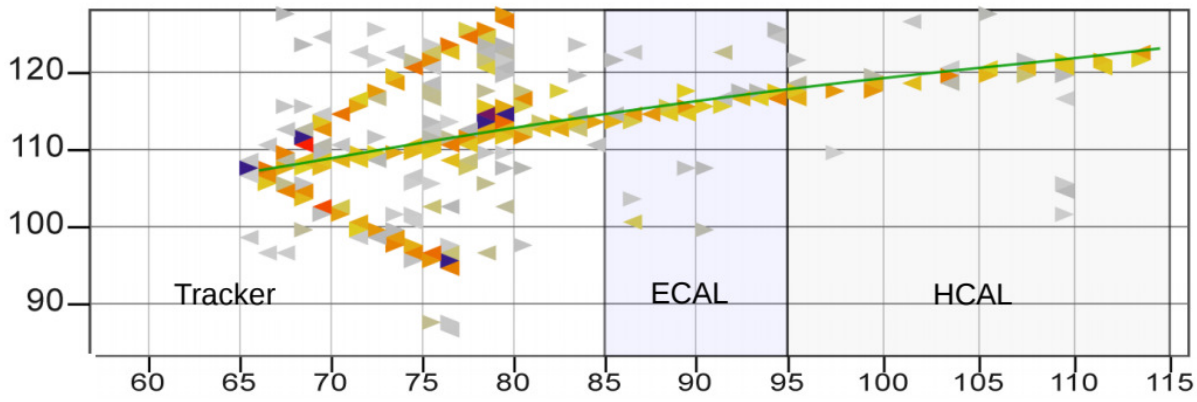

Figure 4.7. Event display of a neutrino interaction in the MINERνA detector. The spectrum of color represent the energy deposited by each scintillator strip. The green line is the muon reconstructed trajectory. Figure from the reference [17].

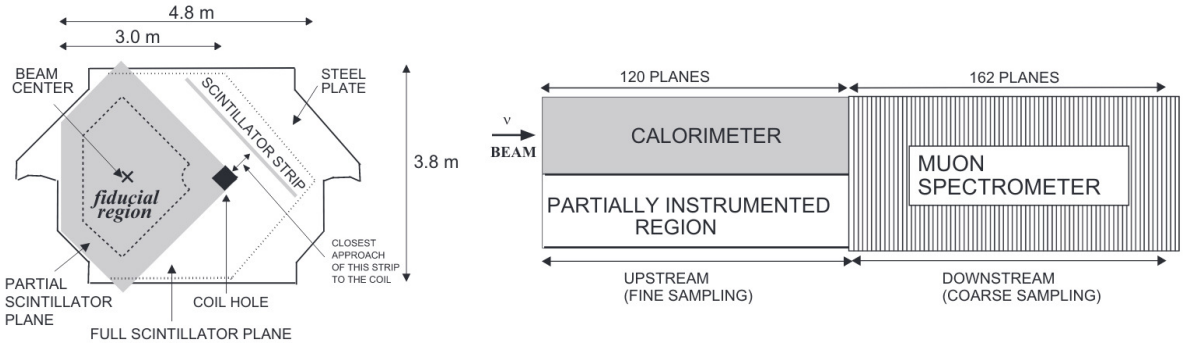

Figure 4.8. Scheme of the MINOS near detector located to 2.1 m downstream of the MINERνA detector. This detector is used as spectrometer of muons to validate the events measured in MINERνA. Figure from the reference [21].

a muon spectrometer of the muons created by the interactions of neutrinos at MINERνA. These muons travel through the MINERνA detector and leave it, coming to the MINOS detector, where they are reconstructed using two methods of detection that will be discussed in chapter 8.

A diagram of the MINOS detector is shown in the figure 4.8, this is constructed of a stack of 282 steel plates, each with a thickness of 1 in. Furthermore, the detector is immersed in a magnetic field of 1.3 T, this is very useful to reconstruct the muons and identify their charge.

After knowing and understanding the components of the MINERνA detector and how

the events are measured, in chapter 5 a distribution of events of the experiment is shown. Also, the discrepancy observed between the data measured and the simulation of events is discussed.

Chapter 5. Wiggle

A brief description of the discrepancy observed between data and simulation in the neutrino flux inside of the MINERvA detector is discussed in this section.

When the NuMI beam-line was set to the medium energy configuration for the neutrino flux, the first studies of the neutrino flux in the MINERvA detector showed a disagreement between data and the simulation of events, which exceeded the region of the uncertainties, this variation was named wiggle, see figures 5.1.

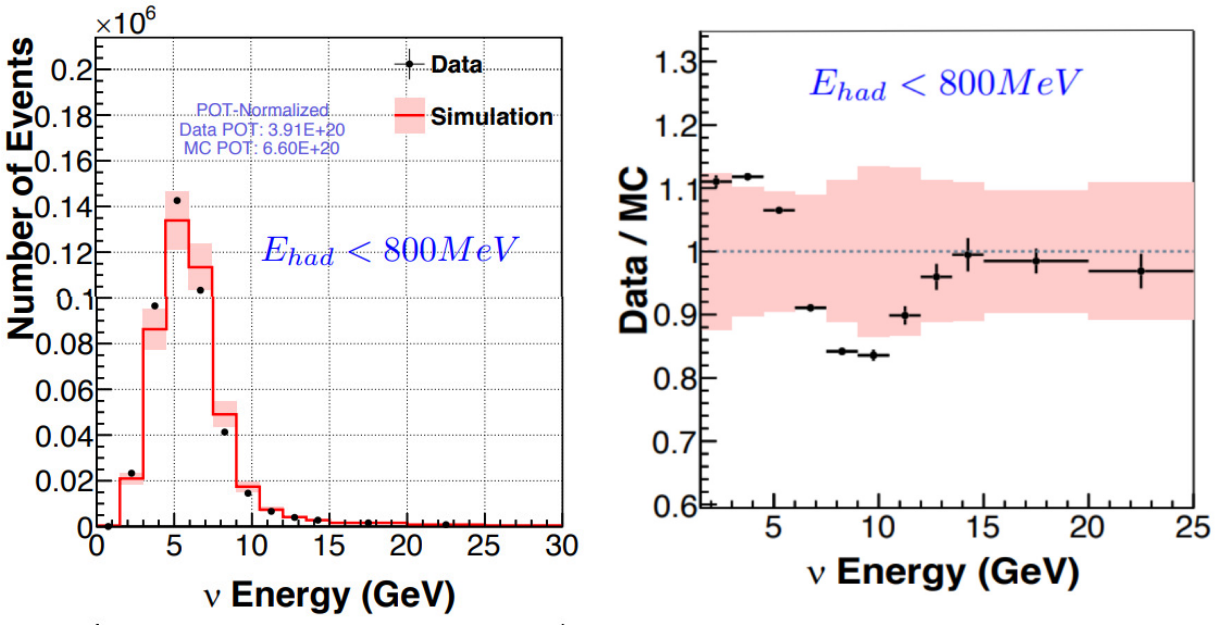

Figure 5.1. Left: Neutrino flux at MINERνA with low-ν cut, and systematic uncertainties in the simulation. Right: Ratio between data and simulation of neutrino flux at MINERνA, the pink band corresponds to the systematic uncertainties, and the error bands to statistical uncertainties. Images taken from [1].

The idea that there might be a malfunction in the hardware of the detector was discarded because the discrepancy was observed on all the channels of the detector. The first studies about the wiggle showed that it was observed for the Inclusive sample, and it has around 20% of variation between data and simulation in the peak region of the neutrino

flux; this corresponds to around 5 GeV [17].

The next work carried out for the wiggle analysis consisted of implementing the low-ν method to get a different sample. The low-ν sample is when a cut is applied to the recoil energy and only the low recoil energy events are considered for the sample, in the next chapter we will discuss in more detail the definition of low-ν and why it is implemented. From the first result of using the low-ν sample, the collaboration identified that the discrepancy between data and simulation was around 10% for the rising edge region and 10% for the falling edge region.

Then, as it was observed that for the inclusive and low-ν samples the wiggle shape was still present for the neutrino energy distribution, the idea of cross-section mismodeling was discarded as a source of the disagreement between data and simulation, and the next ideas were that the wiggle might be coming from a wrong calibration on the modeling on the focusing parameters, or a possible error on the tracking reconstruction of the muons in the MINOS detector. These proposals as sources of the discrepancy resulted in two fits options to apply to the samples and try to remove the wiggle shape. These fits will be mentioned in chapter 8.

Chapter 6. Low-ν method

The explanation of the low-ν method, the implementation of it on the reconstruction of neutrino flux, and the cuts selected to apply to all the neutrino energy spectrum at the MINERνA experiment due to this method are discussed in this chapter.

6.1 Charged Current Neutrino-Nucleus interaction

The low-ν method is a technique very useful to model the shape of the neutrino flux using the neutrino events measured at the MINERνA detector. The pioneers of this method were the CCFR[31] and NuTeV[24] collaborations, and this was implemented by MINOS[25], and MINERvA[22]. The Feynman diagram of the Charged Current neutrino nucleus interaction is needed to explain the definition of the low-ν method implement in this study, see figure 6.1.

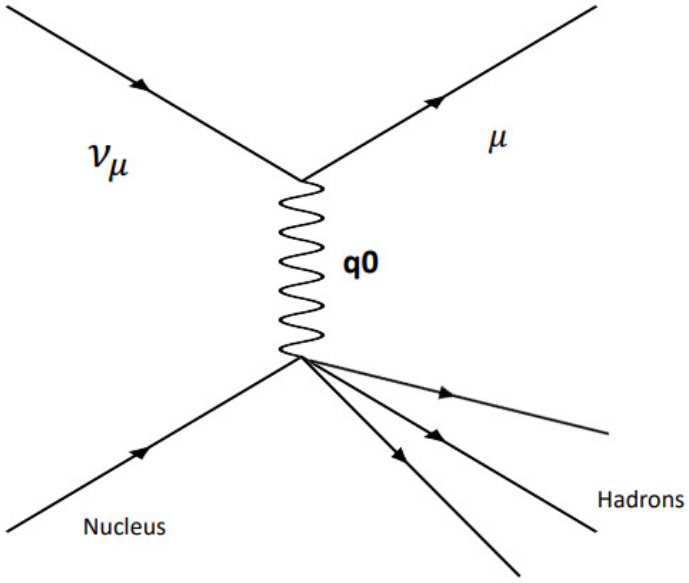

Figure 6.1. Feynman diagram of the Charged Current neutrino nucleus interaction.ν_μ is the muon neutrino incoming, μ is the muon produced, and q_0 is the energy transferred to the hadronic system.

Where the neutrino energy, E_ν, that corresponds to the energy of the incoming neutrino, which is indirectly measured by the equation:

$$E_\nu = E_\mu + q_0 \,. \tag{6.1}$$

In the previous equation, E_μ represents the energy of the muon that corresponds to the final state lepton in the interaction model, and q_0 is the recoil energy transferred to the hadronic system. To understand the low-ν technique, it is necessary to mention the definition of ν for a charged-current neutrino interaction, that is the energy transfered to the recoil system, and it is obtained subtracting from the incoming neutrino energy the energy of the lepton in his final state (muon in this case):

$$\nu \equiv E_\nu - E_\mu \,. \tag{6.2}$$

Then, low-ν technique is considered the approximation for very low recoil energy in the charged current cross section, because for this case the cross section of the interaction is constant as a function of the neutrino energy. With this a direct measurement of the shape of the flux can be performed.

6.2 Charged current scattering cross section

To observe and understand the changes in the cross section of neutrino interaction to use the low-ν technique the charged current scattering cross section will be expressed as a function of incoming neutrino energy (E_ν), the energy transfer to the recoil system (ν), and the Bjorken scaling variable (x), the equation is given by [17]

$$\frac{d\sigma}{d\nu} = \frac{G_F^2 M}{\pi} \int_0^1 \left(F_2 - \frac{\nu}{E_\nu}[F_2 + xF_3] + \frac{\nu}{2E_\nu^2}\left[\frac{Mx(1-R_L)}{1+R_L}F_2\right] + \frac{\nu^2}{2E_\nu^2}\left[\frac{F_2}{1+R_L} + xF_3\right]\right) dx\,, \tag{6.3}$$

where G_F is the Fermi coupling constant, M is the mass of the struck nucleon, F_2 and xF_3 are structure functions that contain the information of the nucleon, and R_L is the ratio of the structure functions defined by $R_L \equiv \frac{F_2}{2xF_1}$.

In the cross section a definition of the limit of very small recoil energy is implemented, $\nu \ll \nu_0$, for some value of $\nu \ll E_\nu$. Where ν_0 is the limit value to restrict the recoil energy. From this limit, the terms proportional to $\frac{\nu}{E_\nu}$, and the next terms of high order, are very small, there for getting a cross section equation approximately constant for all neutrino energies, E_ν. This approximation is not perfectly constant, because for some higher order terms the limit of $\nu \ll E_\nu$ can not perfectly be realized; also, the small Q^2 dependence of the structure functions due to the Bjorken scaling violation.

6.3 Low-ν in the flux fit investigation

For the analyses presented in this thesis, the value of ν_0 was chosen equal to the previous low-ν investigation where the three fits to use in this analysis were developed, that will be explained in chapter(8). The value number for ν_0 is **800 MeV**. This means that to implement the low-ν technique, after the events is validated, we apply a cut to the entries on the data and simulation, if the recoil energy variable is less or equal to 800 MeV then this event is saved for the analysis, with this cut we guarantee that the low-ν method is

E_ν [GeV]	ν_0 cut [GeV]
< 3	0.3
< 7	0.5
< 12	1.0
< 25	2.0

Tabla 6.1: Table with the step cut implemented in some low-nu MINERνA analyzes (a flat cut is used in this thesis). If the value of the neutrino energy, E_ν is less than one of the values of the first column, then the numerical value of the cut applied to the recoil energy variable is the corresponding to the second column.

implemented and the shape of the neutrino energy distribution is comparable with the shape of the flux distribution.

There are other analyzes that implement the low-ν technique in the MINERνA experiment, for these the low-ν cut applied depends of the energy of the neutrino incoming, see table 6.1, if E_ν increases, then the value of ν_0 increases for the cut. This step cut generates a better approximation to the cross section model, but for the analysis shown in this thesis it is not necessary. This is because for the region of interest of the neutrino energy to be analyzed the contribution of the flat cut for all the spectrum does not generate a great difference against the step cut. Furthermore, the weight functions used to fix the neutrino energy distribution were elaborated by applying the flat cut to the recoil energy.

Before the discussion of the different fits implemented, the next topic of the investigation to analyze is the systematic uncertainties, see chapter (7).

Chapter 7. Systematic uncertainties

Conducting a detailed investigation of the systematic uncertainties is very important for the study of the events measured at the MINERνA detector. Doing a deep analysis of the sources of uncertainty, we get a better result of the models to identify the particles, which allows a better study of the type of interaction that occurred for each event into the detector.

The collaboration works to reduce these uncertainties with the goal to get the best performance of the models to apply to the simulation of events and then compare with data measured to understand the phenomenon observed in the data. Furthermore these studies to reduce the uncertainties could be used in future investigations.

7.1 Central Value and the universes

To understand how we obtain the systematic uncertainties, the origin of the central value must first be understood. To simulate a physic interaction on MINERνA detector a collection of the best values for many physical parameters were chosen to be implemented in the simulation, and every value of these parameters affect our measurements. These values were chosen trying to make the reconstruction as similar as possible to the real conditions in the detector. Furthermore, each collaboration analysis group implemented a particular physics model to the simulation according to the investigation that they are doing.

Sometimes these models are not the best reflection of what happens in the physical systems, but those are used because maybe it is the best way to perform the final measurement; then after applying the model, we can compare the results of the simulation with the data measured on the detector and evaluate this model of theory with the real experiment. After choosing the values of the physical parameters and the physics model, we can define our central value universe obtained from the chosen conditions.

Assuming that the measurement was performed and the central value was obtained for

Parameter	Nominal Value	1 σ shift from Nominal Value
Beam Position (X)	0 mm	1 mm
Beam Position (Y)	0 mm	1 mm
Beam Spot Size	1.5 mm	0.3 mm
Horn Water Layer	1.0 mm	0.5 mm
Horn Current	200 kA	1 kA
Horn 1 Position (X)	0 mm	1 mm
Horn 1 Position (Y)	0 mm	1 mm
Horn 1 Position (Z)	30 mm	2 mm
Horn 2 Position (X)	0 mm	1 mm
Horn 2 Position (Y)	0 mm	1 mm
Target Position (X)	0 mm	1 mm
Target Position (Y)	0 mm	1 mm
Target Position (Z)	-1433 mm	1 mm
POT Counting	0	0.02% of Total POT
Baffle Scraping	0	0.25% of POT

Tabla 7.1: Table with the Beam Focusing Parameters that are considered in the MINERνA analysis for the run configuration of the beam-line by Medium Energy. This information was consulted from the low-ν flux investigation [3].

the particular conditions of each parameter, the next stage to analyze individual sources of uncertainty is to shift the value of one of the physical parameters, then the final value of the measure will change. For each shift to parameters, we got a new measure that we associate to a new universe. Then each universe corresponds to one specific variation of a particular parameter.

7.2 Source of the uncertainties

In the MINERνA experiment the contribution of the systematic effects due to various parameters were simulated and each result is a different universe. For the models with only one parameter, the variation to this parameter corresponds to two alternatives from the central value, those are $\pm 1\sigma$. Then, the average shift gives the uncertainty on the sample of the simulation. In table 7.1 the nominal value and this value with 1 σ shift of the beam parameters for MINERνA are shown.

In the particular case of the systematic uncertainties from the flux and reconstruction

that have multiple parameters and those parameters are correlated, the technique used to get the value of the uncertainties is the multi universe approach. To apply this technique, random shifts were made to the parameters based on a probability distribution that consider the correlation between the parameters. Beside that each shift generates a universe, the average shift between each universe and the central value gives the systematic uncertainty for many parameters.

The systematic uncertainties implemented to this analysis are four and correspond to the reconstruction of the muon particle, focusing parameters, and some corrections applied to the simulation of the events in the GENIE software. The systematic uncertainties used are listed below, accompanied by a short description of each one. For more details of the development of each one, you are invited to review the publications of the MINERνA collaboration shown in the references attached to each uncertainty in the list below.

- Neutrino flux uncertainties (*Flux*), the source of this uncertainty is attributed to the models of hadron production in the target, and other materials inmersed in the beamline of NuMI; and furthermore, some contributions by the simulation of the beam and the focusing system [20].
- GENIE interaction model uncertainties (*Genie_interactionModel*), this is attributed to aspects of the initial neutrino-nucleon interaction probabilities modeled and simulated by GENIE software [7] [6].
- MINERνA modifications to GENIE (*Genie_FSI*), this uncertainty corresponds to the final state interactions (FSI) in the model of GENIE, in addition to some modifications that were made to the GENIE software to get a better modeling of the interactions for the MINERνA experiment [9] .
- Uncertainties associated with the reconstruction of the muon tracks in MINERνA detector, and MINOS detector (*EmuRangeCurve*). Recalling that for MINOS two techniques of reconstruction of tracks by curvature, and by range are used [18] .

A summary of the fractional uncertainties with the four sources mentioned before as a function of the neutrino energy with the low-nu cut is shown in figure 7.1. For this figure the principal source of contribution is the GENIE interaction model uncertainties.

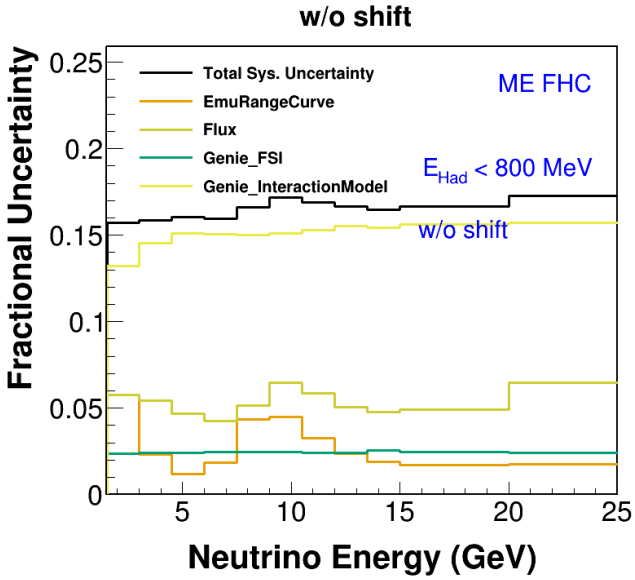

Figure 7.1. Summary of the fractional systematics uncertainties, on the neutrino energy distribution for low-ν events for the simulation sample with all the playlist set of the MINERνA experiment of the medium energy era for neutrino beam.

7.3 Systematic error band in the ratio of the data and simulation

For the analysis of the different fits in this thesis is very important to add the contribution of the systematic errors to the plots of the events to identify if the discrepancy observed between data and simulation is covered by the systematic uncertainties. Because if this is covered, then we can find the source of the disagreement.

The neutrino energy distribution plots for data and simulation of the low-ν events with the systematic uncertainties are shown in the figure 7.2. For these plots two different normalizations were applied. One of the normalizations corresponds to absolute normalization, in the plots this normalization is identified with the label "POT Normalized", and it means that the simulation distribution was scaled by the factor obtain by the number of Protons on Target of the data divided by the number of Protons on Target of the simulation ($\frac{Data\_POT}{MC\_POT}$).The second normalization of the simulation events corresponds to area normalization, in this case the area under the curve of the distribution is measured of the data and the simulation distributions, and the simulation distribution is scaled by

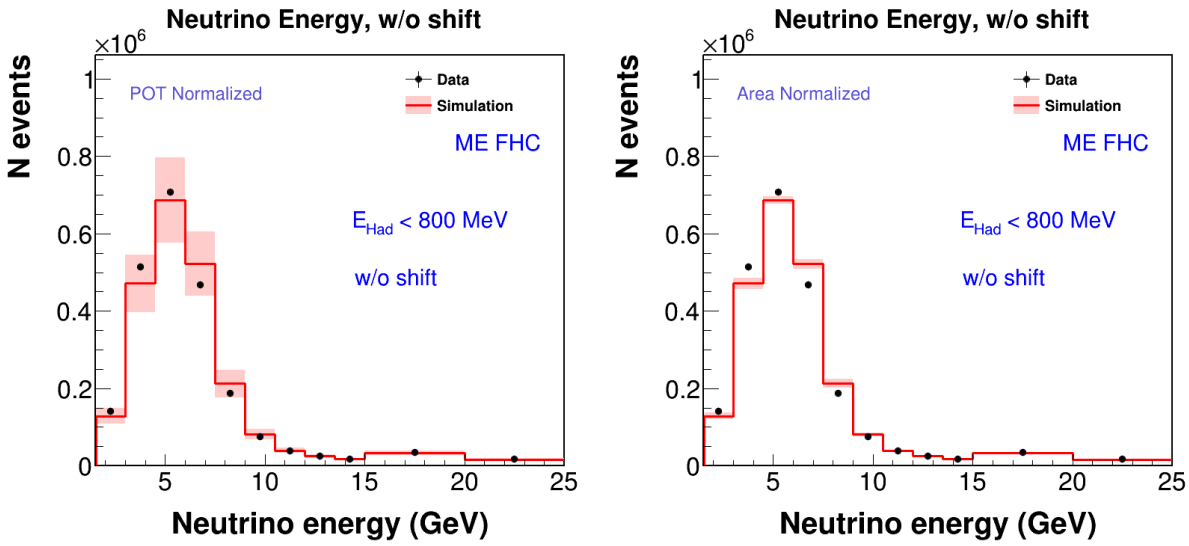

Figure 7.2. Plots of the neutrino energy distribution for the low-ν events. All the run playlists of the Medium Energy era for neutrino beam-line are used for this histograms. The black lines correspond to the statistical errors, and the pink bands are the systematic uncertainties applied to the simulation. In the left side the plot with the absolute normalization is shown. In the plot of the right side the area normalization is applied.

the factor of the area under the data distribution divided by the area under the simulation distribution ($\frac{Data\_Area}{MC\_Area}$). The plots with this normalization are identified with the label "Area Normalized".

For a better identification of the discrepancies between the data distribution and the simulation distribution, the plots of the ratio between the data and the simulation of low-ν events for each normalization is shown in the figure 7.3. In these plots it is possible to observe that the discrepancy is well-covered by the systematic uncertainties in the case of the absolute normalization. But for the case of the area normalized distribution that has the shape-only component of the systematic uncertainty, the shape of the discrepancy is much larger than the systematic uncertainty band.

After seeing that, the idea is to find the proper fit to reduce the disagreement between data and simulation. The fits applied and the justification of each one are discuss in chapter 8.

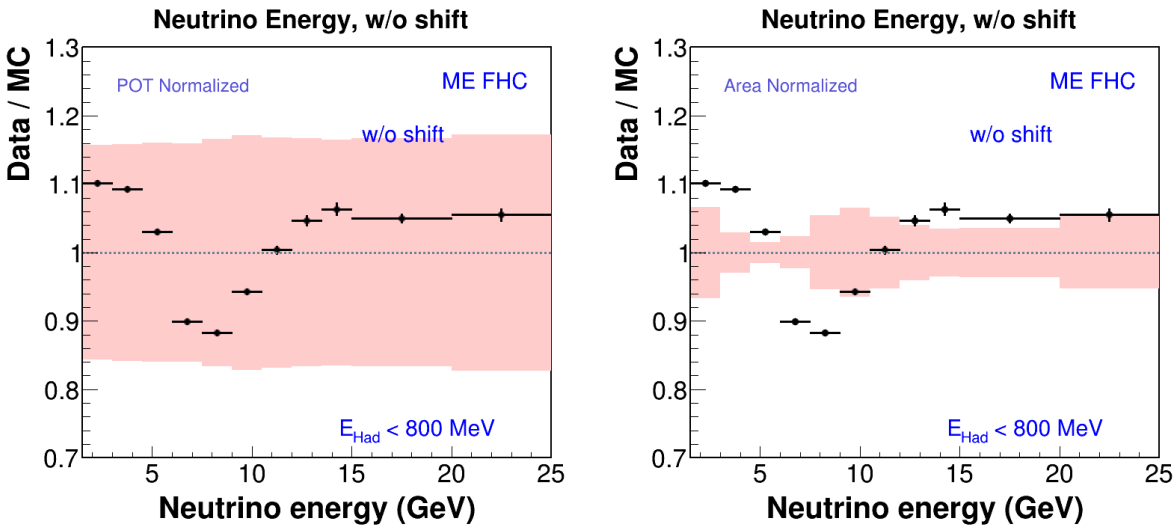

Figure 7.3. Plots of the ratio between data and the simulation of the neutrino energy distribution for the low-ν events. All the run playlists of the Medium Energy era for neutrino beam-line are used for this histograms. The black lines correspond to the statistical errors, and the pink bands are the systematic uncertainties applied to the simulation. The plot with the absolute normalization is shown in the left. In the plot of the right the area normalization is applied, in this plot the shape of the systematic uncertainties shows only the contribution to the variation in the shape of the distribution.

Chapter 8. Fits implemented

In previous chapters the disagreement observed between the data and the simulation of the neutrino energy distribution was shown, and the importance of the systematic uncertainties to identify and understand the sources of the possible mis-modelings. In this chapter a brief description of how three fits were developed to be applied to the neutrino energy distribution with the goal to reduce or remove the discrepancy in the sample are mentioned.

8.1 Measurement of E_μ and ν

To understand the process of developing a weight function that works to perform a fit to sample, first we need to know how the main variables of this analysis are measured. When the Charged Current Neutrino Nucleus interaction was explained, it was mentioned that the energy of the incoming neutrino (E_ν) was reconstructed by the addition of the outgoing muon energy (E_μ) and the energy transfered to the recoil system (ν). Then, the next step is to identify how these two variables are measured in the experiment, which are described below.

The measurement of (E_μ) is the principal reason to keep the MINOS near detector working after that the MINOS experiment finished. Because to measure the energy of the muon is necessary the information provided by MINOS and MINERνA detectors. In the process of identification and reconstruction of the events occurred into the MINERνA detector a tracking algorithm is implemented, which is based on the topology of the particles. The algorithm of reconstruction for muons in MINOS is independent of the use in MINERνA.

Comparing muons with other kinds of particles produced by the neutrino interactions in the same level of energy, they tend to travel long distances. Due to the high mass the probability to produce a shower of particles is low. They leave behind a small amount of energy in each strip through which they pass on the tracker region of the detector, this creates an easy way to predict the energy loss for the particle.

Inside of the MINOS detector the process is similar, but the structure of this works as a big calorimeter immersed in a magnetic field. Then, the affectation to the muon trajectory due the magnetic field is used to measure the curvature of the track knowing that this curvature is proportional to the magnitude of the muon momentum and the electric charge sign. But, it is not the only way to measure the muon energy in MINOS. The muon detected in MINOS can be reconstructed by the curvature of the particle's track, or by the range of its trajectory.

For the **muon reconstruction by curvature**, as mentioned in the previous paragraph, the curvature of the particle's track is measured and this is proportional to muon momentum. Also the energy deposited in each plastic scintillator is measured. This method of reconstruction is implemented when the muon leaves the MINOS detector.

For the **muon reconstruction by range**, this is implemented when the muon stops in the MINOS detector. In this case the energy loss by the muon is measured based on the amount of material through which it passes in the active scintillators and the passive materials such as the steel planes. Generally the energy of the muons measured by this method are ($E_\mu \lesssim 5\ GeV$).

Comparing both methods of reconstruction, for the case of curvature the systematic uncertainty is larger, because for a right reconstruction both methods are used. In the case of reconstruction by range, only this method is used. This generates a muon momentum with less systematic uncertainty.

Finally, the muon momentum measured by MINERνA and the measured by MINOS are associated with a matching algorithm when the muon tracks appear simultaneously in both detectors. Then, the momenta are added resulting in the total muon momentum of the interaction, from this we can measure the muon energy (E_μ).

To measure the transfered energy to the recoil system (ν), this is an inclusive analysis, the total deposited energy in the calorimeters is added together, subtracting the contribution of the muon. To get the total deposited energy the energy of the active regions of the detector and the deposited in the passive regions of the detector are considered. For a right measure of the total energy, we need to do some corrections to the account, these corrections depend on location in the detector. If the observed activity has a lower frac-

tion on the active material, then the correction that needs to be applied will be greater, this is because the account must be corrected for the activity in the unobserved region (corresponding to the steel and lead planes of the calorimeters). With the goal to quantify the effects of these different regions, calorimetric constants are implemented. For this analysis, the values of these constants are the used for the sample events processed by the toolkit of CCQENu developed by MINERνA collaboration.

With the knowledge of each stage for reconstructing the neutrino energy (E_ν), we can start to find which parameters could be affecting the shape of the neutrino energy distribution, to begin to do shifts in each one of these parameters.

8.2 Vertical and lateral affectation generated by shifts to the parameters

When we apply a shift to one of the parameters, we see variations on the systematic uncertainties and some changes to the shape of the distribution of events in the plot. But these differences depend of the type of systematic shift that we are doing, we can identify these shifts in two categories: vertical shifts, and lateral shifts.

The source of the **vertical shifts** is when the systematic uncertainty does not directly affect the kinematic variable, for this reason the effects that we observe are only a modification in the weight of a particular event. These weights correspond to correction factors that are applied to the events when the collaboration finds corrections to implement to the sample of simulation. In the histograms these changes can be seen as an increase or decrease in the content of a bin, but will never lead to event migration between bins, in addition to this, the events that are into the selected sample will never leave this sample by a vertical shift. For example apply a shift in the flux universes, this kind of shift does not change the final reconstructed neutrino energy but the weight of this event could be changed.

The second, **lateral shifts**, are found when the source of the shift in the systematic uncertainty does a direct affectation to the kinematic variable. In this case, this shift generates the migration of events between bins of the histogram. For this reason, some

of the events that were part of the sample could be remove after the shift is applied. An example is the shift that we applied to the muon energy scale parameter trying to fix a disagreement between the events simulated and the measured in the detector, we will discuss this shift later.

To understand the importance of the 1 σ shift to the nominal value of the focusing parameters, the ratio between the predicted and the nominal flux values is shown in figure 8.1. In this figure the distortion on the shape by some of the parameters is clearly observed. The parameters that have a big distortion are Horn 1 transverse position, the horn current, the size of the horn water layer, and the proton beam position. Also, the region affected by this distortion corresponds between 6 and 15 GeV.

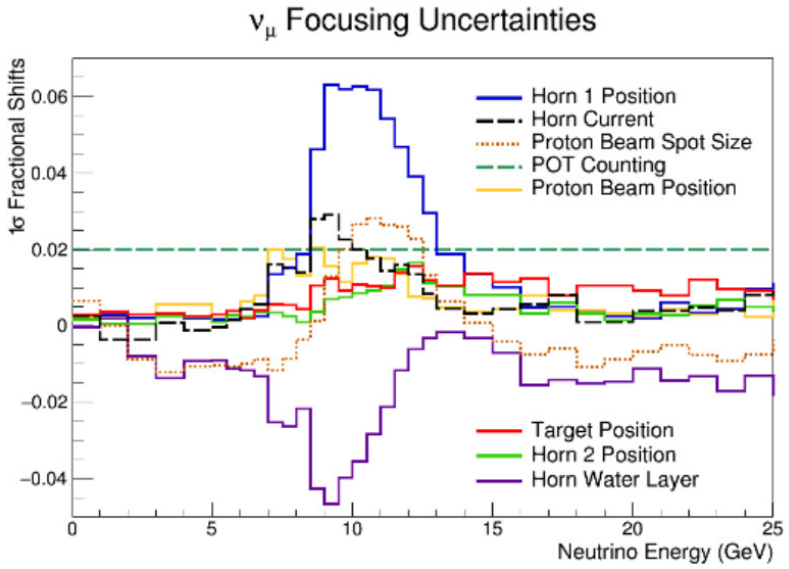

Figure 8.1. Figure of the ratio between the predicted neutrino flux applying shift of one standard deviation to the beam parameters and the nominal neutrino flux. This plot was taken from the documentation of neutrino energy flux with low hadronic recoil [3].

By analyzing figure 8.1, it was possible to identify that the alignment parameters affect differently depending of the region of the detector. This can be noted if we apply a transversal shift to one of the beam parameters, causing the alignment of the beam in the detector to change. If we expected to see a similar distribution of events for all the detector seen in a transversal cut, then it would be expected that this would no longer happens when making shifts to the parameters.

To be able to analyze the possible change on the alignment of the beam due by the shift of the focusing parameters. The event sample was separated according to the position of the vertex for a spatial transverse cut of seven regions in the frontal view of the MINERνA detector, the seven bins are shown in figure 8.2.

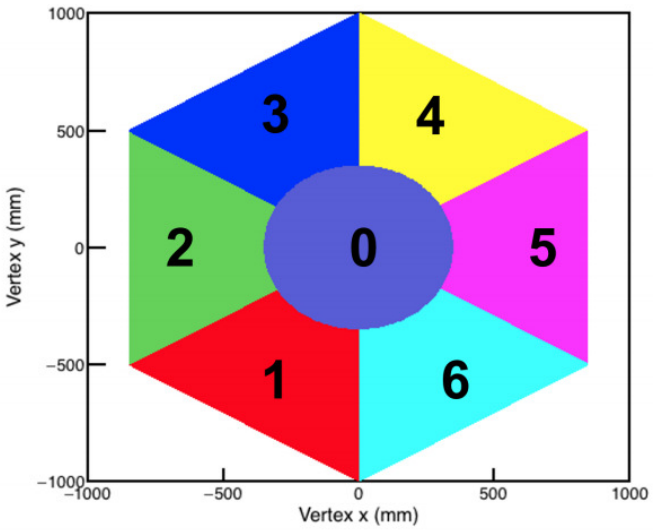

Figure 8.2. Figure of the seven regions (bins) of interaction vertex transverse position implemented to analyze the variations on the number of events occurred by bin, when a shift is applied to the focusing parameters. This plot was taken from the documentation of neutrino energy flux with low hadronic recoil [3].

No big changes were expected, because the radius of the NuMI beam is larger than the radius of the MINERνA detector, there for any shift of the parameters could make a big difference with the nominal position of the beam.

To analyze the possible shifts for each bin of the seven regions, some focusing parameters were shifted. The shift of 1 σ for the primary proton beam spot, and for transverse position on target are shown in figure 8.3. It was identified that some parameters affect all the regions equally, it is the case of the proton beam spot size parameter. But other parameters have different effects according to the position of the bin in the detector.

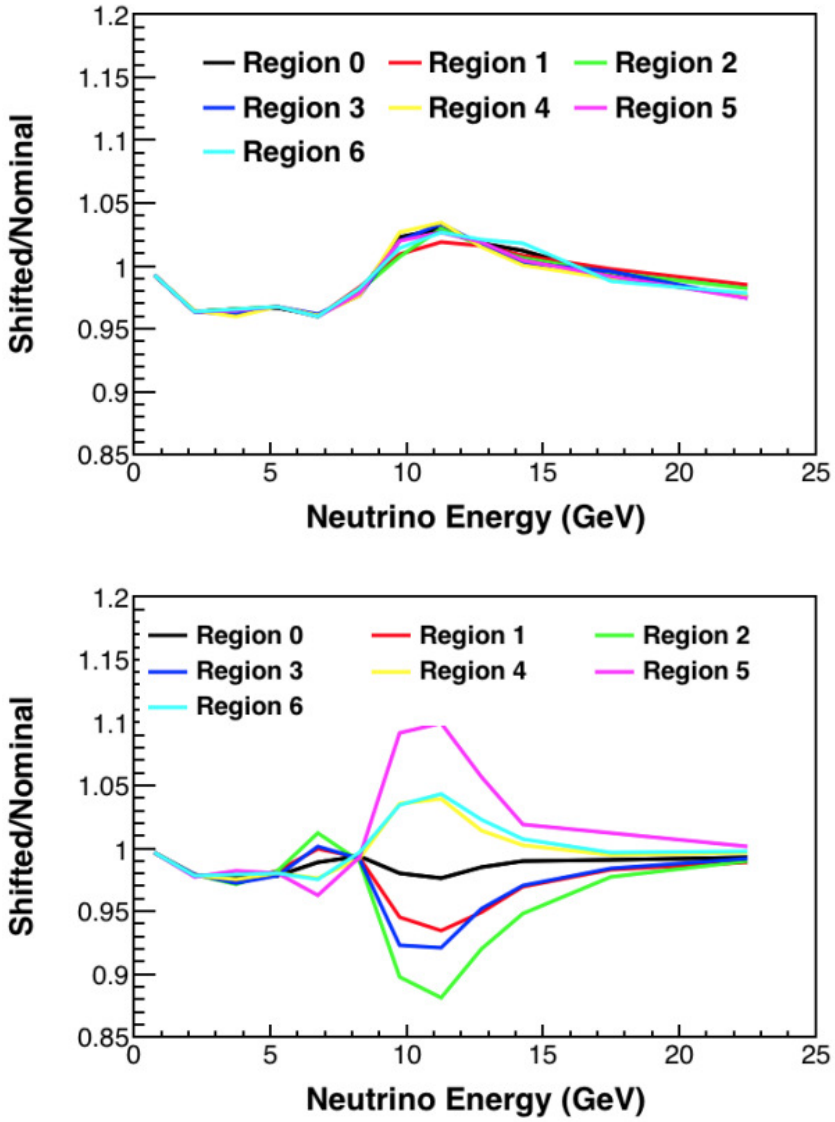

Figure 8.3. Ratio plots between the neutrino flux for 1 σ shift and the nominal value for the seven regions of interaction vertex transverse position. Applying only the shift in the primary proton beam spot size parameter (above), and only to the transverse position on target (below). This plot was taken from the documentation of neutrino energy flux with low hadronic recoil [3].

To see the shape of the variations between the nominal value of the parameter and the shifted value for some of the bins, the collaboration considered the possibility that the origin of the wiggle could be a mis-modeling in the focusing parameters, because the shape observed in the figure 8.3 is similar to the shape of the wiggle. Then the proposal for removing the wiggle on the neutrino energy distribution was to develop a weight function

shifting the focusing parameter until the best fit was found.

Before starting to shift the values of the focusing parameters, the ratio between the data and simulation for each of the seven bins was elaborated, see in figure 8.4. In this ratio plot the discrepancy is similar for all the bins, for this reason the collaboration identifies that the mis-modeling is not consistent only with a transverse shift of the beam parameters. This generates a new proposal to also consider the source of the discrepancy in the muon energy scale, this will be discussed later.

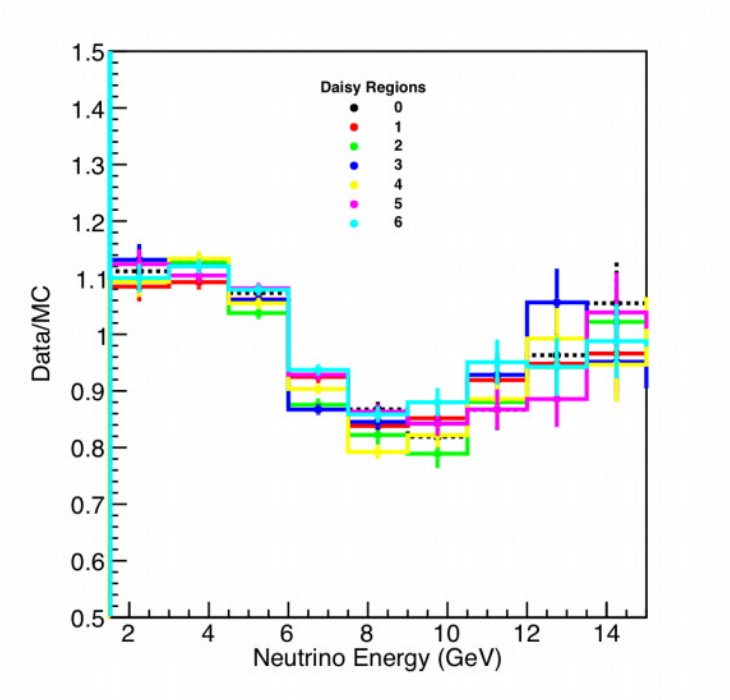

Figure 8.4. Plot of the ratio between the neutrino flux data and the simulation for the seven bins of interaction vertex transverse position. The shape of the distribution is similar for the seven regions. This plot was taken from the documentation of neutrino energy flux with low hadronic recoil [3].

8.3 Performing a weight function

The idea to develop a weight function arises to reduce the disagreement observed between the data and simulation events of the neutrino energy distribution, this, through a correction of the simulation events, implementing a reweight to the nominal simulation values.

The reweight is made by the weight function.

To perform the weight function, first you need to identify the parameters that will be shifted. After having the parameters with their nominal value, the next step is to start to do the shift for each parameter, getting a set of events for each region of the seven bins mentioned before. Subsequently with the seven event samples, the idea is to get a set of the best fit shift parameters and that will converge to a minimum total χ^2. This guarantees that it is the best fit to implement, when we use the set of parameters selected.

The idea is to perform the fit for the spectrum of energy between 1.5 GeV to 15 GeV, divided in nine bins. After 15 GeV the weight function value will be 1. The equation to get a weight to apply for each energy bin on the distribution is given by:

$$w = \frac{MC_{best}}{MC_{nominal}}\,, \tag{8.1}$$

where the MC_{best} is the best value for the simulation, and it is conformed by:

$$MC_{best} = MC_{nominal} \times R_{best}\,, \tag{8.2}$$

where R_{best} is the best fraction correction value (reweight) that comes from the shift to the parameters. But it is different for each bin on the seven bins division for MINERvA detector. For this reason, the best value for the simulation is calculated for the *ith* bin. Then the overall weight function becomes:

$$w = \frac{\sum_{i=1}^{7} MC_{nominal;i} \times R_{best;i}}{\sum_{i=1}^{7} MC_{nominal;i}}\,. \tag{8.3}$$

Finally, when the weight function is implemented to the simulation sample, we expect to reduce the discrepancy between data and simulation events. Subsequently, the validation of the best fit is reviewed with minimizing the χ^2, and this is through the following equation:

$$\chi^2 = \sum_{ij} \frac{(Data'_{ij} - MC'_{ij})^2}{\sigma^2_{ij}}\,, \tag{8.4}$$

where $Data_{ij}$ is the number of events of data in the *ith* energy bin (of the nine energy

bins) and the jth vertex bin (of the seven vertex position regions), MC_{ij} is the number of predicted events of the simulation with the reweight by shifted parameters. In addition, σ_{ij}^2 is the uncertainty given by the combination of the statistical uncertainty of the data and simulation, it is shown next:

$$\sigma_{ij}^2 = \sqrt{\sigma_{Data'_{ij}}^2 + \sigma_{MC'_{ij}}^2}\,. \tag{8.5}$$

To get the systematic propagation on the weight function from the simulation sample for the uncertainty, where each universe on the weight function has a error by the fit implemented in the corresponding universe, the next equation is used:

$$RMS = \sqrt{\frac{\sum_i (w_i - \overline{w})^2}{N^2}}\,, \tag{8.6}$$

where, the w_i is the weight of some ith universe for one of the parameters. This summation is over all the given universes. In addition, the average weight $\overline{w}$ is given by:

$$\overline{w} = \sum_i \frac{w_i}{N}\,, \tag{8.7}$$

where, the w_i is again the weight in some ith systematic universe, and N is the total universes for the parameter. From this propagation of the uncertainties, the next step is to get the total systematic uncertainty, that is the sum of all the individual systematic uncertainties in quadrature, as in the next equation:

$$\sigma_{sys} = \sqrt{\sum_s RMS_s^2}\,, \tag{8.8}$$

where s is the index that runs over all the systematic uncertainties of the weight function. The final error bars that we see in the plots correspond to the addition of the quadrature of the systematic uncertainties and the statistical errors, given by:

$$\sigma_{tot} = \sqrt{\sigma_{sys}^2 + \sigma_{stat}^2}\,. \tag{8.9}$$

After understanding the process to perform the weight function, the idea is to elaborate the best fit that implements shifts to the focusing parameter. Furthermore, a second weight function was developed, but for this case the shift was applied to the focusing parameters and the muon reconstruction parameters. Both fits will be discussed, starting with the weight function elaborated exclusively with the focusing parameters.

Bin Number	Value of Energy (GeV)	Fractional Correction
1	[1.5 , 3.0)	1.06
2	[3.0 , 4.5)	1.00
3	[4.5 , 6.0)	0.99
4	[6.0 , 7.5)	0.90
5	[7.5 , 9.0)	0.82
6	[9.0 , 10.5)	0.83
7	[10.5 , 12.0)	0.89
8	[12.0 , 13.5)	0.92
9	[13.5 , 15.0)	0.94

Tabla 8.1: Table with the values of the fractional corrections for each bin between 1.5 GeV and 15 GeV. These values correspond to the weight function performed assuming a mis-modeling in the focusing parameters only. The plot to see the shape of the weight function is shown in figure 8.5.

8.4 Weight function of the focusing parameters

This fit was performed only applying the shifts to the focusing parameters. That is because the hypothesis considers that all the discrepancy between the data and the simulation events is coming from the mis-modeling of the focusing parameters only. This fit was labeled in the plots as **flux fit**.

After doing all the processes mentioned above to developed the weight function, the values of the fractional correction for each bin between 1.5 GeV to 15 GeV are shown in table 8.1. The width of the bin is the same for all the nine bins, that corresponds to 1.5 GeV.

The shape of the weight function is shows in figure 8.5. The plot shows the region with the fractional correction, in addition to the region with energies greater than 15 GeV, but for this region the value of the weight function is 1, because this is not a region of interest in the weight function for the neutrino energy distribution. As shown in previous plots, this region shows no discrepancy in the ratio of data and simulation events. The next plots include the label **ME FHC**, that means, the showed plot includes the events of the playlists 1A, 1B, 1C, 1D, 1E, 1F, 1G, 1L, 1M, 1N, 1O, and 1P; for the medium energy era of the NuMI beam.

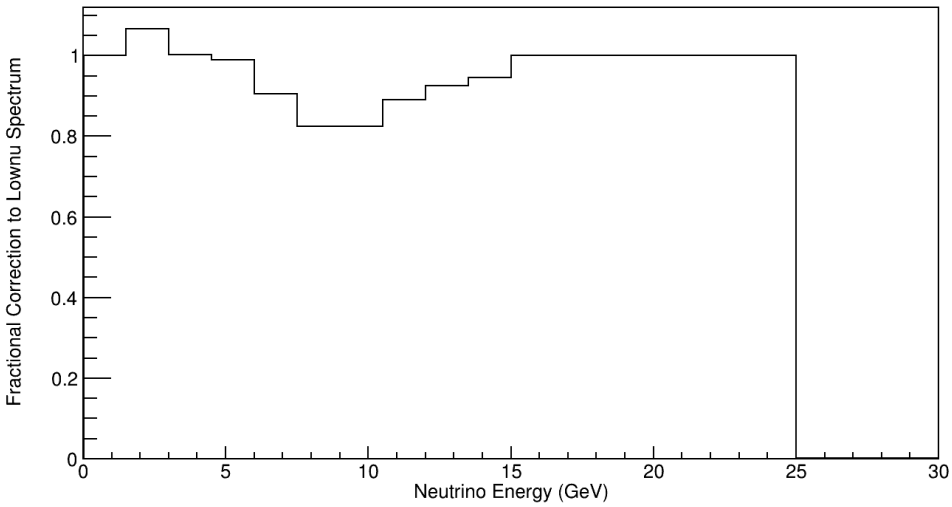

Figure 8.5. Plot of the weight function. The weight function was developed using the focusing parameters only as source for the discrepancy between the data and the simulation of the neutrino flux distribution. The process to develop this weight function is shown in more detail in the technical note for the MINERνA Collaboration [4].

Applying the weight function to the neutrino energy distribution with area normalization for the low-ν events showed in figure 7.2 (right side), the distribution of the neutrino flux events obtained is shown in figure 8.6 (left side). Some variations on the number of events (entries by bin) are possible to identify in the peak region, around 5 GeV. To have a better visualization of the differences, the ratio plot of the data and the simulation events is shown in figure 8.6 (right side). In this plot we see a reduction in the discrepancy between data and the simulation with the flux fit implemented.

For the region between 1.5 GeV to 9 GeV of energy, the largest discrepancy observed is around 6 %, and all this region is almost covered by the systematic uncertainties. But in the intermediate region of the energy spectrum, between 9 GeV to 15 GeV, we see a similar disagreement of 9 % for all the region, and this is not covered by the shape of the systematic uncertainties.

The last region of high energy, between 15 Gev to 25 GeV, is the region without correction for the weight function. In this region we only see a vertical displacement due to the area normalization that works as a scale factor for all the distribution of the simulation events.

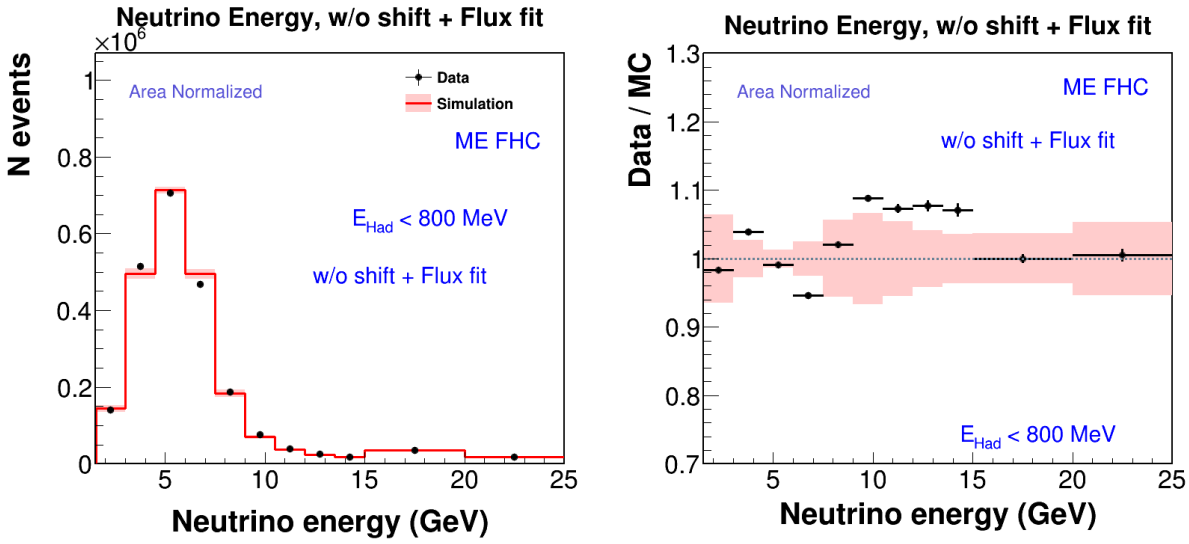

Figure 8.6. Plots of the neutrino flux for the low-ν events implementing the **flux fit** hypothesis to the simulation events. All the run playlists of the Medium Energy era for neutrino beamline are used for this histograms. The plot of the distribution is shown in the left side. In the plot to the right, the ratio between the data and the simulation is shown.

To identify which is the greatest contribution to the shape of the systematic uncertainties in the intermediate region of the spectrum of the neutrino energy, the plot with the summary of the systematic uncertainties is shown in figure 8.7.

In the plot of the summary of systematic uncertainties, the entry with the label *"EmuRangeCurve"* is the variable that increases in the region between 9 GeV to 15 GeV, and this variable is associated with the muon reconstruction parameters. Then, as we discussed in previous sections, if we want to reduce the discrepancy between data and simulation, we need to consider a mis-modeling in the muon reconstruction parameters and not only in the focusing parameters. For this reason a second fit was performed to test another hypothesis.

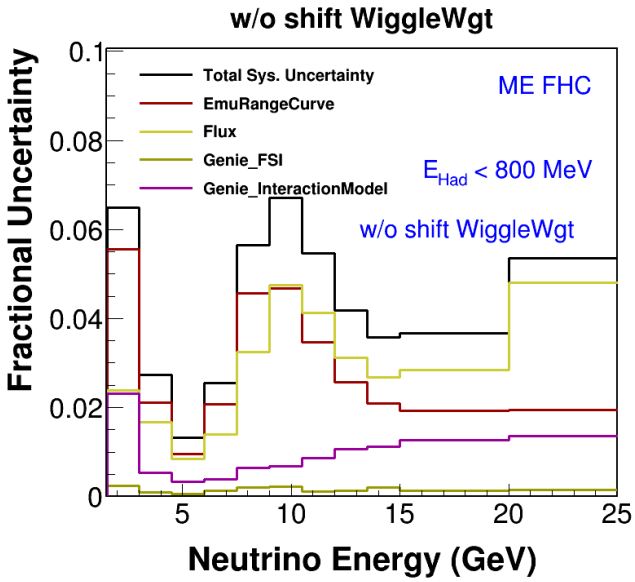

Figure 8.7. Plot of the summary of all the systematic uncertainties included for this analysis of low-ν events. In this plot the label "w/o shift WiggleWgt" means that only the flux fit is implemented. This distribution of uncertainties is for all the medium energy playlists of MINERνA for the neutrino beam-line configuration.

8.5 Shift to the muon energy scale

For this second hypothesis, we are assuming that the value of the focusing parameters are right, and the source of the wiggle in the neutrino flux shape is a mis-modeling in the muon reconstruction parameters. In previous sections it was mentioned that the muon energy (E_μ) is measured adding the energy loss by the muon in the MINERνA detector do the energy deposited in the MINOS detector. But the muon energy in MINOS is reconstructed by two methods, curvature and range. For this reason, the systematic uncertainty of the muon energy consists of four contributions, these are shown in table 8.2, with their corresponding error.

In previous analyzes of the collaboration the right shift to the muon reconstruction parameters was found. To get the best fit between the data and the simulation events for low-ν samples is necessary to apply a shift to the MINOS muon energy scale of 1.8 standard deviations, which means that the MINOS muon energy scale is shifted 3.6 %. But this shift is applied to the data events, the reason is that the collaboration considers this mis-modeling as an error in the reconstruction of events, and not a correction factor

Error Source	Error
MINOS Range	2 %
MINOS Curvature ($p_\mu < 1$ GeV)	2.5 %
MINOS Curvature ($p_\mu > 1$ GeV)	0.6 %
MINERνA	53.94 MeV

Tabla 8.2: Table of the sources of the error for the systematic uncertainties in the Muon Energy reconstruction for the MINERνA experiment. The variable p_μ corresponds to the reconstructed MINOS muon momentum. These values were taken from the technical note of low-ν analysis for the flux in MINERνA [4].

to add in the simulation.

The shift to the muon energy scale only applies to the contribution of MINOS for the reconstruction of the total muon energy, because the contribution of the muon energy loss in the MINERνA detector is small. Something similar happens with the contribution of a mis-modeling in the hadronic recoil energy. This is not considered because the contribution of this variable is too small compared with the energy incoming of the muon. To identify the plots where the muon energy scale shift is applied, a label with the text "Muon Energy Scale fit" was added.

The plot of the neutrino flux distribution applying the shift of 3.6 % (1.8 σ) to the data for the low-ν sample is shown in figure 8.8 (left side). This plot is considering all the playlists of the medium energy era with the neutrino beam configuration.

To get a better comparison between data with the shift to the muon energy scale and the simulation events, the plot with the ratio of data over simulation is shown in figure 8.8 (right side). In this plot, we observe a very good agreement for the region of energies between 1.5 GeV to 9 GeV, for almost all the bins in this region the systematic uncertainties cover the discrepancy. But after this region a big disagreement is observed, of around 10 %. One of the possible reasons is the low-ν cut applied to the sample, which generates a low number of events for this region. Furthermore, the shift to the muon energy scale causes a lateral shift in the bins, moving the events measured for this region of high energy.

Analyzing the shape of the systematic uncertainties using the muon energy scale fit, see figure 8.9, we see that the shape does not have significant change compared with the

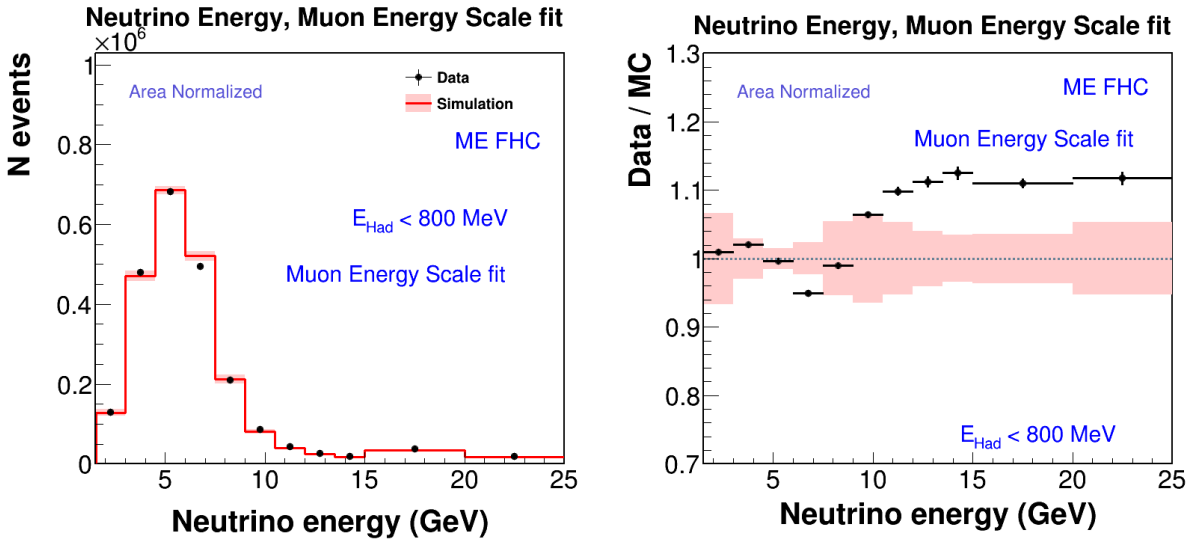

Figure 8.8. Plots of the neutrino flux for the low-ν events implementing the **muon energy scale fit** hypothesis to the data events, that correspond to apply a shift of 3.6 % to the MINOS muon energy reconstruction. All the run playlists of the Medium Energy era for neutrino beam-line are used for this histograms. The plot of the distribution is shown in the left side. In the plot of the right, the ratio between the data and the simulation is shown.

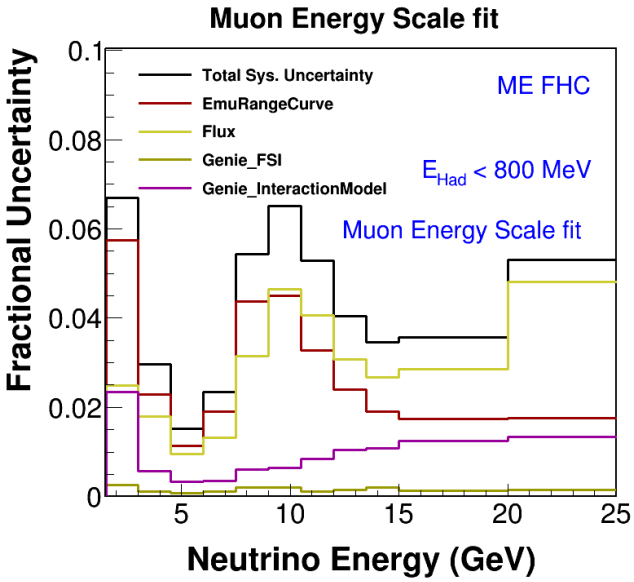

Figure 8.9. Plot of the summary of all the systematic uncertainties included for this analysis of low-ν events. In this plot the label "Muon Energy Scale fit" means that only the muon reconstruction shift is implemented. This distribution of uncertainties is for all the medium energy playlists of MINERνA for the neutrino beam-line configuration.

shape with the flux fit shown before.

A last hypothesis was considered due to the disagreement in the neutrino flux distribution, this is considering the two previous hypotheses in the same case. This will be discussed in the next section.

8.6 Weight function of the focusing parameters and muon reconstruction parameters

To perform this fit the previous two fits are considered. For this hypothesis we are assuming a mis-modeling in the focusing parameters (as in the flux fit), and also the muon energy scale shift is considered as source of the disagreement in the neutrino flux distribution, but now it is added as a fit parameter.

Since the two sources of error are being considered as fit parameters, a weight function is developed to be applied to the simulation events as a correction to these values. Again

Bin Number	Value of Energy (GeV)	Fractional Correction
1	[1.5 , 3.0)	1.07
2	[3.0 , 4.5)	1.02
3	[4.5 , 6.0)	1.00
4	[6.0 , 7.5)	0.91
5	[7.5 , 9.0)	0.82
6	[9.0 , 10.5)	0.81
7	[10.5 , 12.0)	0.87
8	[12.0 , 13.5)	0.92
9	[13.5 , 15.0)	0.96

Tabla 8.3: Table with the values of the fractional corrections for each bin between 1.5 GeV and 15 GeV. These values correspond to the weight function performed assuming a mis-modeling in the focusing and the muon reconstruction parameters as fit parameters. The plot to see the shape of the weight function is shown in figure 8.10.

this weight function is only implemented for the spectrum of energy between 1.5 GeV to 15 GeV, and the fractional corrections for each bin are shown in table 8.3, reminding that all the bins have the same width of 1.5 GeV.

The graph with the fractional correction is shown in figure 8.10, in this plot the first bin corresponds to the fractional correction for the energies between 0 and 1.5 GeV, but this bin has the value of 1, because for that region we are not interested in modifying, the same for the region for energies greater than 15 GeV. If we compare this weight function with the performance for the flux fit, we see similar fractional corrections for both hypotheses. This is expected, because the goal of the weight function is the same, to remove the disagreement between data and simulation for the low-ν sample.

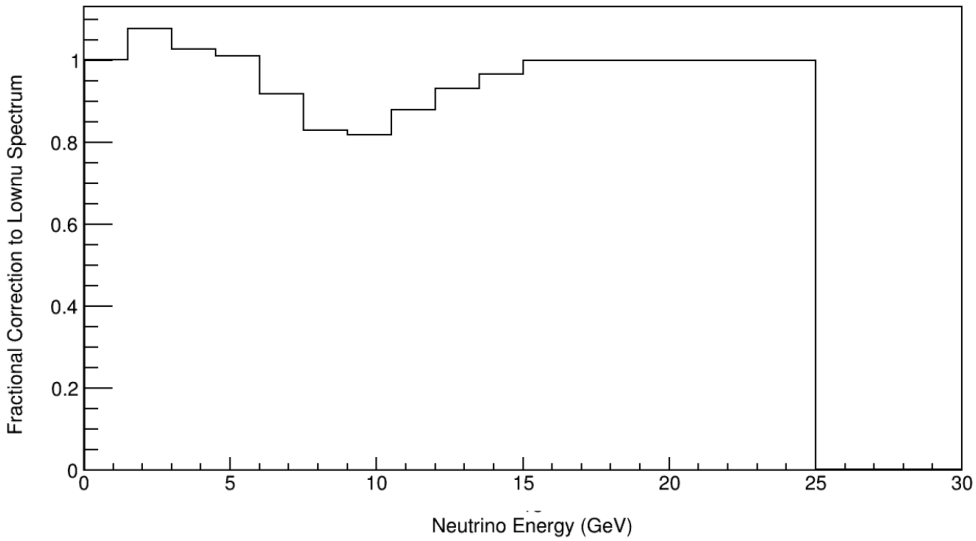

Figure 8.10. Plot of the weight function to observe the shape for all the energy spectrum. The weight function was developed using the focusing and the muon reconstruction parameters as source of the discrepancy between the data and the simulation of the neutrino flux distribution. The process to develop this weight function is shown in more detail in the technical note of the MINERνA Collaboration [4].

After implementing the weight function to the neutrino flux distribution without shift and area normalization that was shown in figure 7.2 (right side). Get the neutrino energy distribution shown in figure 8.11 (left side). All the plots with the weight function developed considering the focusing parameter and the muon energy scale as sources to the discrepancy in the neutrino flux are labeled with the text "Flux/Muon fit".

Again the plot with the ratio between the data and the simulation is shown in figure 8.11 (right side) to better analyze the variation in the shape of the disagreement. We see in this plot a considerable reduction of the original discrepancy for all the spectrum energy showed.

Doing a detailed analysis for each energy region, we again observe three main regions to review. The first region corresponds to the events with a neutrino energy of 1.5 GeV to 9 GeV, we see a good agreement between the data and the simulation events and only one of the five bins is not covered by the systematic uncertainty bars.

The second region with energies between 9 GeV and 15 GeV presents a large wiggle to

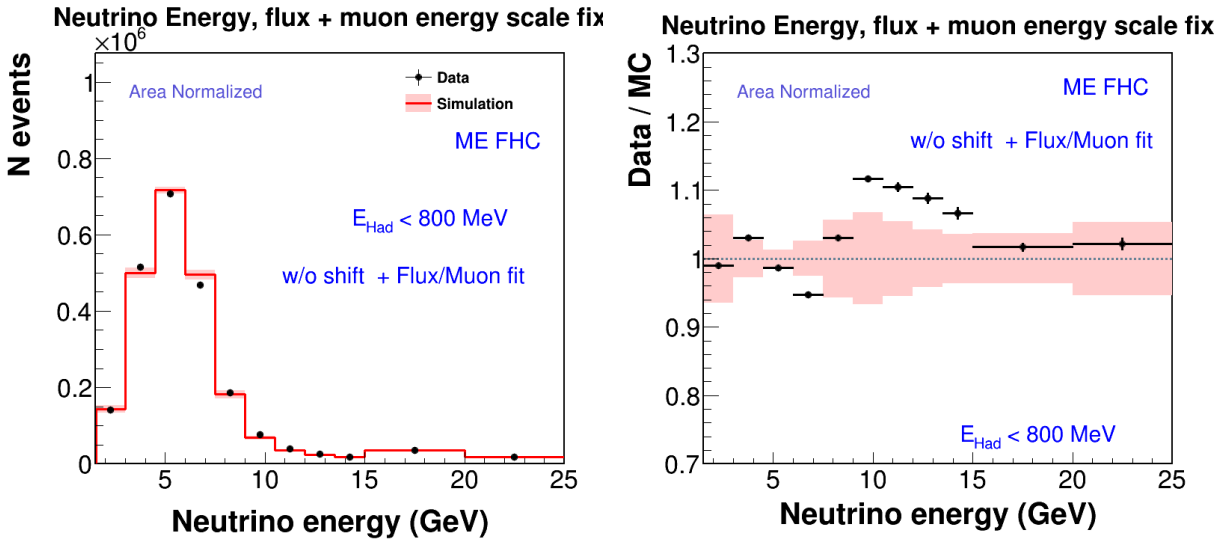

Figure 8.11. Plots of the neutrino flux for the low-nu events implementing the **Flux/Muon fit** hypothesis that corresponds to applying the weight function constructed with the focusing and the muon reconstruction parameters as fit parameters. All the run playlists of the Medium Energy era for neutrino beam-line are used for these histograms. The plot of the distribution is shown in the left side. In the plot of the right the ratio between the data and the simulation is shown.

the data, and it is not covered by the systematic uncertainties. The bin with the largest discrepancy has a 11 % variation, and the one with the least disagreement corresponds to around 8.5 % variation. This could be due to variations between the sample used for this analysis and the sample implemented in previous analysis when the weight functions were performed, this will be discussed later.

For the last region of energies in the neutrino flux distribution, that corresponds to 15 GeV and 25 GeV, the agreement is preserved and the shape is covered by the bars of the systematic uncertainties.

The shape of the total systematic uncertainty stays similar to the shape observed in the other two hypotheses, the summary of the systematic uncertainties for the hypothesis with the focusing and the muon reconstruction parameters as fit parameters is shown in figure 8.12.

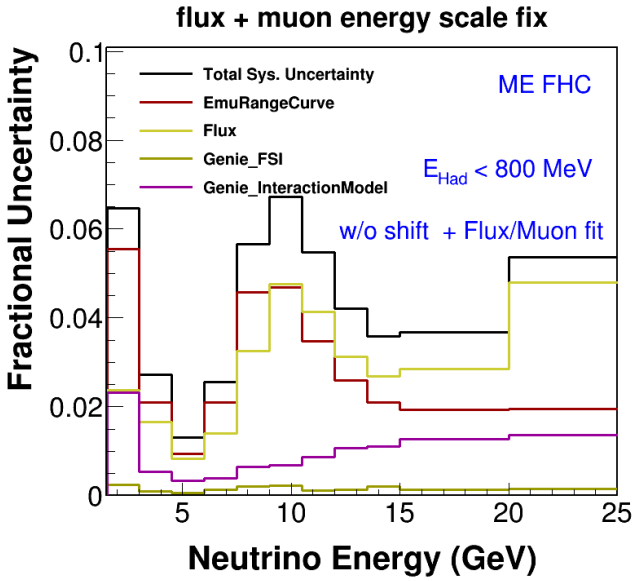

Figure 8.12. Plot of the summary of all the systematic uncertainties included for this analysis of low-ν events. In this plot the label "Flux/Muon fit" means that the weight function developed with the focusing and the muon reconstruction parameters are implemented. This distribution of uncertainties is for all the medium energy playlists of MINERνA for the neutrino beam-line configuration.

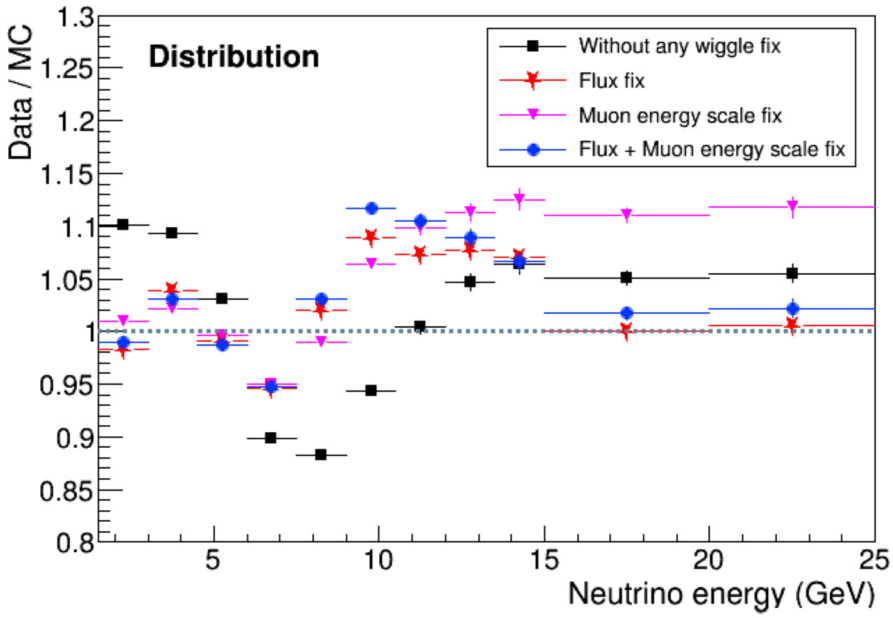

Figure 8.13. Plot with the three ratio distributions corresponding to each hypotheses, in addition to the ratio distribution for the original case without any fit to remove the wiggle. All distributions are using all the playlists of MINERνA for the medium energy era with the beam-line configured for neutrino generation.

8.7 Comparing between the shape distribution of all hypotheses

In order to have a better visualization of all the shapes of the ratio between data and simulation for each hypothesis, figure 8.13 was elaborated. In this plot the ratio distribution for each fit implemented was added, besides the shape distribution without any wiggle fix, the shape shown in figure 7.3 (right side).

From figure 8.13 we can see that the region of low energies, 1.5 GeV to 9 GeV, which is also the region with the peak of neutrino beam events, presents a good reduction of the wiggle for all the fits. It is possible to identify that there is a better fit in the case of the muon energy scale fit.

In the second region that corresponds to the energies between 9 GeV to 15 GeV, and that we can observe from the distribution of the beam flux, the peak of events decreases.

None of the distributions with the fit have a better agreement than the shape without any fit. But the only shape that remains with the same variation for the entire region is the muon energy scale fit.

For the last region with the high energies, 15 GeV to 25 GeV, we see that the best fit corresponds to the flux fit, and the second best is the hypothesis with the focusing and muon reconstruction parameters as fit parameters. Reminding that the number of events for this region is reduced compared with the first region, and for that reason, greater importance is given to having a good fit of the data and the simulation in the region with a peak of number of events.

Having the comparison of the neutrino energy distribution for the low-ν events implementing the three fits, each separately. The next step to identify which is the appropriate fit to implement in future analysis is observing the distribution of the events for different samples of this low-ν events. To do this, in chapter 9 different cuts will be implemented to the sample to divide this in small samples of events with a particular characteristic of the particle reconstruction process in MINERνA.

In appendix A a version of the plots for neutrino distribution, ratios and summary of the systematic uncertainties for each playlist of the medium energy era for the MINERνA experiment with the NuMI configuration for neutrino beam-line are shown.

Chapter 9. Variations to the sample

In the previous chapter the shape of the ratio between data and simulation events of low-ν implementing three different fits to remove the wiggle was shown. We can identify which fit is the best to reduce the wiggle. But to understand why this fit affects the shape that way, we need to implement more cuts to the sample.

With the goal to identify how different factors, related to the muon reconstruction and the proportion between the hadronic recoil energy and the total neutrino energy, contribute to the variations of the shape in the neutrino flux distribution, a set of new samples were performed. The process to create these samples was beginning with the low-ν sample that we used before, but to this sample a second stage of event cutting was added. The cuts are independent of each other, with the goal to create five different samples of events. The five cuts are the following:

- Dividing into samples of muons reconstructed by the curvature method in the MINOS detector.
- Dividing into samples of muons reconstructed by the range technique in the MINOS detector.
- Dividing into samples with MINOS muon momentum $P_{\mu}^{MINOS} < 1$ GeV.
- Dividing into samples with MINOS muon momentum $P_{\mu}^{MINOS} > 1$ GeV.
- Comparing the contribution of the hadronic energy to the neutrino energy (actually this is not a cut, it just creates a new variable).

For the plots of each one of the new samples the width of the bins is changed to 1 GeV, this in order to observe in more detail all the variations of the shape.

9.1 Samples of muons reconstructed by curvature

The idea of implementing a cut for dividing the events into samples of muons reconstructed using the curvature method in the MINOS detector to measure the energy is because we

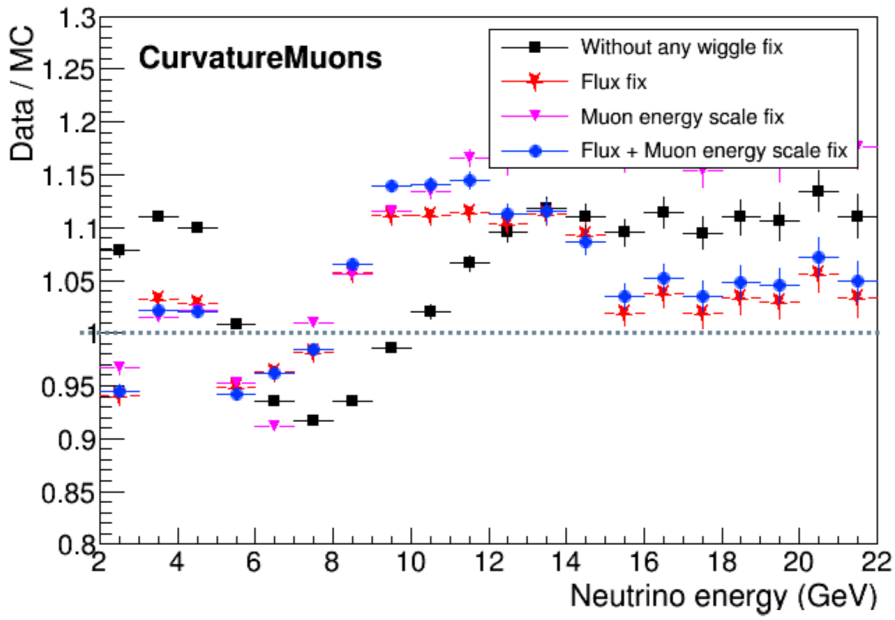

Figure 9.1. Plots of the ratio between data and simulation of the neutrino flux distribution, for the low-nu events with the condition that the muon measured for the event was reconstructed using the **curvature** method in the MINOS detector. All distributions are using all the playlists of MINERνA for the medium energy era with the beamline configured for the neutrino generation.

know that the curvature method is used when the muon particle has high energy, then it does not stop in the MINOS detector. Furthermore when the curvature method is implemented, the propagation of the error on the reconstruction is greater compared with the events reconstructed by range. Besides, if the source of the wiggle is coming from the curvature reconstruction, we expect to see a very marked shape of the wiggle in the distribution for this sample.

The plot with the neutrino flux distribution for the sample of muons reconstructed by curvature is shown in figure 9.1. This plot includes the four versions of the distribution, one without any wiggle fit, and the three fit hypotheses. In addition to these plots, the corresponding plots of the ratio with the bars of the systematic uncertainties for each one of the distributions shown in plot mentioned above are shown in figure 9.2.

From the shape of the distributions seen in the figure 9.1, we see that the shape of the wiggle is present for all distributions, with a considerable reduction in the region of low

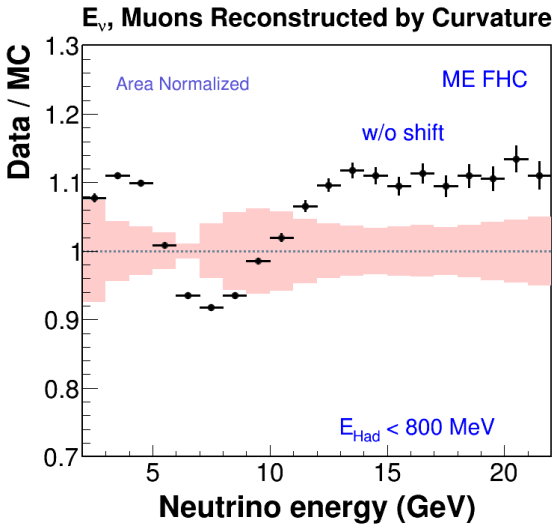

9.2.1. Without any wiggle fit.

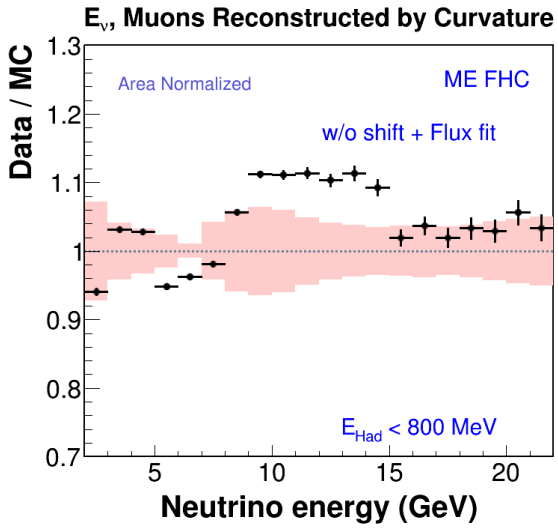

9.2.2. Focusing parameters fit.

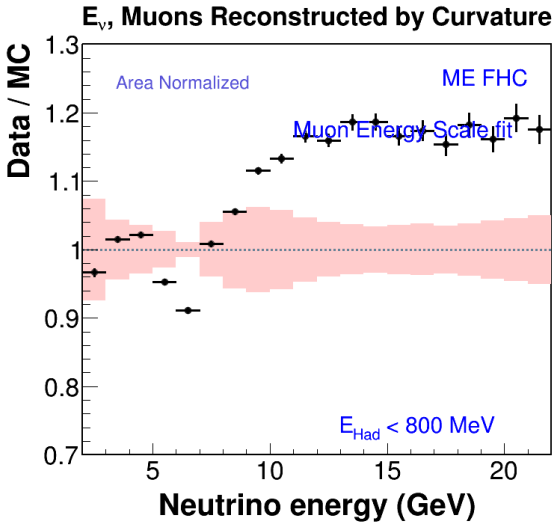

9.2.3. Muon energy scale fit.

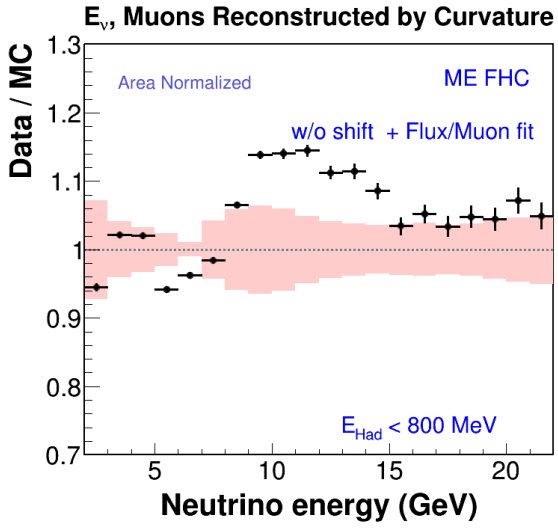

9.2.4. Focusing and Muon parameters fit.

Figure 9.2. Ratios between data and simulation with the systematic uncertainty bars (pink region). The sample of events used for these plots corresponds to the low-ν events with the muon reconstruction by **curvature** into MINOS detector. All the run playlists of the medium energy era for neutrino beam-line are used for these histograms.

energies, from 2 GeV to 5 GeV, for the distribution with a fit applied. But after 5 GeV the shape with the disagreement between data and simulation is observed. Besides in the distributions with a fit, the wiggle shape has a lateral shift compared to the version without any fit. Furthermore, for all the cases with a wiggle fit, we see that the systematic errors covered the discrepancy between data and simulation for the low energy region mentioned above, being the case with the muon energy scale fit the best fit for this region.

The plots with the summary of the systematic uncertainties for each one of the four distributions are shown in figure 9.3. These do not present great variations between the four distributions, just little changes in the amplitude of the total shape attributed to the muon reconstruction uncertainty.

9.2 Samples of muons reconstructed by range

Elaborating the new sample of events with the condition that the muon measured in the MINOS detector must be reconstructed by the range method. An indirect energy cut is made. Because for the muon to be reconstructed by range, this muon needs to stop in the MINOS detector, due the dimensions of the detector, if the muon particles have too high energies these will cross the detector without stopping. From previous studies on the MINOS detector, we know that the greatest muon energy reconstructed by range is around 5 GeV.

If the shape of the wiggle in the distribution of events reconstructed by range is observed, we could think that the source of the discrepancy between data and simulation is coming from a mis-modeling in the algorithm of reconstruction of muon energy in the range method. Knowing that the curvature method is independent of each other, unlike the reconstruction by curvature, that uses a comparison of both methods to get the measurement.

The ratio plot of the data and simulation of events reconstructed by range in MINOS, with the restriction in the hadronic recoil energy is shown in figure 9.4. In this figure, as in the case of muon reconstructed by curvature, the four cases are shown in the same canvas to compare how is the original distribution without any wiggle fit and the distributions

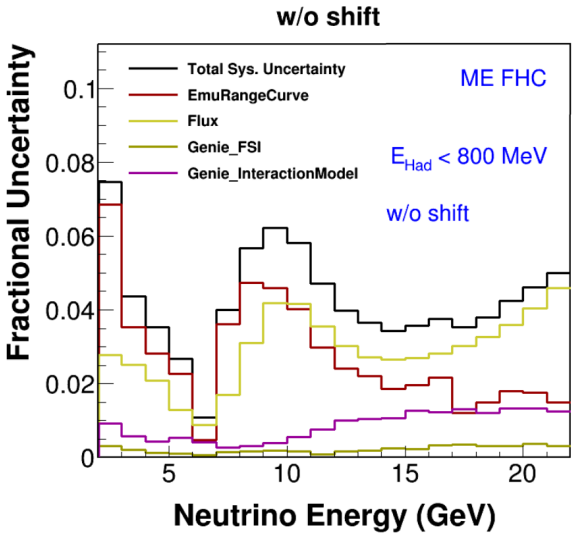

9.3.1. Without any wiggle fit.

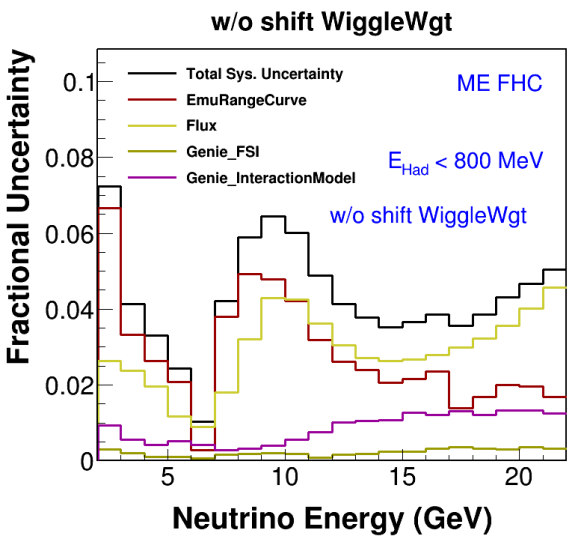

9.3.2. Focusing parameters fit.

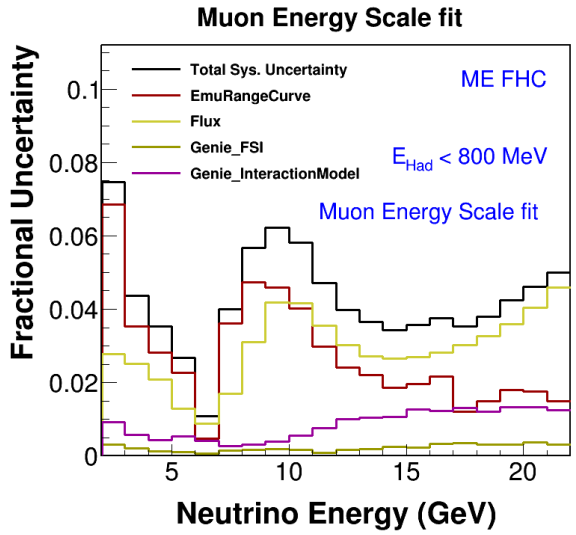

9.3.3. Muon energy scale fit.

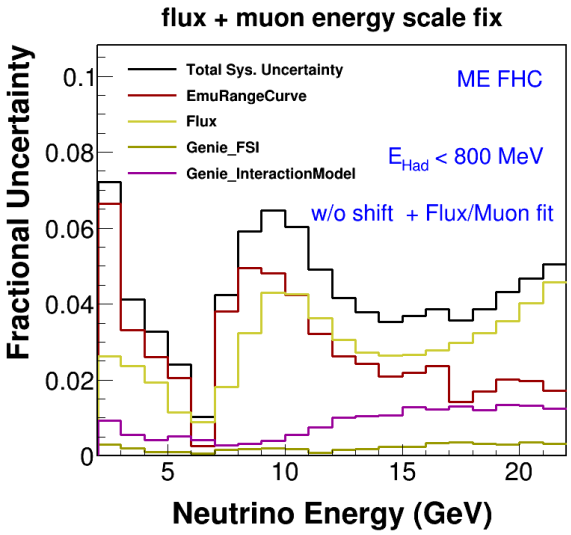

9.3.4. Focusing and Muon parameters fit.

Figure 9.3. Summary of the systematic uncertainties. The sample of events used for these plots correspond to the low-ν events with the muon reconstruction by **curvature** in MINOS detector. All the run playlists of the medium energy era for neutrino beam-line are used for these histograms.

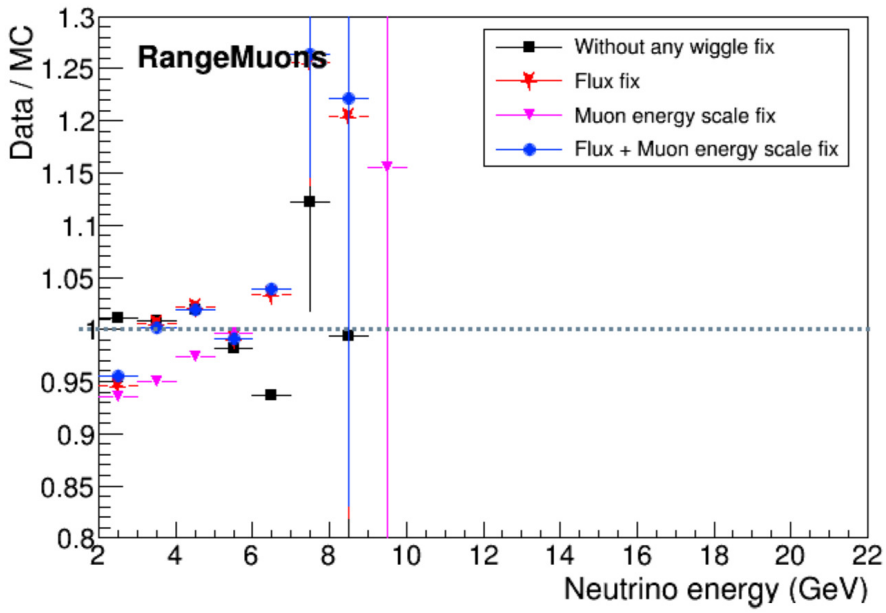

Figure 9.4. Plots of the ratio between data and simulation of the neutrino flux distribution, for the low-ν events with the condition that the muon measured for the event was reconstructed using the **range** method in the MINOS detector. All distributions are using all the playlists of MINERνA for the medium energy era with the beam-line configured for the neutrino generation.

affected by the three different fits described in this analysis.

From the plot of the ratio distribution it is noted that the number of events compared with the original sample is reduced, this is because as mentioned before, the MINOS detector only measures by range method the muons stopped in the detector. In addition to this, if the greatest contribution of the hadronic energy is 800 MeV, then we expect to measure events up to around 6 GeV, that corresponds to the last bin with short statistical error bars. After this bin statistical error bars increase around 20 % compared with the bars of the first bins. This means that the number of events measured in the bins after 6 GeV have a low statistic. Furthermore, from the distribution of events without any wiggle fit it is possible to see that the wiggle shape is not present,but this can be better seen from the individual version of the distribution.

In figure 9.5 the ratio plots on individual canvas are shown, also the systematic uncertainty bars are added. We can note that as mentioned, the shape of the ratio distribution

of events without any wiggle fit implemented does not present the disagreement in the region of energies between 2 GeV to 6 GeV, but in the last bin with the short statistical error bars, we see a discrepancy between the events measured and the events simulated. Besides, this disagreement is covered by the systematic uncertainty bars, as in the rest of bins with short statistical error bars. Only the bin that corresponds to 4 GeV is outside of the systematic uncertainty region, and presents a discrepancy of 2 % between data and simulation.

Analyzing the plots with the summary of the systematic uncertainties (seen in figure 9.6), we found that for the last bin with the short statistical error bars , that corresponds to 6 GeV, the systematic uncertainty attributed to the muon reconstruction parameters increased. This gives an idea that the discrepancy observed in this last bin with high statistics perhaps has a mis-modeling in the reconstruction of energy. Recalling that this bin corresponds to the limits of measurement for the range method of muon reconstruction in MINOS detector.

In addition to the increase of the systematic uncertainty attributed to the muon reconstruction parameters, for the region with neutrino energy greater than 6 GeV, the contribution to the total systematic uncertainty associated to the GENIE parameters have a progressive increase when the energy of the neutrino increases.

9.3 Samples of MINOS muon momentum $<$ 1 GeV

The idea to implement a division of the sample for events with the MINOS muon momentum less than 1 GeV arises to identify that in the previous sample of muon events reconstructed by curvature the wiggle shape was observed.

Analyzing with more detail the uncertainty of the muon reconstructed by curvature in MINOS, we see that the error source of this uncertainty is divided in two cases: for $p_{\mu}^{MINOS} < 1$ GeV and $p_{\mu}^{MINOS} > 1$ GeV. In table 8.2 the contribution of each one to the uncertainties are shown.

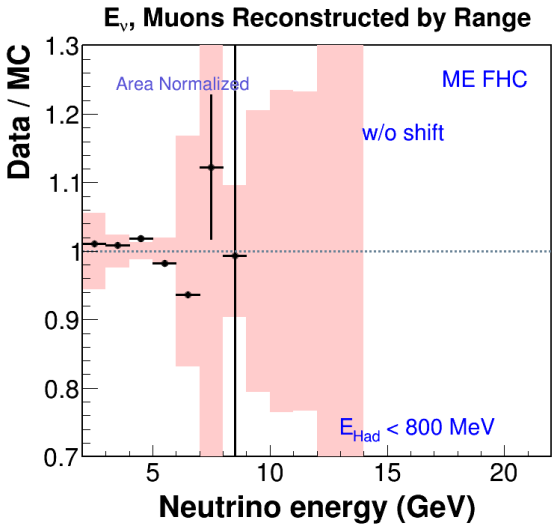

9.5.1. Without any wiggle fit.

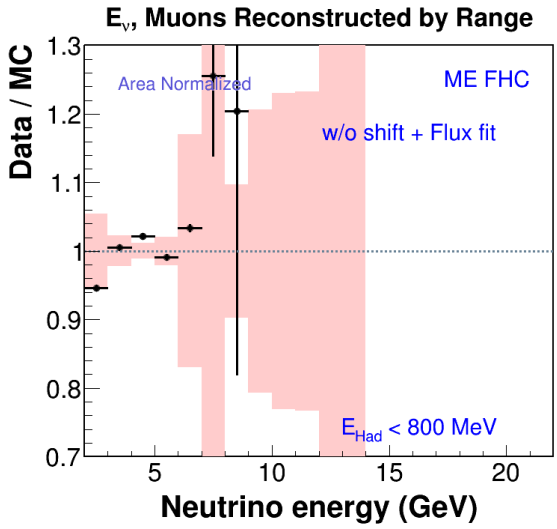

9.5.2. Focusing parameters fit.

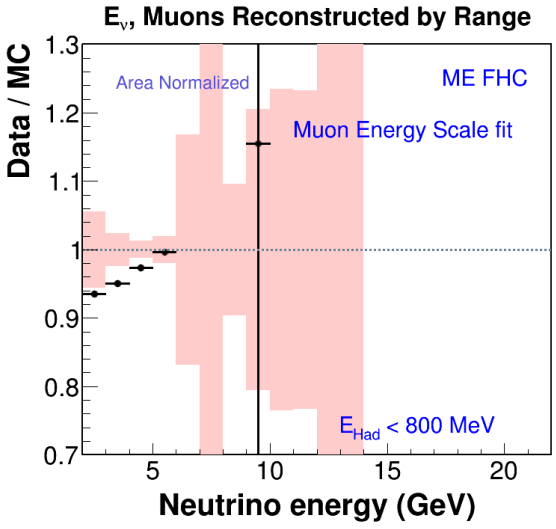

9.5.3. Muon energy scale fit.

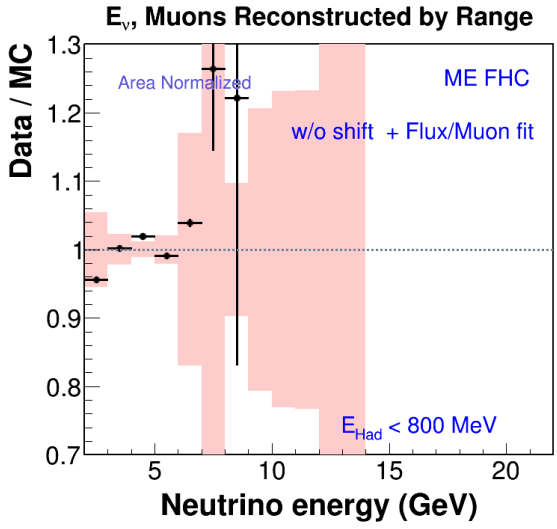

9.5.4. Focusing and Muon parameters fit.

Figure 9.5. Ratios between data and simulation with the systematic uncertainty bars (pink region). The sample of events used for these plots corresponds to the low-ν events with the muon reconstruction by **range** into MINOS detector. All the run playlists of the medium energy era for neutrino beam-line are used for these histograms.

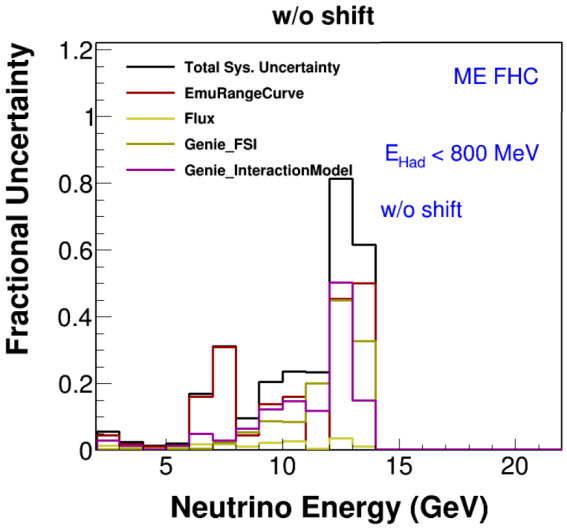

9.6.1. Without any wiggle fit.

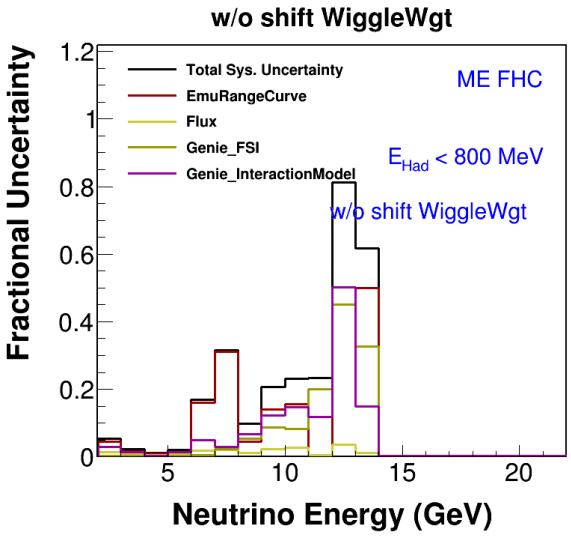

9.6.2. Focusing parameters fit.

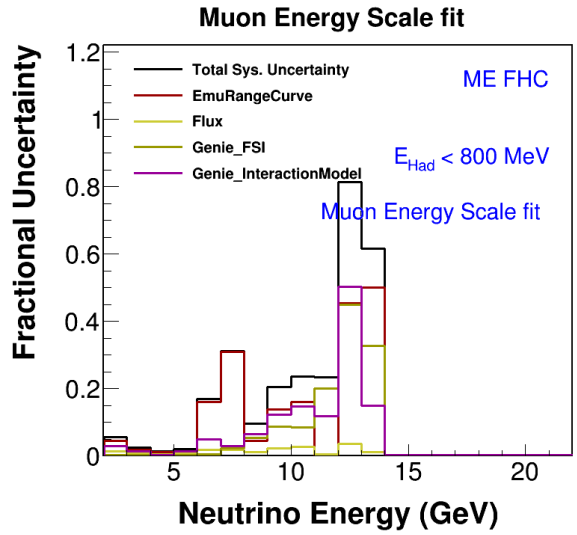

9.6.3. Muon energy scale fit.

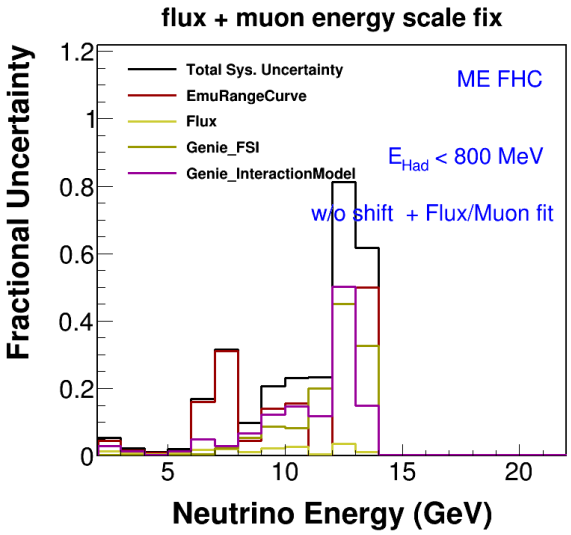

9.6.4. Focusing and Muon parameters fit.

Figure 9.6. Summary of the systematic uncertainties. The sample of events used for these plots corresponds to the low-ν events with the muon reconstruction by **range** into MINOS detector. All the run playlists of the medium energy era for neutrino beam-line are used for these histograms.

For the sample of the events with a $p_{\mu}^{MINOS} < 1$ GeV, the expectation is to get a sample with a reduced number of events, and also with low energy. Because, the reconstruction of the neutrino energy used in this analysis is conformed by two variables: the muon energy and the hadronic recoil energy, as mentioned in chapter 6. Due to the restriction in energies of less than 1 GeV for the muon momentum reconstructed in MINOS, and the restriction of low energies for the recoil system with has less than 800 MeV. Therefore the values of the neutrino energy for this sample must be low.

In figure 9.7 the ratio distribution for the three fits and the original distribution are shown. For these plots the range of the horizontal axis changes compared to the rest of plots shown in this investigation. As expected from the mentioned above, the events with the greater neutrino energy for this sample correspond to around 3.2 GeV. For this reason a change in the range of the horizontal axis was made, this axis corresponds to the neutrino energy. We note that the shape of the distribution does not change with the flux fit nor with the flux/muon fit. We only see a minimum change when the muon energy scale fit is implemented.

To analyze the shape of the distribution with the systematic uncertainties, the plots with the four distributions each one in different canvas and including the systematic error bars are shown in figure 9.8. In addition to noticing that the shape of the ratio distributions does not show changes other than in the last two bins, we see that the shape distribution is almost covered in all the regions by the systematic uncertainty bars. Furthermore, the shape of the distribution for the plot of the ratio between data and simulation seems not to have the same wiggle affectation than other samples, because the shape of the distribution is different to the wiggle shape observed in the original distribution of low-ν.

From the plots with the summary of the systematic uncertainties for the four different fits, see figure 9.9, it can be observed that the shape of the total systematic uncertainties is the same for all the distribution. Besides, the main contribution to the total is the variable attributed to the muon reconstruction parameters.

The distribution observed for this sample of events is not significant for the analysis, because the number of events is too small. As a sample of this, figure 9.10 shows the distribution of events for the sample without any wiggle fit implemented. In this plot the number of entries in the bin with the peak of events (2.3 GeV to 2.5 GeV) is around

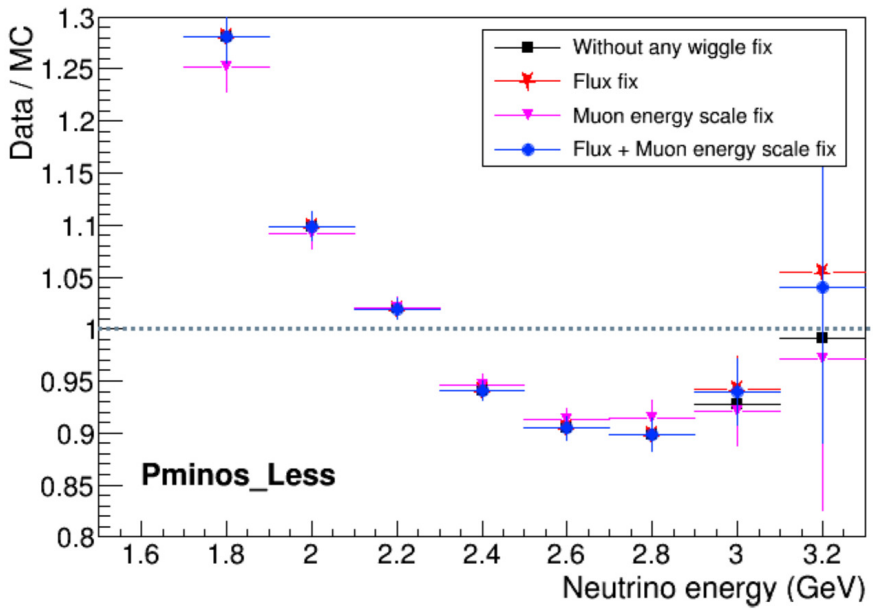

Figure 9.7. Plots of the ratio between data and simulation of the neutrino flux distribution, for the low-ν events with the condition that the MINOS muon momentum measured was less than 1 GeV, $\boldsymbol{p_{\mu}^{MINOS} < 1}$ **GeV**. All distributions are using all the playlists of MINERνA for the medium energy era with the beam-line configured for the neutrino generation.

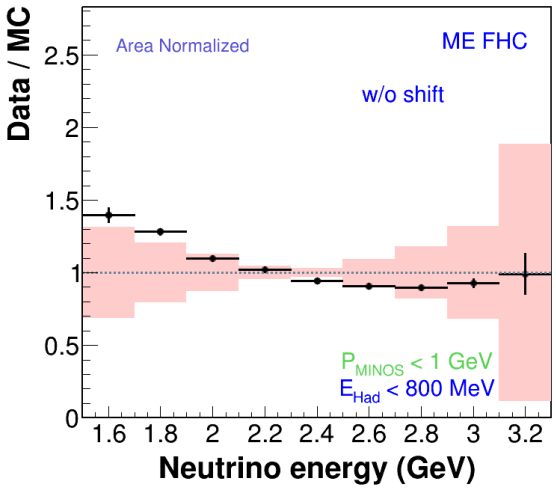

9.8.1. Without any wiggle fit.

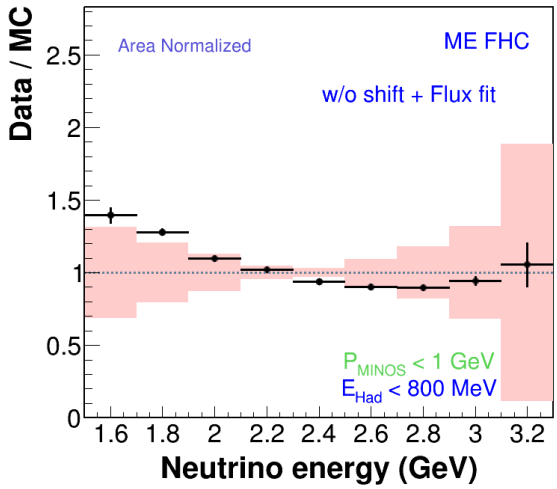

9.8.2. Focusing parameters fit.

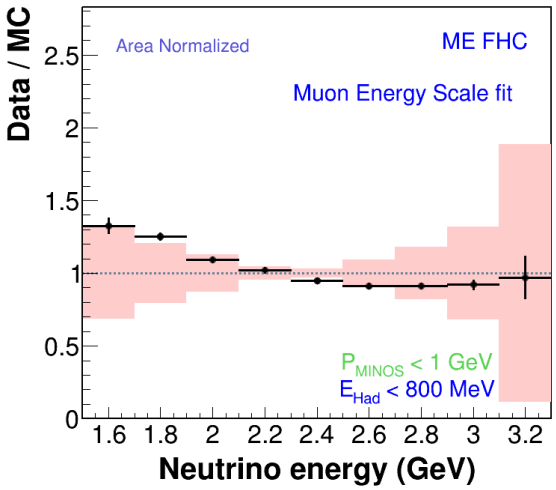

9.8.3. Muon energy scale fit.

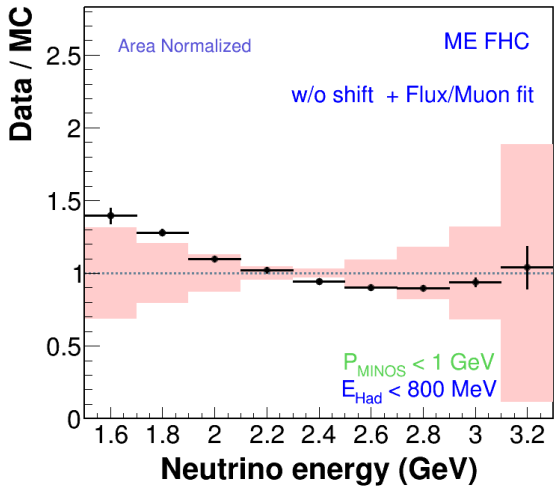

9.8.4. Focusing and Muon parameters fit.

Figure 9.8. Ratios between data and simulation with the systematic uncertainty bars (pink region). The sample of events used for these plots corresponds to the low-ν events with the condition that the MINOS muon momentum to be less than 1 GeV, $\boldsymbol{p_{\mu}^{MINOS} < 1}$ **GeV**. All the run playlists of the medium energy era for neutrino beam-line are used for these histograms.

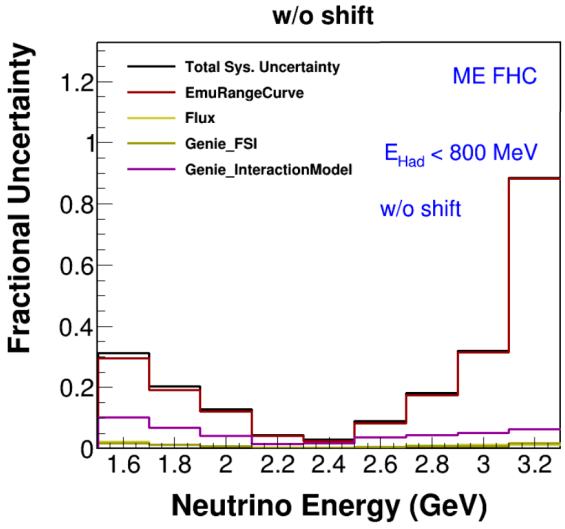

9.9.1. Without any wiggle fit.

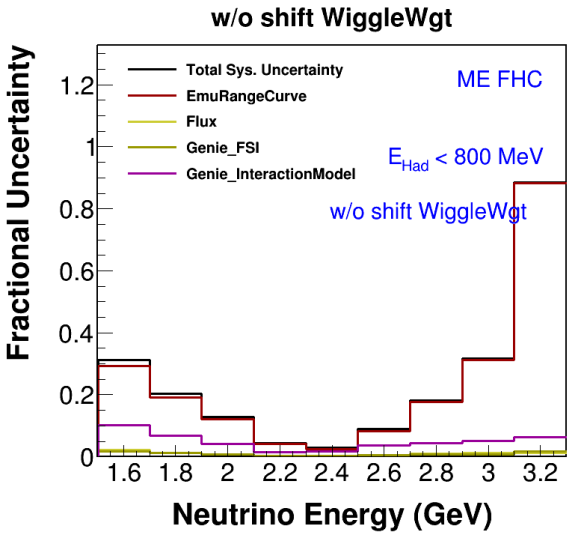

9.9.2. Focusing parameters fit.

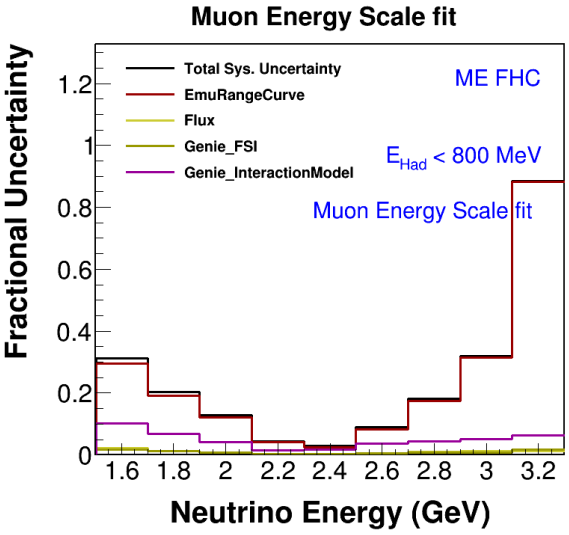

9.9.3. Muon energy scale fit.

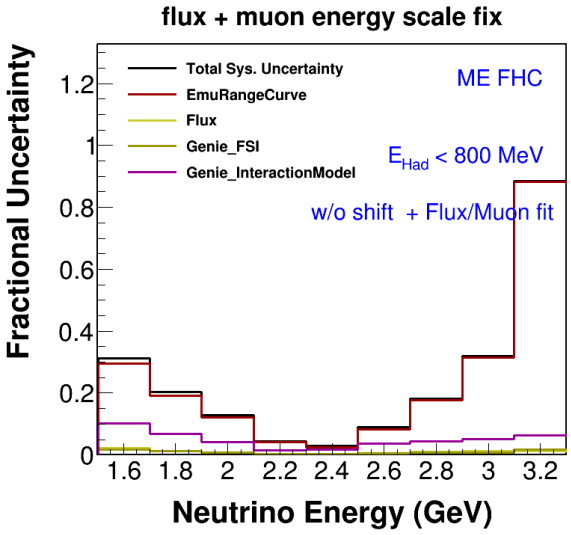

9.9.4. Focusing and Muon parameters fit.

Figure 9.9. Summary of the systematic uncertainties.The sample of events used for these plots corresponds to the low-ν events with the condition that the MINOS muon momentum to be less than 1 GeV, $\boldsymbol{p_{\mu}^{MINOS} < 1\ \mathbf{GeV}}$. All the run playlists of the medium energy era for neutrino beam-line are used for these histograms.

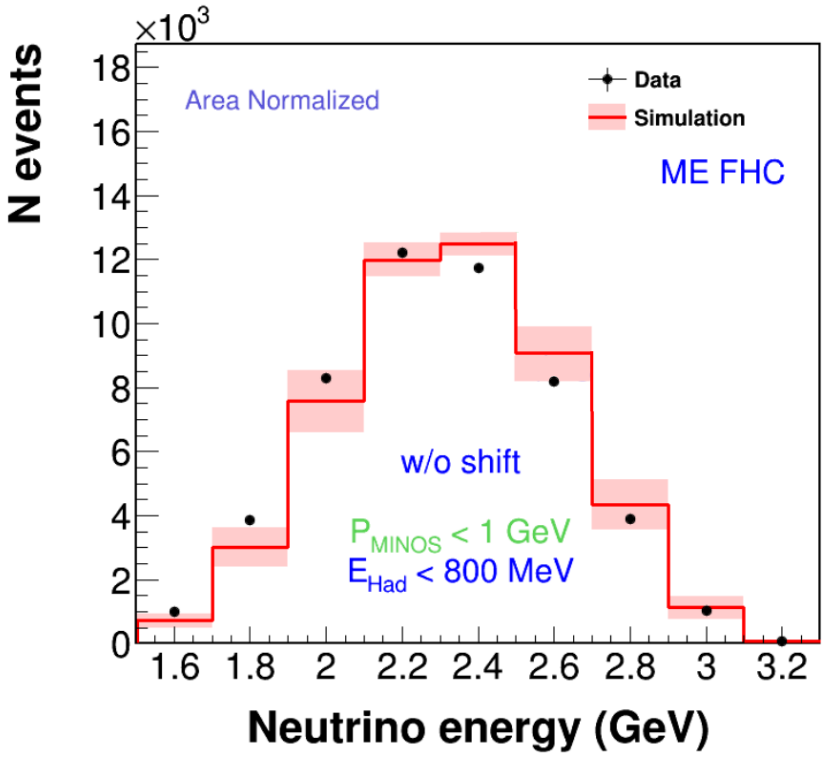

Figure 9.10. Plot of the neutrino flux distribution, for the low-ν events with the condition that the MINOS muon momentum measured was less than 1 GeV, $\boldsymbol{p_{\mu}^{MINOS} < 1}$ **GeV**. The horizontal axis is only from 1.6 GeV to 3.2 GeV because it is the only region with entries in the sample. These distributions are obtained using all the playlists of MINERνA for the medium energy era with the beam-line configured for the neutrino generation.

12000 events. Considering that this sample of events includes the events measured for all the playlists of the medium energy era with the NuMI beam-line configured for neutrinos, then 12000 events is a very small sample.

9.4 Sample of MINOS muon momentum $>$ 1 GeV

For this sample with the cut that only includes the events measured in MINOS with a muon momentum greater than 1 GeV, the expectation is to observe a similar shape distribution of the events as in the original low-ν sample. But unlike the original sample, the discrepancy between data and simulation for the first two bins could be different, since

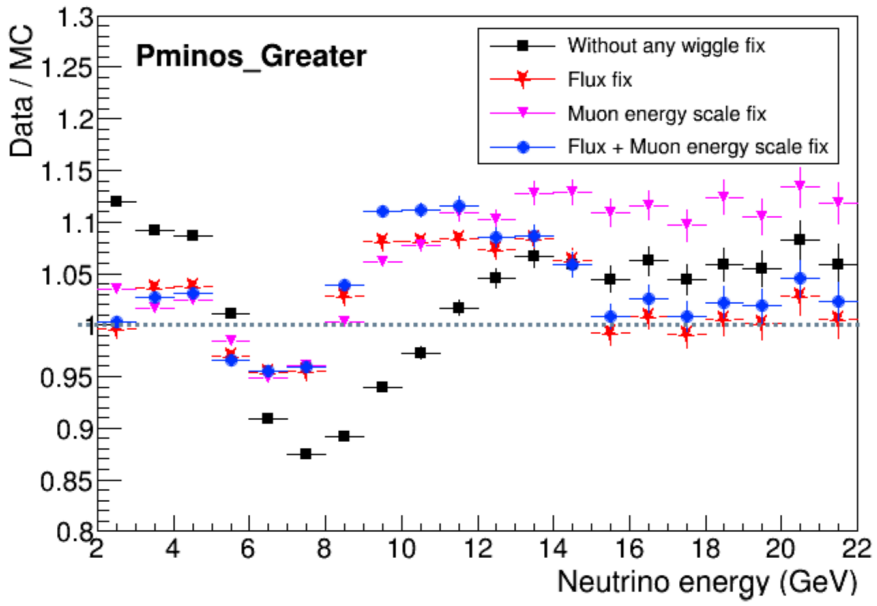

Figure 9.11. Plots of the ratio between data and simulation of the neutrino flux distribution, for the low-ν events with the condition that the MINOS muon momentum measured to be greater than 1 GeV, $\boldsymbol{p_{\mu}^{MINOS} > 1}$ **GeV**. All distributions are made all the playlists of MINERνA for the medium energy era with the beam-line configured for the neutrino generation.

these bins present a reduction of entries due to the cut of $p_{\mu}^{MINOS} > 1$ GeV.

As could be seen in the previous section, the region of events excluded when the sample is divided in p_{μ}^{MINOS} around the 1 GeV corresponds to the low energies region between 2 GeV and 4 GeV, according to the division of the bins used for the plots of this sample. All the bins have the same width of 1 GeV, with the spectrum of neutrino energy beginning from 2 GeV, and finishing at 22 GeV.

In figure 9.11 the four distributions with and without a fit are shown. Just as expected, the shape of the distributions is almost the same as for the low-ν sample without the cut of $p_{\mu}^{MINOS} > 1$ GeV. But for the versions that include a fit to remove the wiggle a much better agreement between data and simulation is observed for the first bin of the distribution.

To analyze if the cut implemented to this sample has influence in the distributions and

how these are cover by the systematic uncertainty bars, the plots with the ratio between data and simulation for the neutrino flux distribution in different canvas adding the systematic bars are shown in figure 9.12. In the four distributions it is observed how they remain very similar to the original low-ν sample.

For the plots with the summary of the systematic uncertainties, see figure 9.13, the only difference observed is that for these plots the region of high energies have a smooth shape between 8 GeV and 22 GeV, but this is due to the change in the width of the bins, because for the plots with the low-ν original sample the width of the bins was 1.5 GeV, and for this sample is 1 GeV. In addition to this difference, the first bin of 2 GeV has a greater contribution of the systematic uncertainty attributed to the muon reconstruction parameters.

To compare both samples, $p_{\mu}^{MINOS} > 1$ GeV and $p_{\mu}^{MINOS} < 1$ GeV, we can identify that most of the errors and the shape of the distribution is coming from the events with a MINOS muon momentum greater than 1 GeV. For the next section is time to identify the proportions of the hadronic recoil energy contribution to the total neutrino energy.

9.5 Contribution of the hadronic recoil energy to the E_{ν}

To identify the proportion of the hadronic recoil energy when the neutrino energy is reconstructed, the variable $y = \frac{\nu}{E_{\nu}}$ is defined, where ν is the energy transfer to the hadronic recoil system, and E_{ν} is the total neutrino energy. Then, with the plot of the distribution for y we can observe which is the greater contribution of the hadronic recoil energy in the reconstructed neutrino energy.

For the horizontal axis the expected values run from almost 0 to 1, the contribution can not be 0, because the conditions of the model is to have one muon outgoing and also have energy transfered to the hadronic recoil system. But due to the low-ν cut, $\nu < 800$ MeV, and considering that the minimum energy of the muon measured in the MINERvA detector must be 1.5 GeV to be able to cross the calorimeters and be measured in the MINOS detector. Then the contribution of the hadronic recoil energy could never be greater

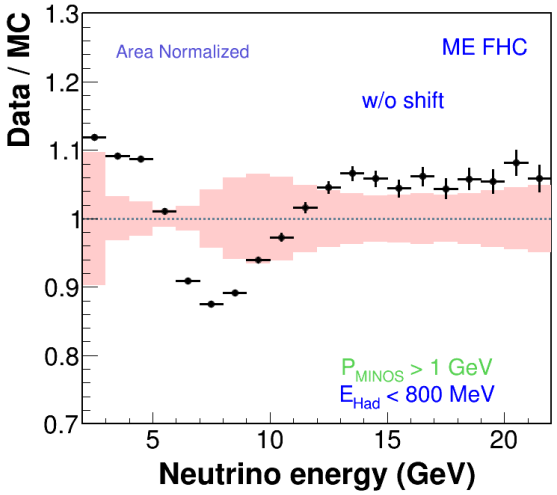

9.12.1. Without any wiggle fit.

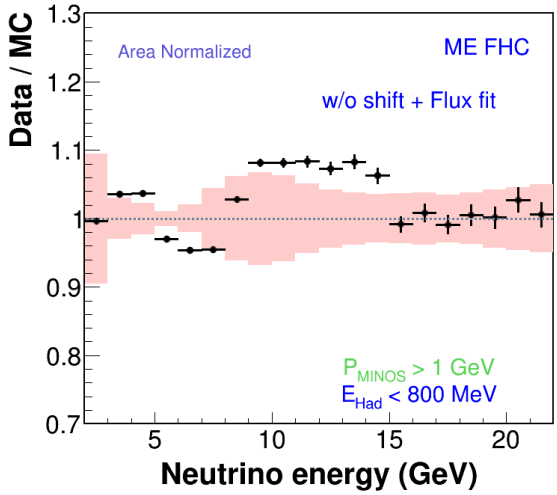

9.12.2. Focusing parameters fit.

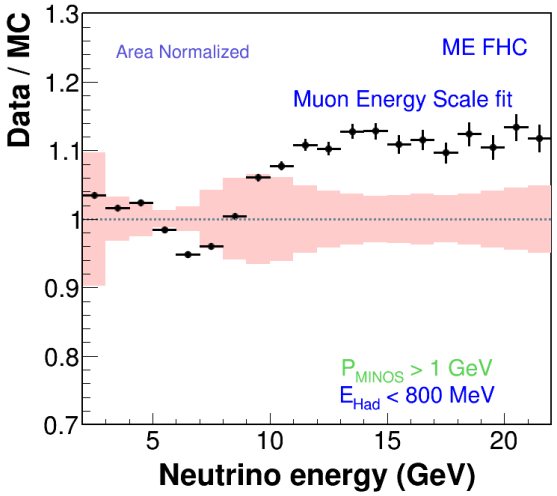

9.12.3. Muon energy scale fit.

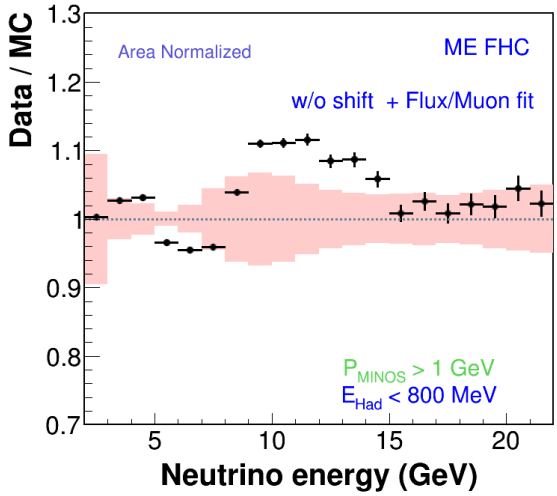

9.12.4. Focusing and Muon parameters fit.

Figure 9.12. Ratios between data and simulation with the systematic uncertainty bars (pink region). The sample of events used for these plots corresponds to the low-ν events with the condition that the MINOS muon momentum to be greater than 1 GeV, $\boldsymbol{p_{\mu}^{MINOS} > 1\ \mathbf{GeV}}$. All the run playlists of the medium energy era for neutrino beam-line are used for these histograms.

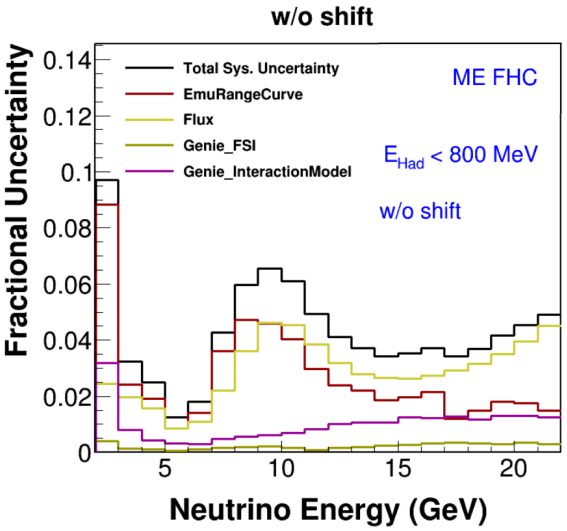

9.13.1. Without any wiggle fit.

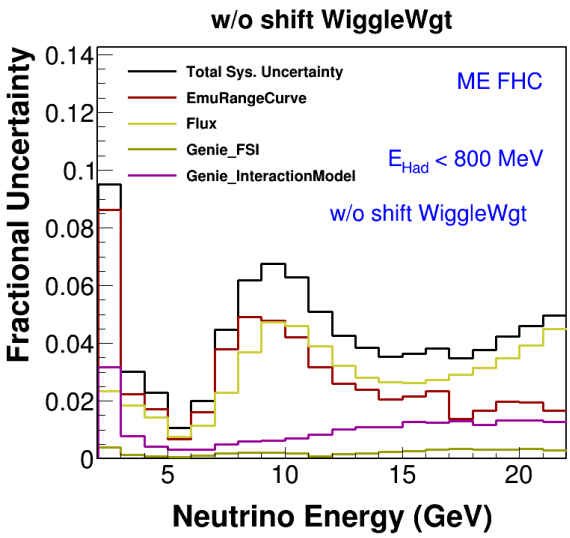

9.13.2. Focusing parameters fit.

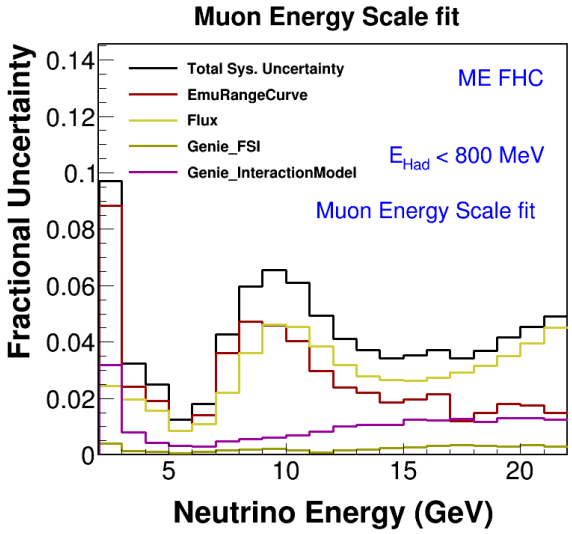

9.13.3. Muon energy scale fit.

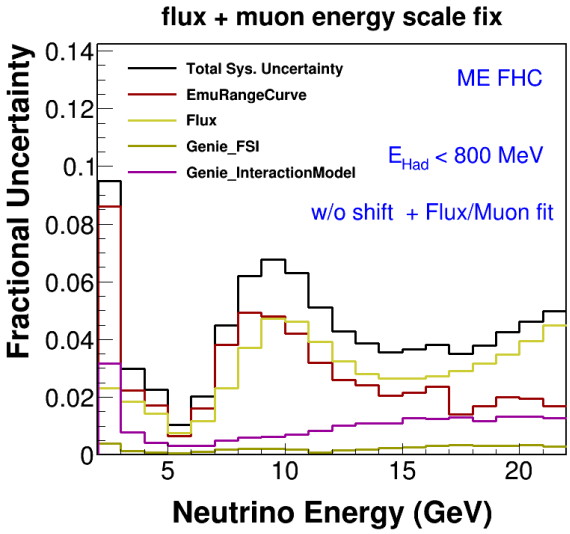

9.13.4. Focusing and Muon parameters fit.

Figure 9.13. Summary of the systematic uncertainties.The sample of events used for these plots corresponds to the low-ν events with the condition that the MINOS muon momentum be greater than 1 GeV, $\boldsymbol{p_{\mu}^{MINOS} > 1\ \mathbf{GeV}}$. All the run playlists of the medium energy era for neutrino beam-line are used for these histograms.

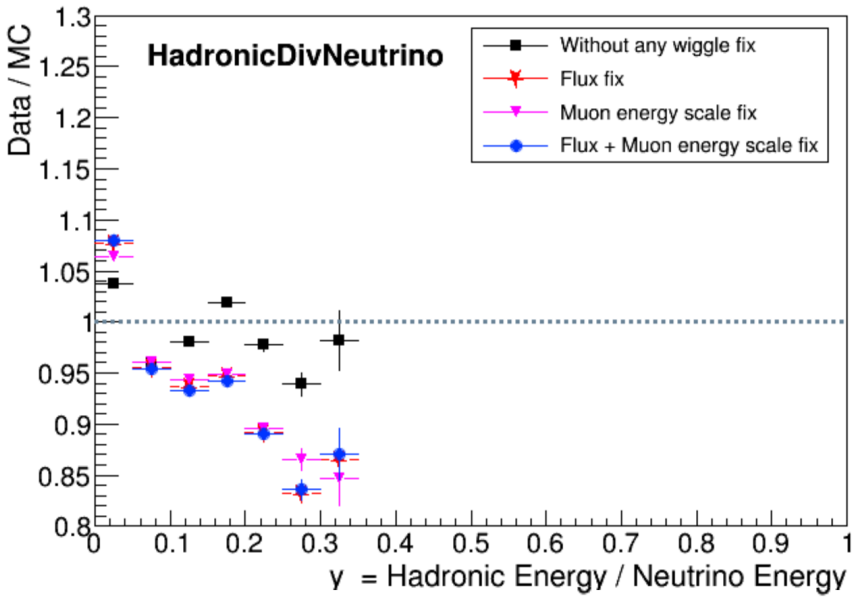

Figure 9.14. Plots of the ratio between data and simulation of the neutrino flux distribution, for the low-ν events. In the horizontal axis the proportion of the hadronic recoil energy in the total neutrino energy reconstructed, $\boldsymbol{y = \nu/E_\nu}$ variable, is shown. All distributions are using all the playlists of MINERνA for the medium energy era with the beam-line configured for the neutrino generation.

than 50 %.

In the plot of figure 9.14, the shape of the ratio between the data and simulation events for different proportions of the hadronic recoil energy contribution to the neutrino energy is shown. Also, in the same plot are shown the three variants of the distribution when the fits to remove the wiggle are applied. From this plot, we see that the greatest contribution of the hadronic recoil energy to the neutrino energy is around 30 %.

To be able to perform a better analysis of the influence to the shape of the neutrino flux distribution for different proportions of the hadronic recoil energy contribution to the neutrino energy, the y variable was divide in three region: [0, 0.1), [0.1, 0.3), and [0.3, 0.5). The idea is to divide the low-ν sample according to the value of y.

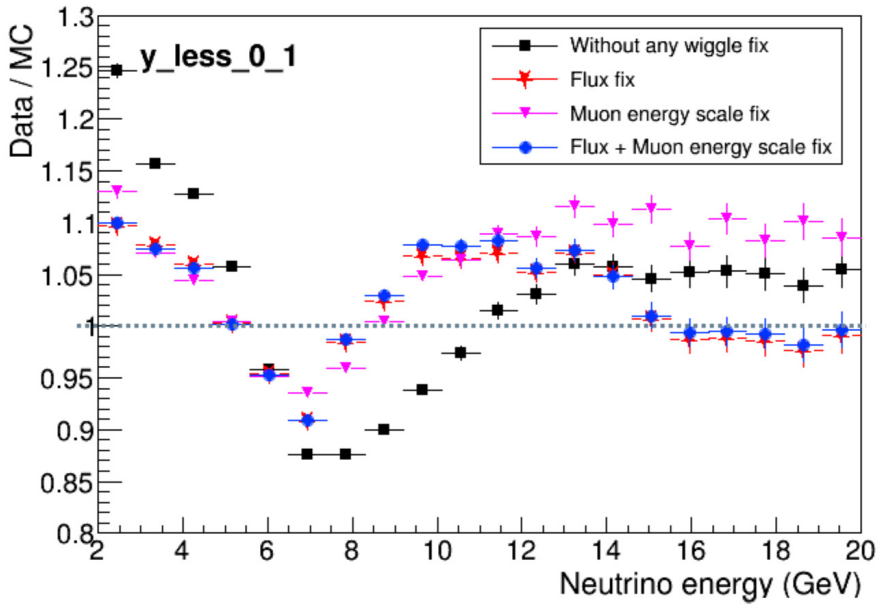

Figure 9.15. Plots of the ratio between data and simulation of the neutrino flux distribution, for the low-ν events with the condition that the contribution of ν to the E_ν to be between almost 0% and 10%, $\mathbf{0 < y < 0.1}$. All distributions are using all the playlists of MINERνA for the medium energy era with the beam-line configured for the neutrino generation.

9.5.1 Sample of $0 < y < 0.1$

In this region of y, the value of $0 < y < 0.1$ means that the contribution of the muon energy is much bigger than the contribution of the hadronic recoil energy. And due to the low-ν cut the number of events for this region is expected to be big. In plot 9.15 the shape of the ratio between data and simulation for the neutrino energy distribution is shown. This plot includes the three versions of the distribution with the three different fits, in addition to the distribution without any wiggle fit. For this region of y a similar wiggle shape is observed in the plot.

The version of the ratio plots with the systematic uncertainty bars for each fit are shown in figure 9.16. From these plots we can observe that the disagreement between data and simulation is present in the four distributions, having some variations when the fits are implemented, but none of the fits could perform a good agreement between the data and the simulation.

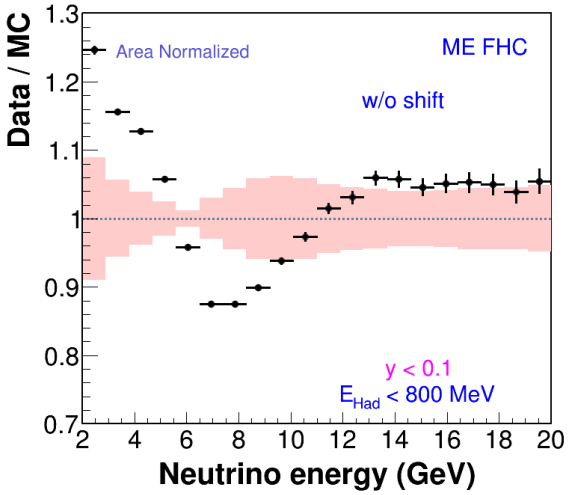

9.16.1. Without any wiggle fit.

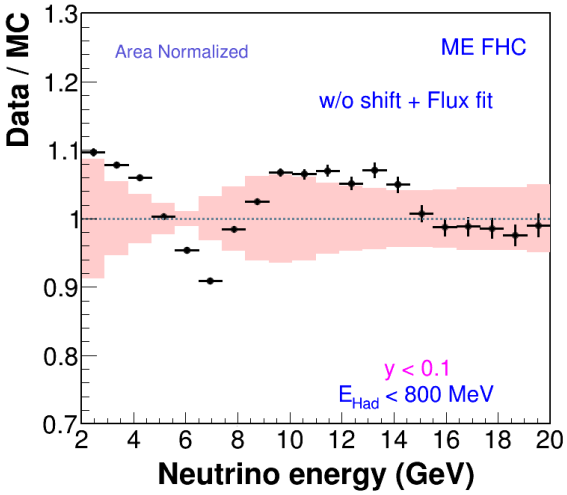

9.16.2. Focusing parameters fit.

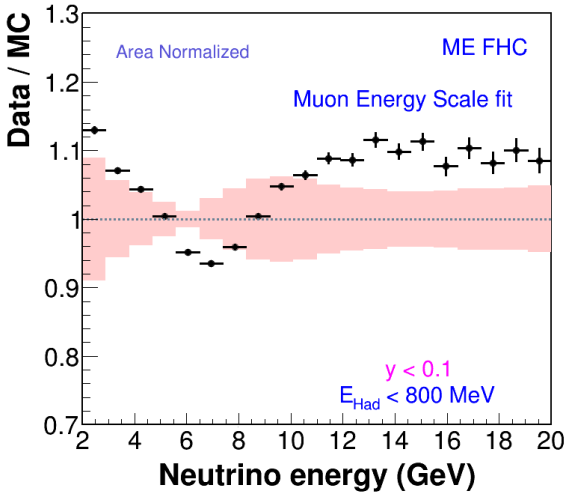

9.16.3. Muon energy scale fit.

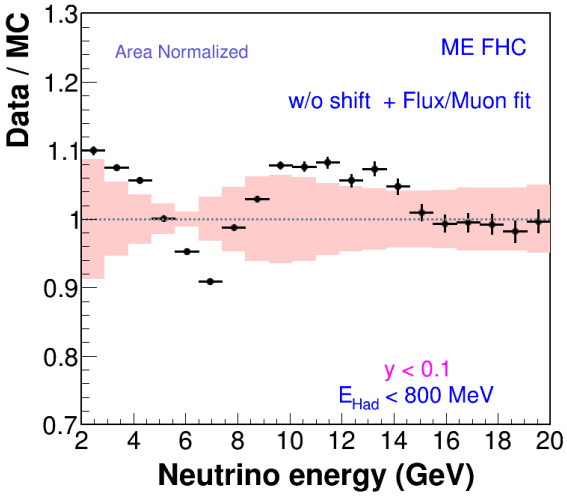

9.16.4. Focusing and Muon parameters fit.

Figure 9.16. Ratios between data and simulation with the systematic uncertainty bars (pink region). The sample of events used for these plots corresponds to the low-ν events with the condition that the contribution of ν to the E_ν to be between almost 0% and 10%, $\mathbf{0 < y < 0.1}$. All the run playlists of the medium energy era for neutrino beam-line are used for these histograms.

Reviewing the plot with the summary of the systematic uncertainties, see figure 9.17, it is observed that the shape of the total systematic uncertainties is almost the same for the four distribution of events. But comparing the shape of this sample version with the original version of low-ν sample, we see an increase of the genie interaction model parameter, this increase of the variable is observed around the peak region of events, but not in the peak (≈ 5 GeV).

9.5.2 Sample of $0.1 < y < 0.3$

For the second slice of events according to the y variable, the contribution of the hadronic recoil energy to the neutrino energy is between 10% and 30%. This region covers almost all the distribution of events observed in figure 9.14, but in comparison with the previous slice, the number of events measured decreases.

In figure 9.18 the plot of the ratio between data and simulation for the low-ν sample with the restriction of $0.1 < y < 0.3$ is shown. Again it includes the distribution with each one of the fits discussed in this investigation, in addition to the distribution without any wiggle fit. From this plot, it is possible to observe that the wiggle shape seen in the original low-ν sample is different to the shape of the distribution for the plot with the ratio between data and simulation of events for this sample. In the region of low energies, around 2 GeV to 4 GeV, for the distribution of events in this sample, we observe a good agreement between the data and simulation. The disagreement observed for the region mentioned above is less than the observed in the same region for the original low-ν sample (see plot of the right side in figure 7.3).

The improvement of the agreement in the ratio distribution for the low energy region mentioned above, may be due to the events of $y < 0.1$ that were removed from this sample. Because if we check the disagreement between data and simulation for this region of low energy observed in the previous slice of y, see figure 9.15, we found a great discrepancy unlike the observed for the slice of $0.1 < y < 0.3$.

To better analyze the performance of the fits implemented to remove the wiggle shape, the plots of the ratio for the neutrino flux distribution with the systematic uncertainty bars are shown in figure 9.19. In the plot it is observed that after implementing the fits

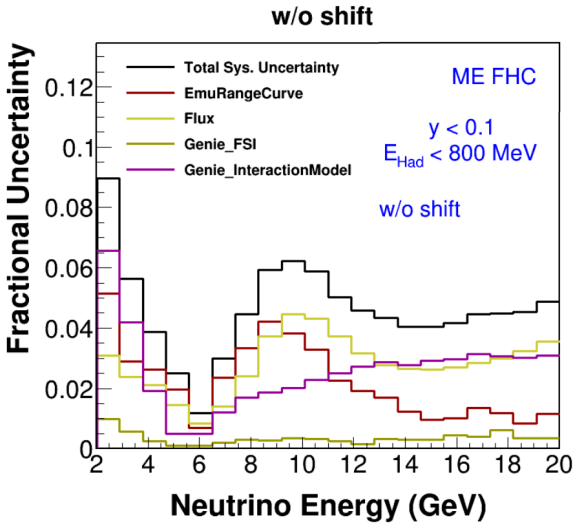

9.17.1. Without any wiggle fit.

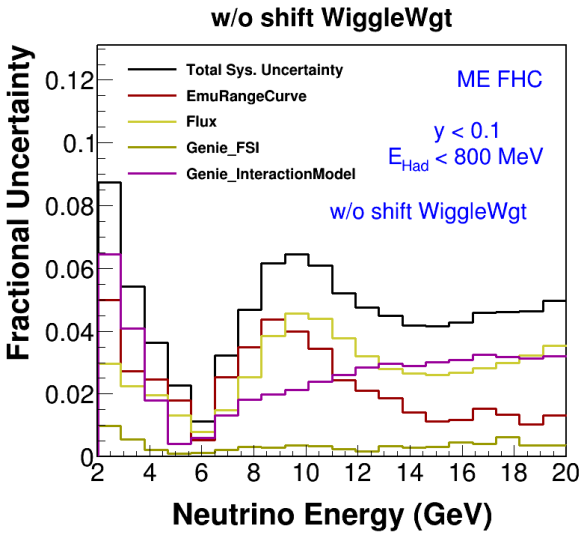

9.17.2. Focusing parameters fit.

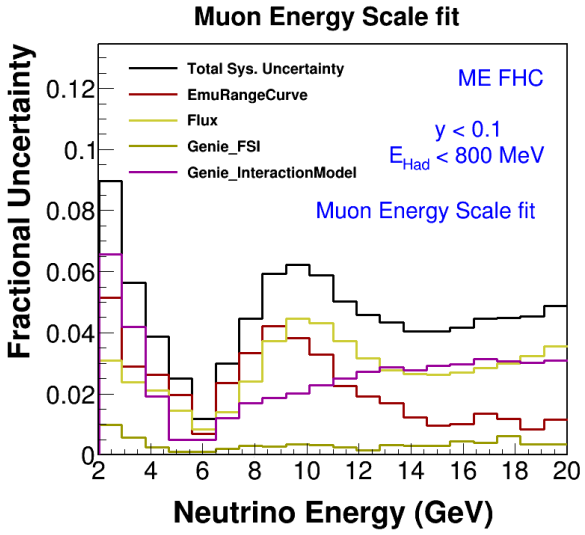

9.17.3. Muon energy scale fit.

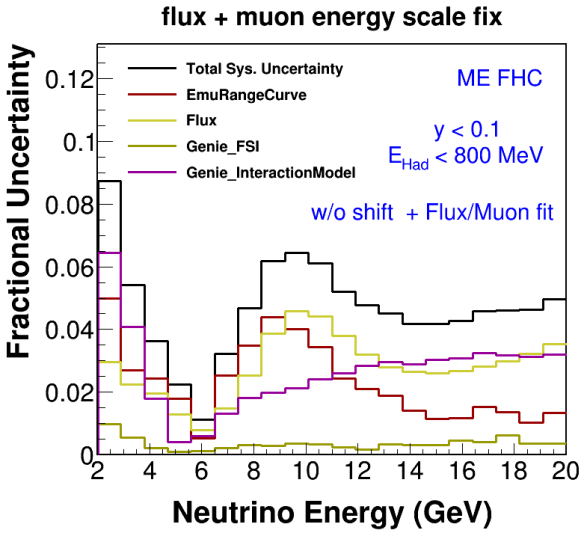

9.17.4. Focusing and Muon parameters fit.

Figure 9.17. Summary of the systematic uncertainties.The sample of events used for these plots corresponds to the low-nu events with the condition that the contribution of ν to the E_ν to be between almost 0% and 10%, $\mathbf{0 < y < 0.1}$. All the run playlists of the medium energy era for neutrino beamline are used for these histograms.

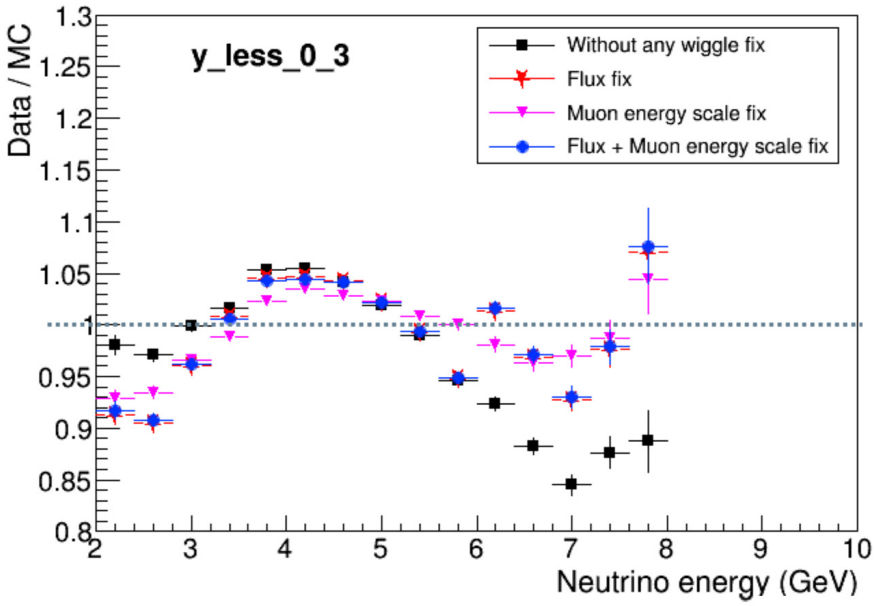

Figure 9.18. Plots of the ratio between data and simulation of the neutrino flux distribution, for the low-nu events with the condition that the contribution of ν to the E_ν to be between 10% and 30%, $\mathbf{0.1 < y < 0.3}$. All distributions are using all the playlists of MINERνA for the medium energy era with the beam-line configured for the neutrino generation.

to remove the wiggle shape, the disagreement observed in the region between 5 GeV and 8 GeV is reduced, and the shape of the resulting distribution is covered by the systematic uncertainty bars. Furthermore, the fit that generates the best agreement between data and simulation is the muon energy scale fit.

Considering all the distribution of events, the best fit for all regions is the muon energy scale fit for this slice of y. There is only one region where the variation between data and simulation is not covered by systematic errors, this region corresponds to the energies between 4 GeV to 5 GeV, that is because for this region the systematic uncertainty bars are small.

To analyze the contribution of the systematic uncertainties for the different fits, the plots with the summary of the systematic uncertainties are shown in figure 9.20. In these plots it is observed that the main contribution to the total systematic uncertainty is coming from the muon reconstruction parameters, followed by the genie interaction model entry, that corresponds to the uncertainties in the simulation of events by the GENIE software. After this the uncertainty of the flux is a great contribution to the total shape, remembering that this corresponds to the focusing parameters of the neutrino beam.

9.5.3 Sample of $0.3 < y < 0.5$

For the last slice of the y variable, we observe from the plot with the y distribution, see figure 9.14, that the number of events measured for this slice is reduced, because for the last bin in this plot the statistical error bars are too long. If an event enters in this sample it means that the neutrino energy reconstructed has a contribution of the hadronic recoil energy around the 30% or 50%, this implies a low contribution of the muon energy to the reconstruction of the neutrino energy.

To get entries in this sample taking into account that the low-ν cut is implemented, $\nu < 800$ MeV, the muon energy reconstructed has to be of around 1.8 GeV, but also the minimum muon energy measured by MINERνA detector is 1.5 GeV, this so that the muon can reach to the MINOS detector. Then, with all these conditions the number of events in this sample is too small. For example, the plot with the neutrino energy distribution without any wiggle fit is shown in figure 9.21. In the plot the bin with the greater entry of

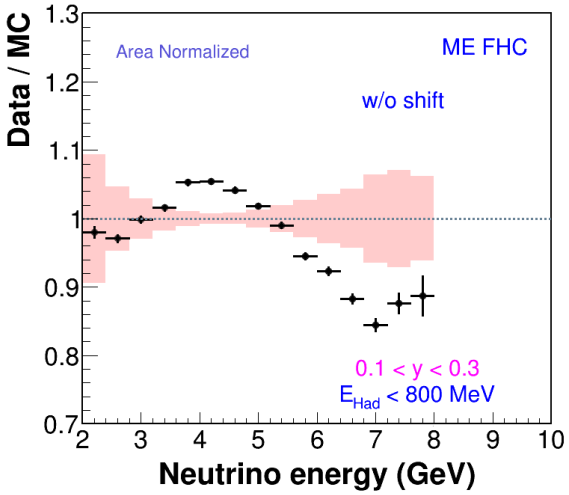

9.19.1. Without any wiggle fit.

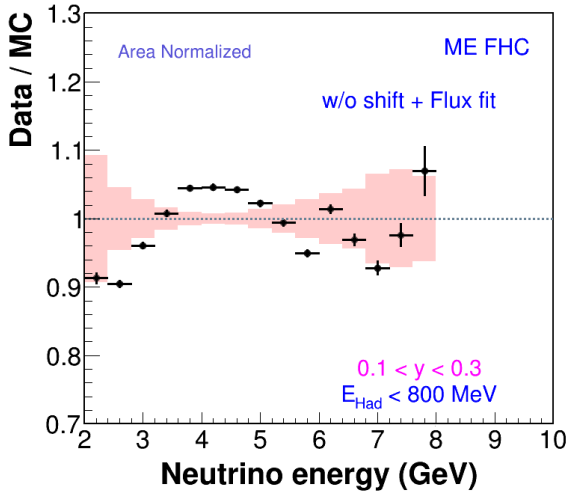

9.19.2. Focusing parameters fit.

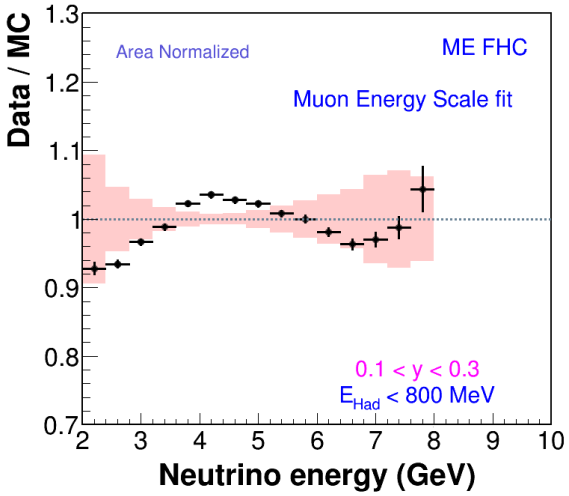

9.19.3. Muon energy scale fit.

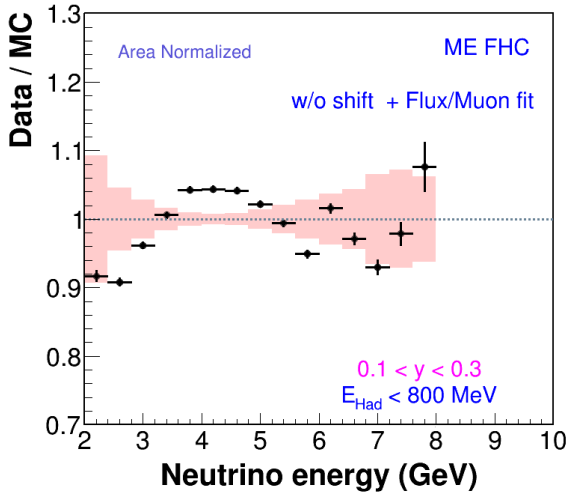

9.19.4. Focusing and Muon parameters fit.

Figure 9.19. Ratios between data and simulation with the systematic uncertainty bars (pink region). The sample of events used for these plots corresponds to the low-ν events with the condition that the contribution of ν to the E_ν to be between 10% and 30%, $\mathbf{0.1 < y < 0.3}$. All the run playlists of the medium energy era for neutrino beam-line are used for these histograms.

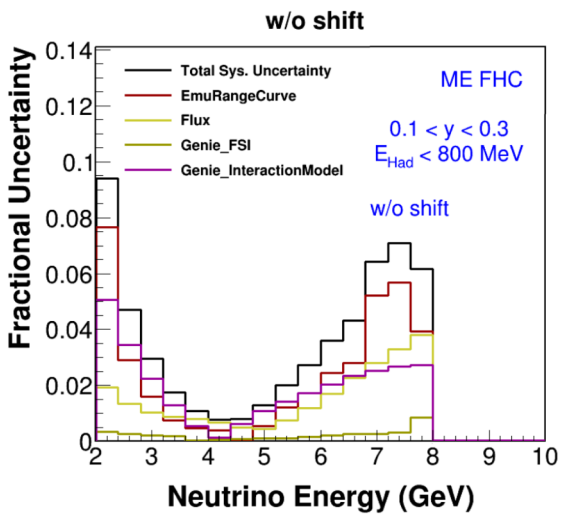

9.20.1. Without any wiggle fit.

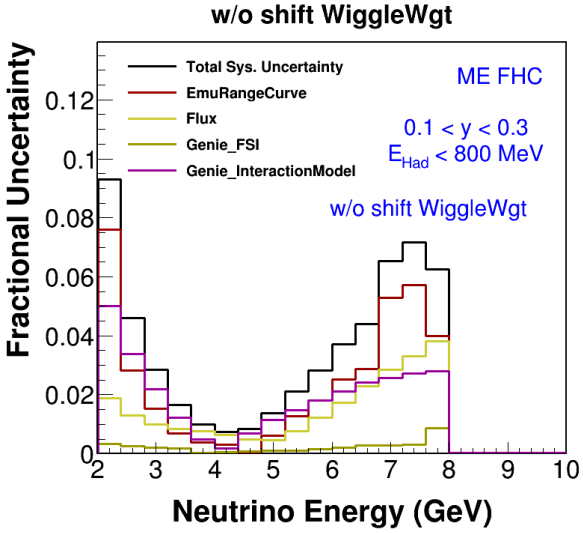

9.20.2. Focusing parameters fit.

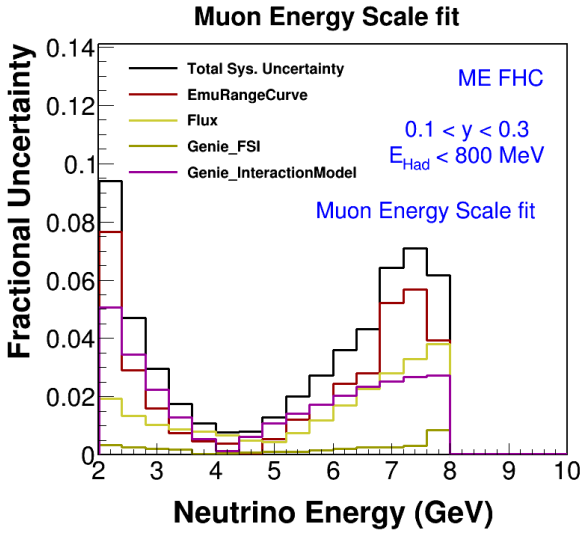

9.20.3. Muon energy scale fit.

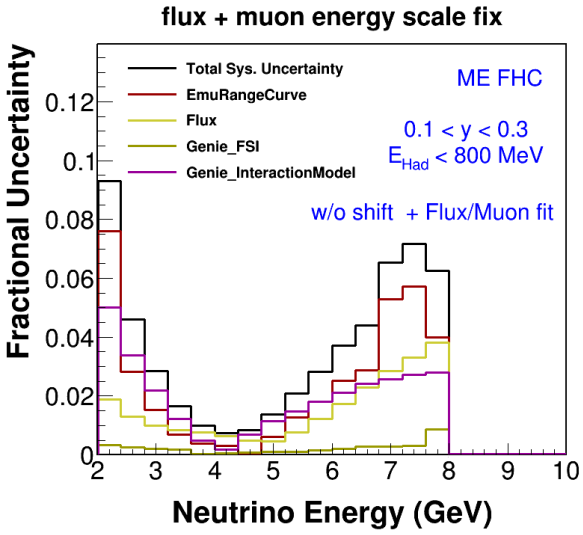

9.20.4. Focusing and Muon parameters fit.

Figure 9.20. Summary of the systematic uncertainties.The sample of events used for these plots corresponds to the low-ν events with the condition that the contribution of ν to the E_ν to be between 10% and 30%, $\mathbf{0.1 < y < 0.3}$. All the run playlists of the medium energy era for neutrino beam-line are used for these histograms.

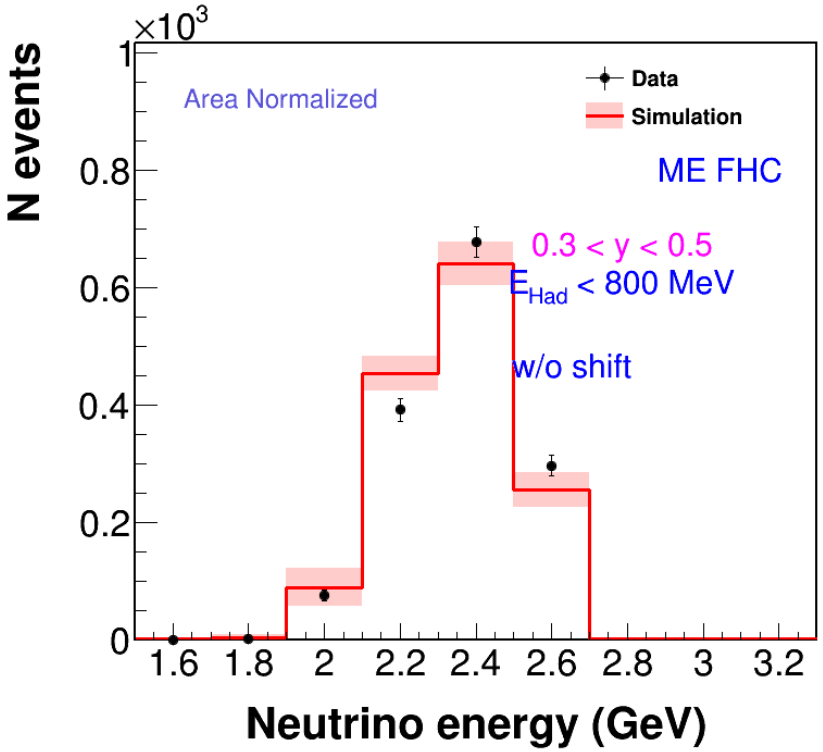

Figure 9.21. Plot of the neutrino flux distribution without any wiggle fit implemented, for the low-ν events with the condition that the contribution of ν to the E_ν to be between 30% and 50%, $\mathbf{0.3 < y < 0.5}$. The distribution was performed using all the playlists of MINERνA for the medium energy era with the beam-line configured for the neutrino generation.

events corresponds to around 650 entries, between 2.25 GeV to 2.45 GeV. For this plot a change in the range of the horizontal axis was implemented, because we only have entries between 2 GeV and 2.6 GeV.

Due to the low number of entries in this slice of y, this sample was discarded to be analyzed. Only as an example the ratio of the distribution of events is shown in figure 9.22. The wiggle fits have a minimum effect on this sample of events. In the summary of the systematic uncertainties the only contribution observed in this sample corresponds to the muon reconstruction parameters, the other parameters are almost zero. In figure 9.23 the plot of the ratio between data and simulation for the distribution without any wiggle fit, and the plot with the summary of the systematic uncertainties of the same distribution are shown.

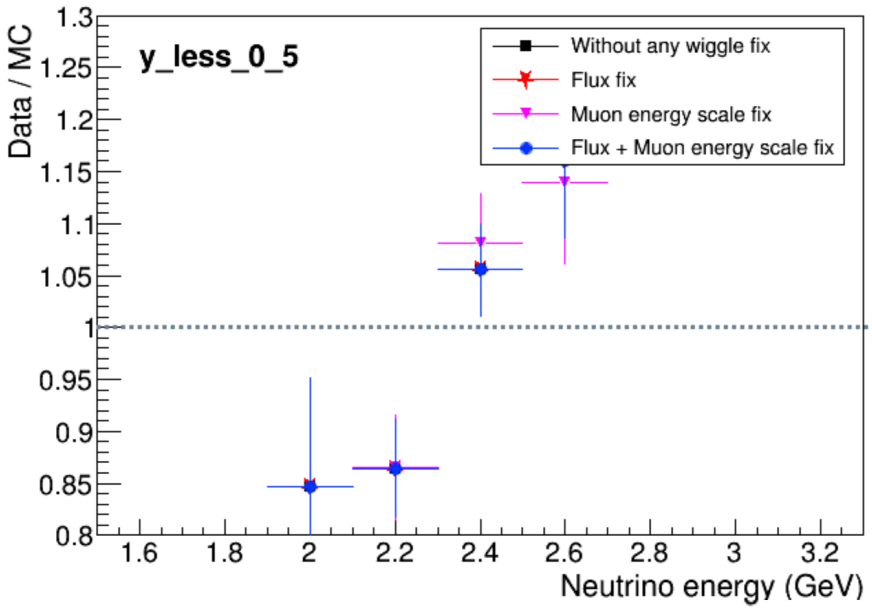

Figure 9.22. Plots of the ratio between data and simulation of the neutrino flux distribution, for the low-ν events with the condition that the contribution of ν to the E_ν to be between 30% and 50%, $\mathbf{0.3 < y < 0.5}$. All distributions are using all the playlists of MINERνA for the medium energy era with the beam-line configured for the neutrino generation.

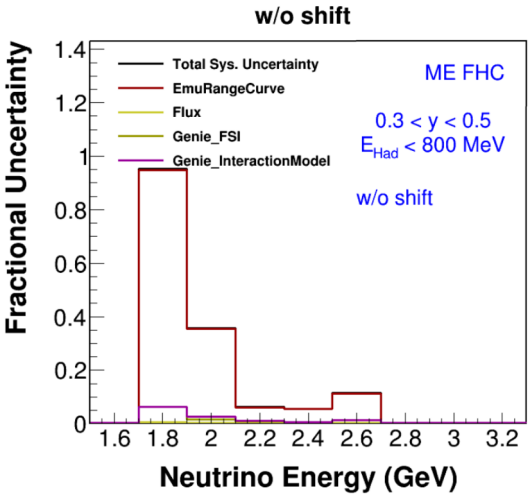

9.23.1. Summary of the systematic uncertainties.

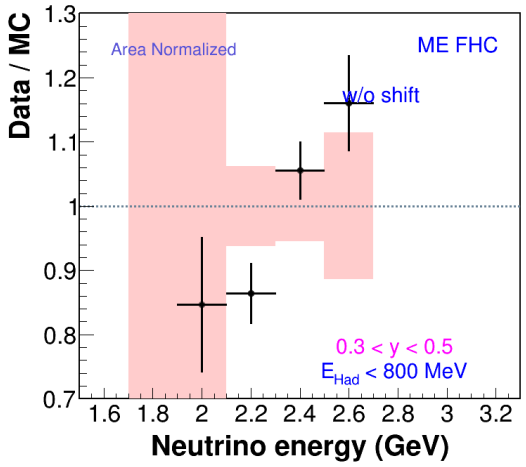

9.23.2. Ratio between data and simulation.

Figure 9.23. Plots of the neutrino flux distribution without any wiggle fit implemented, for the low-ν events with the condition that the contribution of ν to the E_ν to be between 30% and 50%, $\mathbf{0.3 < y < 0.5}$. The sample was performed using all the playlists of MINERνA for the medium energy era with the beam-line configured for the neutrino generation.

Chapter 10. Conclusions

For the analysis of the neutrino flux in the MINERνA experiment a sample of charged current neutrino-nucleus interactions was used, implementing a cut to the sample for the low hadronic recoil energy, ν. Which allows the shape of the neutrino energy distribution to be comparable to the shape of the neutrino flux distribution.

Three different fits were applied to the neutrino flux distribution, each separately, in order to find the origin of the discrepancy observed between the events measured in the detector and the simulated events, and also perform a correction to reduce this discrepancy. The three hypotheses of which was the source of the discrepancy were the following:

- A mis-modeling in the focusing parameters of the neutrino beam-line.
- A shift in the muon reconstruction parameters in the MINOS detector.
- A mis-modeling in the muon reconstruction and the focusing parameters, considering both as fit parameters.

After testing the three hypothesis, the best fit that removes the wiggle shape observed in the neutrino flux distribution was the fit considering a mis-modeling in the focusing and muon reconstruction parameters. But using this fit implies that some of the focusing parameters have a big shift to the nominal values, for example: the target longitudinal position by 13.6 mm. The NuMI beam experts mentioned that the target position was within its tolerance value. This led to the second hypothesis of the muon energy scale of the MINOS detector as the source of the discrepancy to be the best option.

The best shift to apply to the MINOS muon reconstruction parameters is 3.6%, that corresponds to 1.8 times the *a priori* standard deviation of this parameter. This shift only affects the contribution of the muon energy reconstructed by the MINOS detector, because after dividing the low-ν sample it was possible to identify that the methods of muon reconstruction used in the MINOS detector are the source of the discrepancy seen between the data and simulation events.

It was possible to identify that using the sample of the Charged-Current Neutrino-Nucleus interaction of the MINERνA experiment, a reduction of the wiggle shape is obtained for the neutrino flux distribution when the muon energy scale is shifted by 3.6%. Only for the region between 9 GeV to 15 GeV a disagreement between the data and simulation events of 10% was observed, unlike previous low-ν studies. This may be because the weight functions used to reconstruct the simulation events had changes to make a better reconstruction, these changes occurred between the creation of the fits shown in this investigation and the implementation of them for this analysis.

For future analysis performed in the MINERνA experiment and other experiments with similar conditions, the shift correction to the muon energy scale is a factor to consider as a possible source of variations in the simulation of events, besides to implementing the low-ν method to analyze the neutrino flux distribution in detectors that use a neutrino beam-line.

Appendix A. Supplementary plots

Plots of the neutrino flux distribution, ratio between data and simulation, and the summary of the systematic uncertainties for each one of the playlist of the MINERνA experiment for the medium energy era and the neutrino beam configuration. The labels of each playlist are 1A, 1B, 1C, 1D, 1E, 1F, 1G, 1L, 1M, 1N, 1O, and 1P; to identify which one of the playlist used in the corresponding plot.

The plots shown in chapter 8 are the summary version of the plots shown in this appendix.

Plots of each playlist for neutrino flux distribution

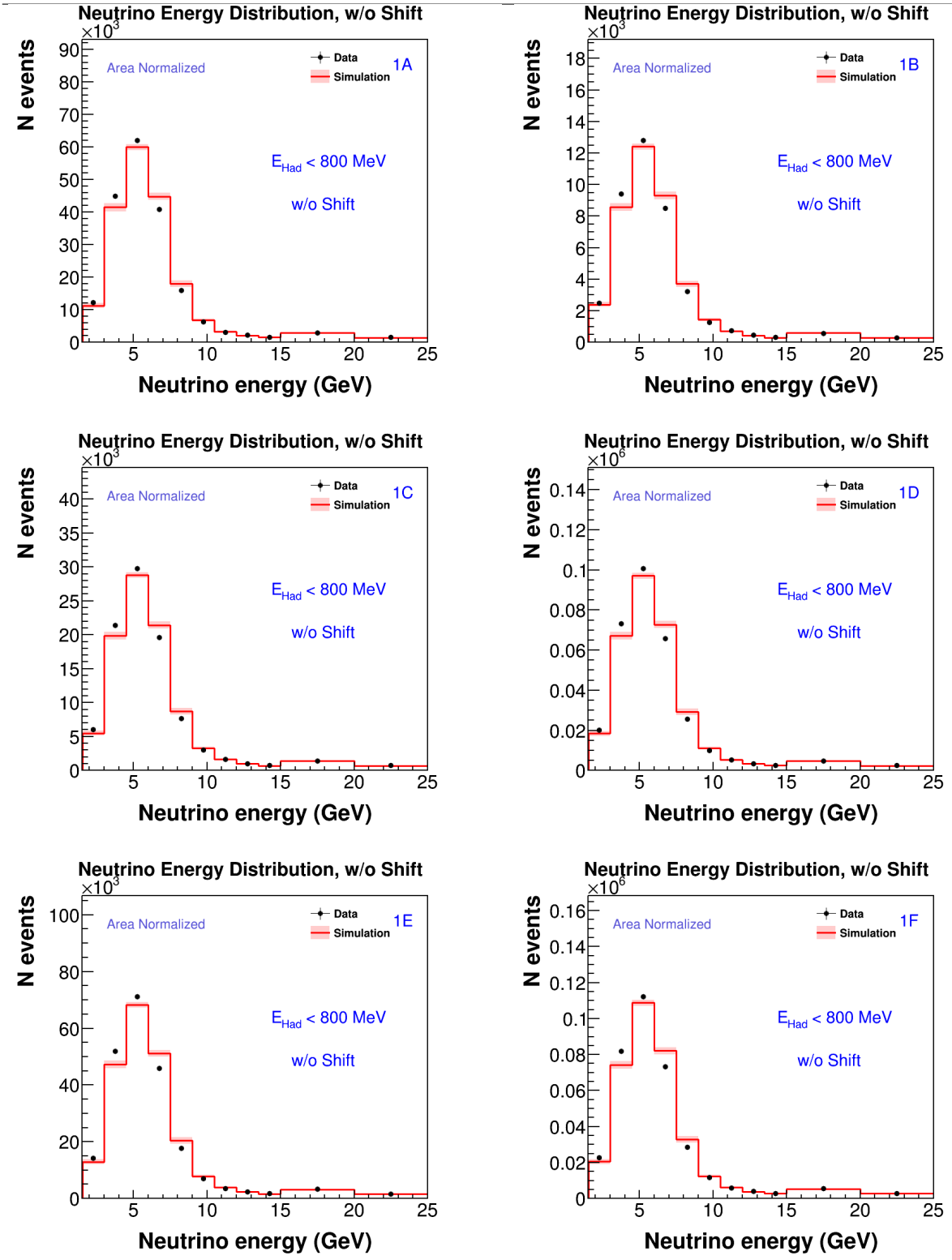

Figure A.1. Neutrino flux distribution for low-nu sample without any wiggle fit applied, 1A to 1F playlists.

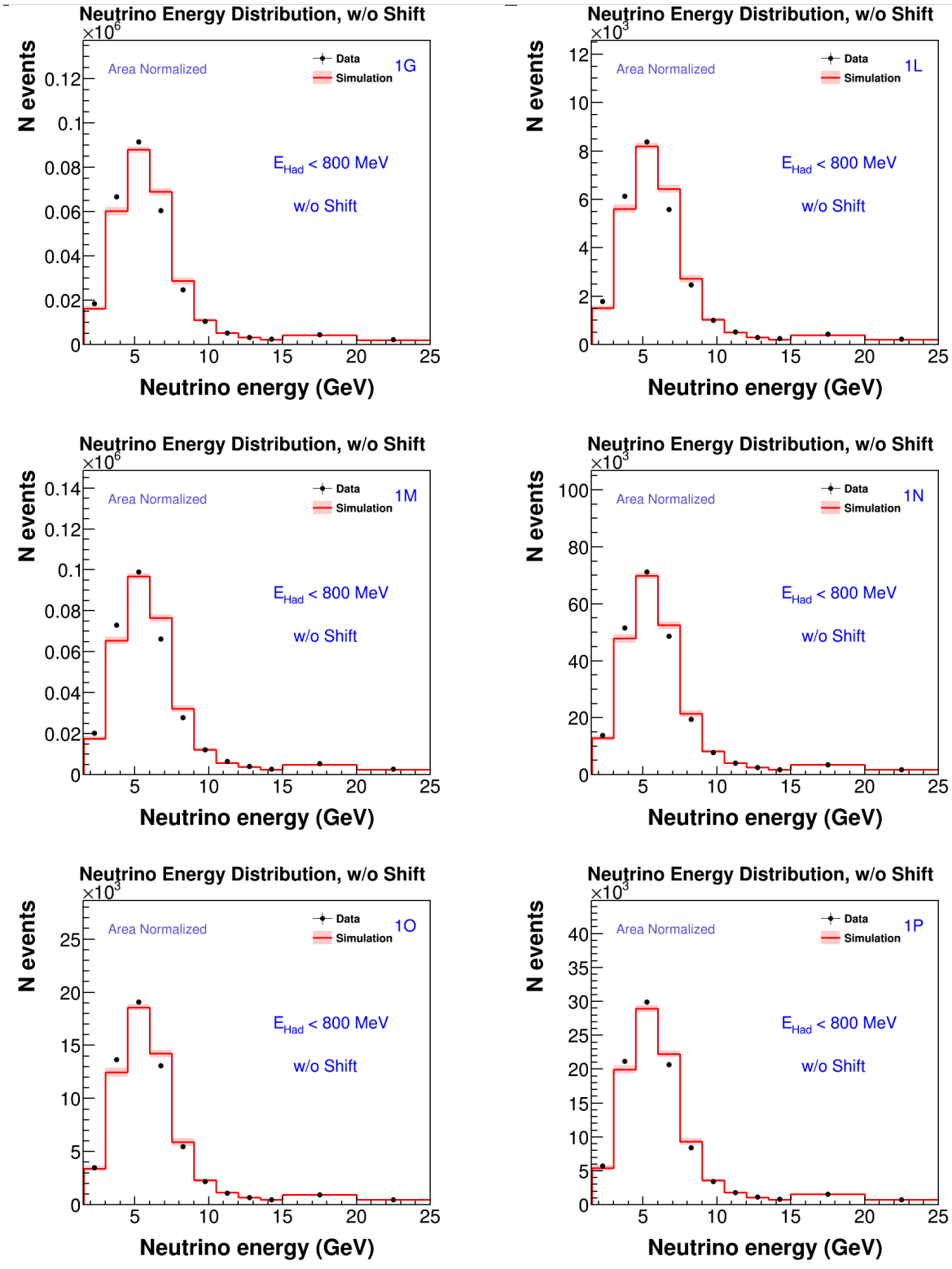

Figure A.2. Neutrino flux distribution for low-nu sample without any wiggle fit applied, 1G to 1P playlists.

Plots of each playlist for the ratio between data and simulation by the neutrino flux distribution

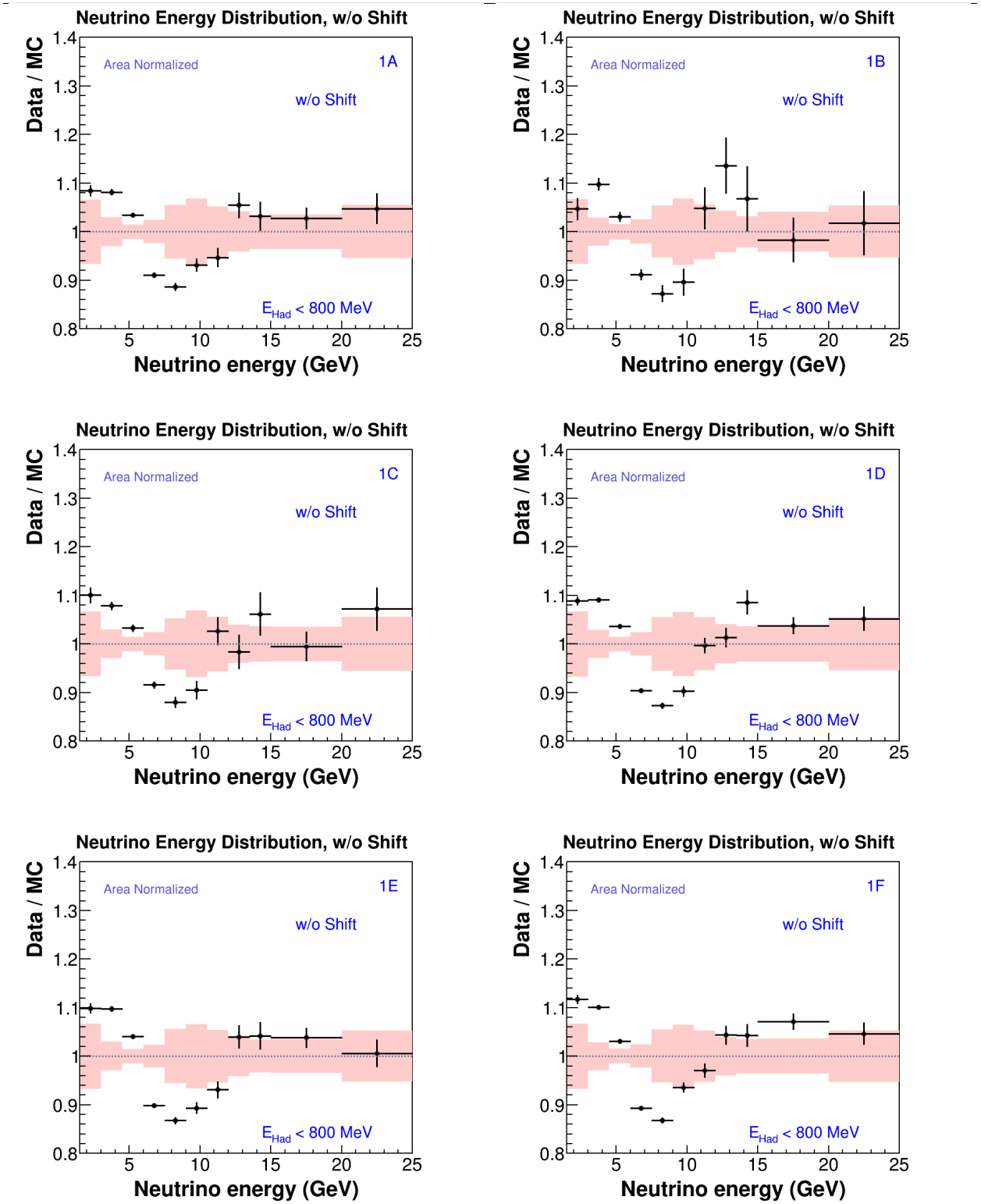

Figure A.3. Ratio between data and simulation for the neutrino flux distribution for low-nu sample without any wiggle fit applied, 1A to 1F playlists.

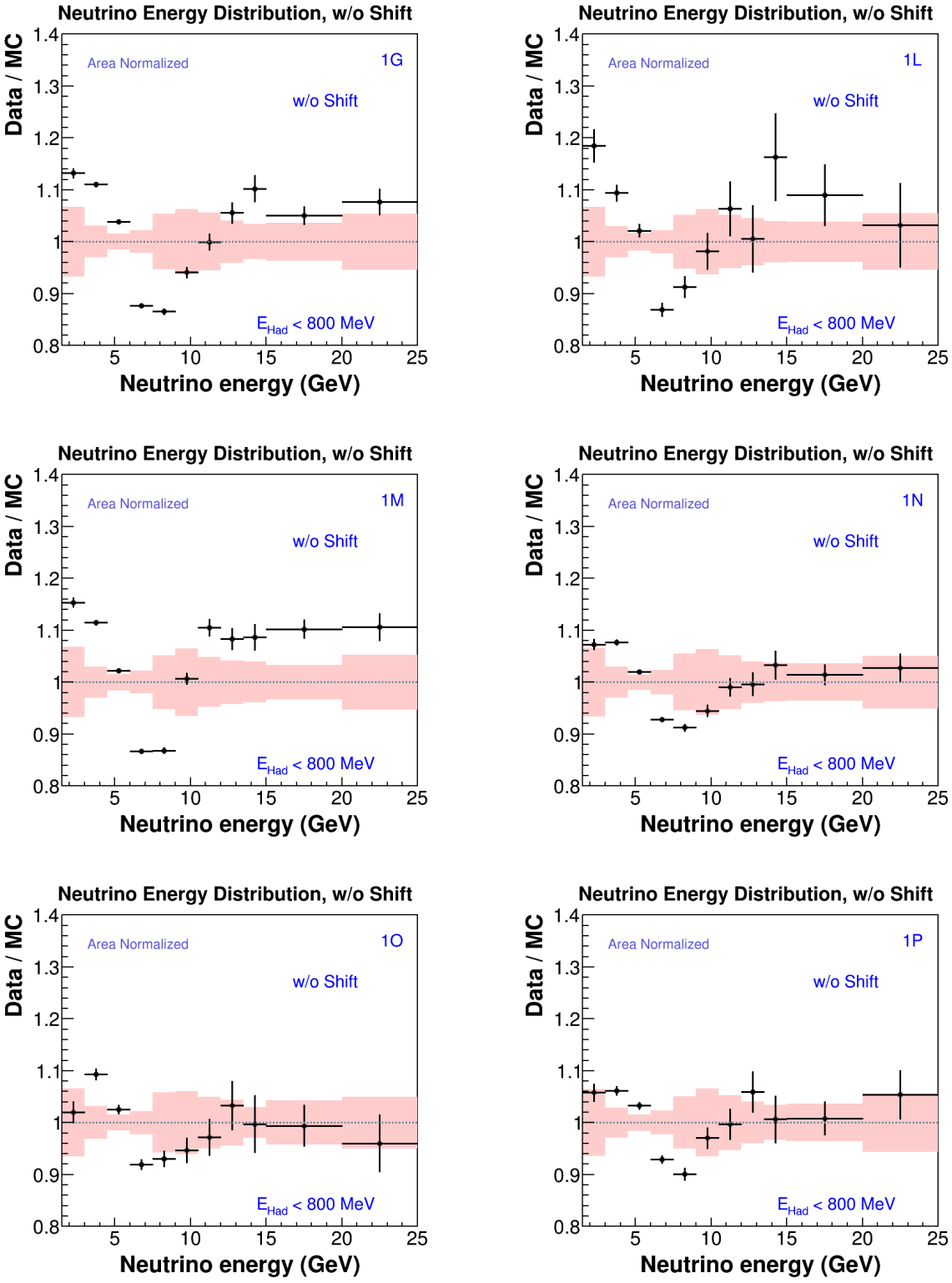

Figure A.4. Ratio between data and simulation for the neutrino flux distribution for low-nu sample without any wiggle fit applied, 1G to 1P playlists.

Plots with the summary of the systematic uncertainties for neutrino flux distribution

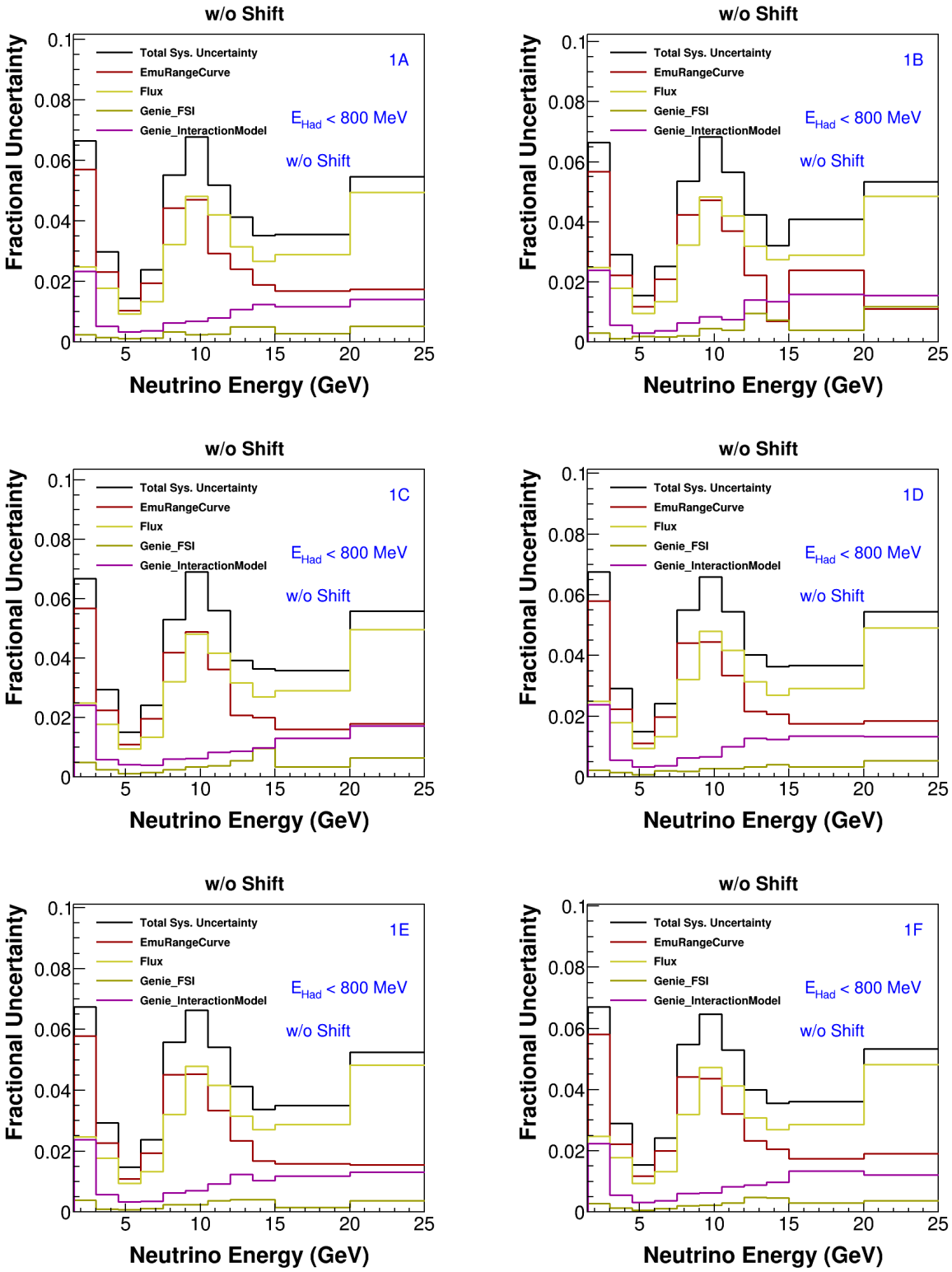

Figure A.5. Summary of the systematic uncertainties for the neutrino flux distribution for low-nu sample without any wiggle fit applied, 1A to 1F playlists.

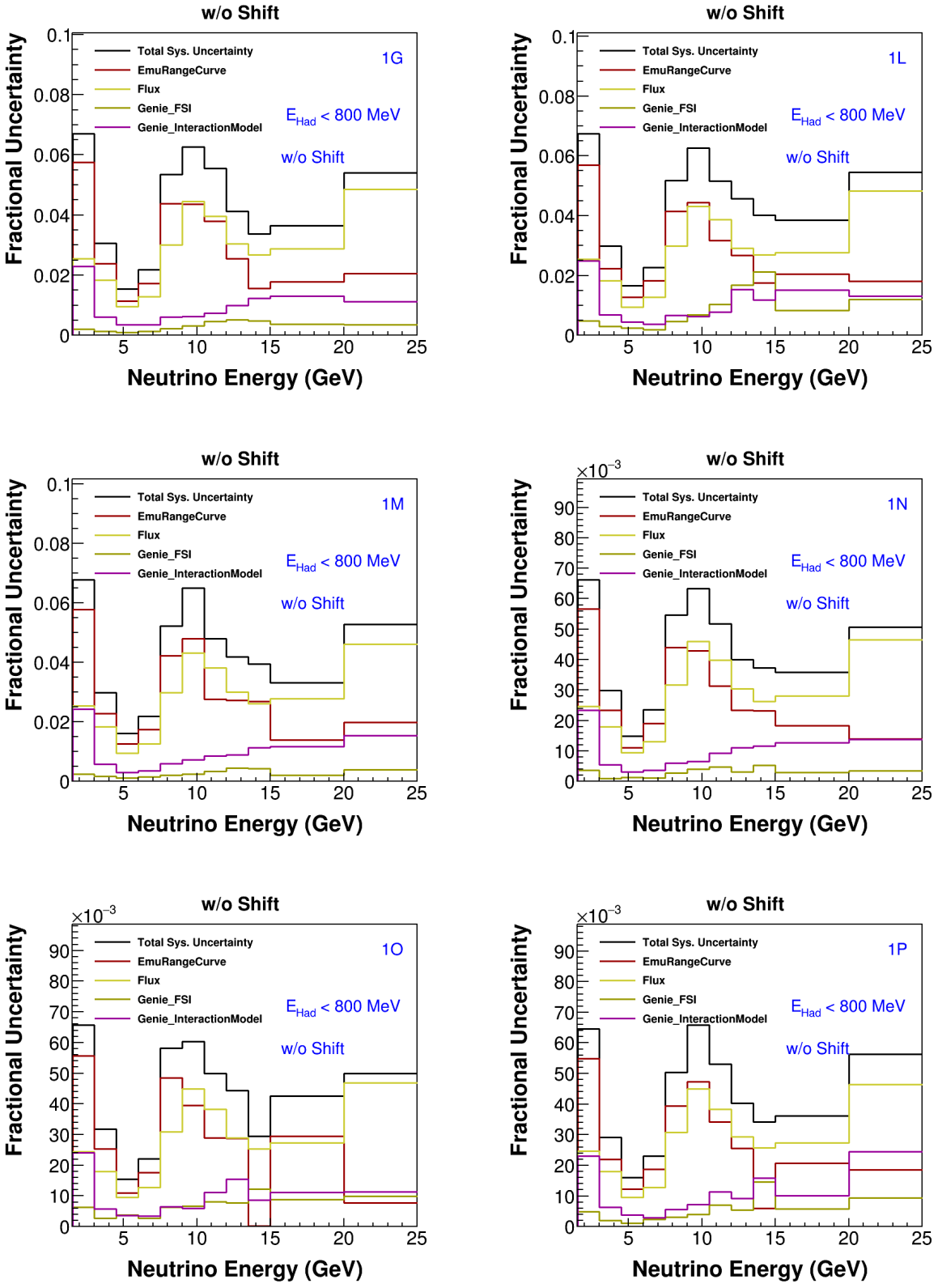

Figure A.6. Summary of the systematic uncertainties for the neutrino flux distribution for low-nu sample without any wiggle fit applied, 1G to 1P playlists.

Bibliography

[1] A. Bashyal. Flux Fit Results, 2019. URL https://minerva-docdb.fnal.gov/cgi-bin/private/RetrieveFile?docid=22908&filename=ABashyal_04192019_FluxFits.pdf&version=3. MINERvA DocDB.

[2] A. Bashyal. NuMI Beamline and Neutrino Flux in MINERvA, 2020. URL https://minerva-docdb.fnal.gov/cgi-bin/private/RetrieveFile?docid=27416&filename=MINERvA101_Flux_2020.pdf&version=10. MINERvA DocDB.

[3] A. Bashyal, D. Rimal, B. Messerly. Use of Neutrino Scattering Events with Low Hadronic Recoil to Inform Neutrino Flux and Detector Energy Scale, 2021. URL https://minerva-docdb.fnal.gov/cgi-bin/private/RetrieveFile?docid=28380&filename=Wiggle_Fit_Paper%20%281%29.pdf&version=4. MINERvA DocDB.

[4] A. Bashyal, D. Rimal, L. Fields, H. Schellman. Flux Fits for NuMI Medium Energy, 2019. URL https://minerva-docdb.fnal.gov/cgi-bin/private/RetrieveFile?docid=25116&filename=NuMI_Medium_Energy_Flux-14.pdf&version=1. MINERvA DocDB.

[5] B. Pontecorvo. Neutrino Experiments and the Problem of Conservation of Leptonic Charge. *Sov. Phys. JETP*, **26**(984-988), 1968.

[6] C. Andreopoulos, C. Barry, S. Dytman, H. Gallagher, T. Golab, R. Hatcher, G. Perdue, and J. Yarba). The GENIE Neutrino Monte Carlo Generator: Physics and User Manual. arXiv:1210.05494v1 [hep-ph], 2015.

[7] C. Andreopoulos et al. (GENIE Collaboration). The GENIE Neutrino Monte Carlo Generator. *Nucl. Instrum. Meth A*, **614**:87–104, 2010. arXiv:0905.2517v2 [hep-ph].

[8] D. Casper. The nuance Neutrino Simulation, and the Future. *Nucl. Phys. Proc. Suppl.*, **112**(161-170), 2002.

[9] D. Ruterbories et al. (MINERvA Collaboration). Measurement of quasielastic-like neutrino scattering at $<E_\nu> \sim 3.5$ GeV on a hydrocarbon target. *Phys. Rev. D*, **99** (012004), 2019. arXiv:1811.02774v1 [hep-ex].

[10] Fermilab. Target Systems: NuMI Beam Absorber, 2017. URL https://targets.fnal.gov/NuMI_beam_absorber.html. Access: February 08, 2021.

[11] Fermilab. Target Systems: NuMI Beam Monitoring System, 2017. URL https://targets.fnal.gov/NuMI_beam_monitors.html. Access: February 08, 2021.

[12] Fermilab. NuMI/NOvA Target, 2017. URL https://targets.fnal.gov/NuMI_target.html. Access: February 08, 2021.

[13] Fermilab. The MINOS Experiment and NuMI Beamline, 2020. URL https://www-numi.fnal.gov/. Access: February 09, 2021.

[14] Fermilab. NuMI Facility: Decay Pipe, 2020. URL https://web.fnal.gov/project/TargetSystems/NuMI/_layouts/15/start.aspx#/SitePages/Decay%20Pipe.aspx. Access: February 08, 2021.

[15] Fermilab. Fermilab is America's particle physics and accelerator laboratory, 2020. URL https://www.fnal.gov/pub/about/index.html. Access: February 08, 2021.

[16] J. A. Formaggio adn G. P. Zeller. From eV to EeV: Neutrino Cross Sections Across Energy Scales. *Rev. Mod. Phys.*, **84**(1307-1341), 2012.

[17] J. D. Devan. *Measurement of Neutrino and Antineutrino Charged-Current Inclusive Cross Sections with the MINERvA Detector*. PhD thesis, Virginia Beach, Virginia, 2016.

[18] J. Mousseau et al. (MINERvA Collaboration). Measurement of partonic nuclear effects in deep-inelastic neutrino scattering using MINERvA. *Phys. Rev. D*, **93**(071101), 2016. arXiv:1601.06313v3 [hep-ex].

[19] Raymond Davis Jr. A HALF-CENTURY WITH SOLAR NEUTRINOS. Nobel Lecture, 2002.

[20] L. Aliaga et al. (MINERvA Collaboration). Neutrino Flux Predictions for the NuMI Beam. *Phys. Rev. D*, **94**(092005), 2016. [Addendum: Phys. Rev. D 95, 039903 (2017)], arXiv:1607.00704v3.

[21] L. Aliaga *et al*. Design, calibration, and performance of the MINERvA detector. *Nucl. Instrum. Methods Phys. Res. A*, **743**(130-159), 2014.

[22] L. Ren et al. Measurement of the antineutrino to neutrino charged-current interaction cross section ratio in MINERvA. *Phys. Rev. D*, **95**(072009), 2017.

[23] M. Hernandez. Flux implications from Horn B-Field Measurements on NuMI and LBNF. *Universidad de Guanajuato*, MsC thesis, Guanajuato, Mexico. 2019.

[24] M. Tzanov et al. Precise measurement of neutrino and antineutrino differential cross sections. *Phys. Rev. D*, **74**(012008), 2006.

[25] P. Adamson et al. Neutrino and antineutrino inclusive charged-current cross section measurements with the MINOS near detector. *Phys. Rev. D*, **81**(072002), 2010.

[26] P. Adamson *et al.* The NuMI Neutrino Beam. *Nucl. Instrum. Meth. A*, **806**(279-306), 2016.

[27] R. Fine. *Measurement of the Medium Energy NuMI Flux Using the Low-ν and High-ν Methods at MINERvA*. PhD thesis, Rochester, New York, 2020.

[28] Tejin Cai. Shared to the MINERvA Collaboration by the official Slack channel of the collaboration, February 2021.

[29] Scott D. Tremaine. *JOHN NORRIS BAHCALL 1934 - 2005*. NATIONAL ACADEMY OF SCIENCES, Washington, D.C., 1 edition, 2011.

[30] V. Shiltsev. Future Accelerator-Based Neutrino Beams. *arXiv:1906.07324v1 [physics.acc-ph]*, 2019.

[31] W. Seligman. *A Next-to-Leading-Order QCD Analysis of Neutrino-Iron Structure Functions at the Tevatron*. PhD thesis, Columbia University, 1997.

[32] Z. Maki, M. Nakagawa and S. Sakata. Remarks on the unified model of elementary particles. *Prog. Theor. Phys.*, **28**(870-880), 1962.

UNIVERSIDAD DE GUANAJUATO

León Guanajuato. Marzo 1, 2021.

DR. DAVID YVES GHISLAIN DELEPINE
DIVISIÓN DE CIENCIAS E INGENIERÍAS
CAMPUS LEÓN, UNIVERSIDAD DE GUANAJUATO
DIRECTOR

Manifiesto que he leído y revisado la tesis de maestría **Validation of muon energy scale fit with medium energy flux using the low-ν method on MINERvA experiment** realizada bajo mi supervisión, que presenta el Sr. **Francisco Javier Rosas Torres,** estudiante de maestría en física en esta División de Ciencias e Ingenierías, para optar por el grado de Maestro en Física.

El mencionado trabajo fue realizado dentro de la colaboración MINERvA (http://minerva.fnal.gov) de la que somos miembros. El contenido tiene la calidad, profundidad, y originalidad, y representa un avance significativo en el desarrollo del tema a nivel internacional, suficientes para optar por el grado de Maestro en Física. El trabajo contribuye a entender las reacciones neutrinos-nucleón que se estudian en el experimento MINERvA.

Si otro particular,

Atentamente,

Dr. Julián Félix
felix@fisica.ugto.mx
Extensiones 8444, 8449, 8458
ASESOR

León, Gto, 17 de Marzo de 2021

Asunto: Carta liberación Francisco Javier Rosas Torres

Dr. David Delepinde
Director de la DCI

Como sinodal del estudiante de Maestría en Física **Francisco Javier Rosas Torres**, me permito comentar que he leído el manuscrito de su tesis ***Validation of muon energy scale fit with medium energy flux using the low-ν method on MINERvA experiment,*** donde el estudiante presenta una buena narrativa de su trabajo, así como los alcances logrados durante su investigación y participación en dicho experimento de Minerva.

Considero que el trabajo de investigación es satisfactorio de acuerdo a los requisitos de la Maestría, por lo que me permito recomendarle que haga los trámites administrativos para que se presente lo más pronto posible.

"LA VERDAD OS HARA LIBRES"

Dr. José Socorro García Díaz
Sinodal

León Guanajuato, a; 16 de marzo de 2021

Dr. David Delepine
Director de la División de Ciencias e Ingenierías
Campus León, Universidad de Guanajuato
PRESENTE

Estimado Dr. Delepine:

Por este medio, me permito informarle que he leído y revisado la tesis titulada **"Validation of muon energy scale fit with medium energy flux using the low-nu method on MINERvA experiment"** que realizó el estudiante de maestría **Francisco Javier Rosas Torres**, como requisito para obtener el grado de Maestro en Física.

Considero que el trabajo de doctorado realizado por Francisco es de interés para la comunidad científica del área de neutrinos y por lo tanto reúne los requisitos necesarios de calidad e interés académico para que sea defendida en un examen profesional, razón por la cual extiendo mi aval para que así se proceda.

Sin más que agregar, agradezco su atención y aprovecho la ocasión para enviarle un cordial saludo.

ATENTAMENTE
"LA VERDAD OS HARÁ LIBRES"

DR. Juan Barranco Monarca
Departamento de Física
DCI, Campus León

DIVISIÓN DE CIENCIAS E INGENIERÍAS, CAMPUS LEÓN
Loma del Bosque 103, Fracc. Lomas del Campestre C.P. 37150 León, Gto., Ap. Postal E-143 C.P. 37000 Tel. +52 (477) 788-5100 Fax:+52 (477) 788-5100 ext. 8410,
http://www.ifug.ugto.mx

UNIVERSIDAD DE GUANAJUATO

Asunto: ***Carta de Aceptación***
León, Gto, Marzo 18, 2021

Dr. David Yves Ghislain Delepine
División De Ciencias E Ingenierías
Campus León, Universidad De Guanajuato
Director

Comunico que he leído y revisado la tesis de maestría titulada "**Validation of muon energy scale fit with medium energy flux using the low-v method on MINERvA experiment**", que presenta el Lic. ***Francisco Javier Rosas Torres***, estudiante en la Maestría en Física de la División de Ciencias e Ingenierías, para optar por el grado de Maestro en Física.

El trabajo es de calidad suficiente para optar por el mencionado grado. Por lo anterior, acepto en contenido, forma, y profundidad la mencionada tesis.

Sin otro particular,

Atentamente,

Dr. Edgar Valencia Rodríguez
e.valencia@ugto.mx
Tel. 472 737 3537